DEVELOPMENT OF ELASTIN-LIKE POLYPEPTIDE FUSION PROTEIN CONTAINING THE BINDING DOMAIN OF RECEPTORS FOR ADVANCED GLYCATION END-PRODUCTS FOR DIABETIC CHRONIC SKIN WOUNDS

by

HWAN JUNE KANG

A dissertation submitted to the

School of Graduate Studies

Rutgers, The State University of New Jersey

In partial fulfillment of the requirements

For the degree of

Doctor of Philosophy

Graduate Program in Biomedical Engineering

Written under the direction of

François Berthiaume

And approved by

_____

_____

_____

_____

New Brunswick, New Jersey

May 2021

ABSTRACT OF THE DISSERTATION

Development of Elastin-like Polypeptide Fusion Protein Containing the Binding Domain of Receptors for Advanced Glycation End-products for Diabetic Chronic Skin Wounds

By HWAN JUNE KANG

Dissertation Director:

François Berthiaume

Chronic and non-healing skin wounds are some of the most significant complications in patients with advanced diabetes. A contributing mechanism to this pathology is the non-enzymatic glycation of proteins due to hyperglycemia, leading to the formation of advanced glycation end products (AGEs). AGEs bind to the receptor for AGEs (RAGE), which triggers pro-inflammatory signals that may inhibit the proliferative phase of wound healing. Soluble forms of RAGE (sRAGE) may be used as a competitive inhibitor of AGE-mediated signaling; however, sRAGE is short-lived in the highly proteolytic wound environment. Previous studies have also found detrimental effects of AGEs on growth factor activities that are critical to the normal wound healing process, including epidermal growth factor (EGF), keratinocyte growth factor (KGF), and stromal cell-derived factor-1 (SDF-1). The aim of this dissertation work was to develop a recombinant fusion protein containing the binding domain of RAGE (vRAGE) linked to elastin-like polypeptides (ELPs) that self-assembles into coacervates to shield from proteolysis and provide a drug depot. This protein could act as a competitive inhibitor of AGEs to restore the AGE-

mediated impaired biological mechanisms in the treatment of diabetic chronic wounds. This dissertation aimed to characterize the physical properties of vRAGE-ELP and investigate the biological activity in vitro and in vivo. Furthermore, a synergistic effect of vRAGE-ELP, when used in combination with another ELP fusion protein, SDF1-ELP that was previously found to accelerate wound healing and promote vascularization, was also investigated. We report that vRAGE-ELP self-assembles into coacervates around 30-31°C. The coacervate size was concentration and temperature-dependent, ranging between 500 and 1600 nm. vRAGE-ELP reversed several AGE-mediated changes in cultured human umbilical vein endothelial cells (HUVECs), including a decrease in viable cell number, an increase in levels of reactive oxygen species (ROS), and an increased expression of the pro-inflammatory marker, intercellular adhesion molecule-1 (ICAM-1). vRAGE-ELP was stable in elastases (common wound fluid proteases) in vitro for 7 days. When used in a single topical application on full-thickness excisional skin wounds in diabetic mice, wound closure was accelerated, with 90% and 100% wound closure on post-wounding days 28 and 35, respectively, compared to 62% and 85% on the same days in animals treated with vehicle control, consisting of ELP alone. Furthermore, the combination of vRAGE-ELP and SDF1-ELP increased viable cell numbers in AGE-stimulated HUVECs, promoted tube formation, and accelerated scratch wound assay in vitro. When used in full-thickness excisional skin wounds of diabetic mice, wound closure in the combination groups reached almost 100% on post-wounding day 35, compared to 62% and 85% on the same days in animals treated with vehicle control, consisting of ELP alone. This coacervate system topically delivering a competitive inhibitor of AGEs has potential for the treatment of diabetic wounds.

ACKNOWLEDGEMENTS

Throughout this journey to my doctorate degree, there have always been people around me with their support and help in the right place at the right time. Without them, I would have not been writing this dissertation. Above all, I would like to first thank God for guiding me in the right direction, to the right place and to the right people.

I would like to thank my advisor, Dr. François Berthiaume for everything he has done for me. By everything, I mean everything. Not only has he supported me in every possible way for my dissertation work and for my personal concerns, but he has also shown me how to be a fine human being. I am truly grateful to have been his student and working under his supervision. Dr. Berthiaume, thank you for always saying "yes" and trusting me with my research plans. I have always told people that you are the best advisor, and you truly are. It has been such an honor to work with you, and more importantly, to know you. I also would like to express my gratitude to Dr. Martin Yarmush. I still vividly remember our conversation when I met him first time in his office and when he suggested me to work with Dr. Berthiaume. Dr. Yarmush, thank you for giving me the opportunity to work in our "big" group. Your passion, dedication to science and mentorship have inspired me to keep moving forward and working hard. I also want to thank my other committee members, Dr. Vikas Nanda and Dr. Henry Hsia. Dr. Nanda, thank you for agreeing to be my committee and always being available whenever I needed your help and advice. With your help and support, my journey has been so much smoother but richer, and I really appreciate it. Dr. Hsia, thank you for being my committee and providing your expertise in clinical aspects.

It has been my pleasure to collaborate with your group and submit several manuscripts on our collaborative work.

There are many other people who I would like to thank. Dr. Rene Schloss has been a leader, a mentor and a supporter, not only to me, but also to everyone in our labs. Dr. Schloss, thank you for your support and dedication to the lab. I cannot imagine our lab without you and my work being done without you. I am very grateful to have worked with you. I also would like to thank Dr. Suneel Kumar whom I have been working with very closely in several projects. Thank you, Suneel, for your help, especially in the animal studies. I would like to thank Dr. Biraja Dash from Yale University for his collaborative work and contribution to our publications. Dr. Rick Cohen from Rutgers BME department has also been an excellent collaborator. Thank you, Dr. Cohen, for sharing your expertise in molecular biology. My special thanks go to Arielle D'Elia, who was an undergraduate researcher in our lab. Arielle, thank you for always trying to help with my experiments, troubleshooting and data analysis. I am grateful that you joined our lab and contributed to my work. I would like to thank Yixin Meng, who was a master's student, for helping me with some of my experiments. Thank you Yixin for your kindness and assistance. I also can't thank enough to the department of Biomedical Engineering for giving me this opportunity to grow as a scientist. Especially, I would like to thank our graduate program administrator, Larry Stromberg, for his support and guidance throughout my study.

I also would like to express my sincere gratitude to Dr. Samuel Sia and Dr. Brian Gillette at Columbia University who opened my eyes to research. Thank you, Sam, for giving me the great opportunity to work in your lab and your advice when I decided to

come to Rutgers. Thank you, Brian, for teaching me priceless research techniques that I could use for my thesis work as well.

All my friends, lab mates and colleagues that I have known are a part of my dissertation work. Their smile and support have made me stronger and my work more enjoyable. A big thanks to Paulina Krzyszczyk and Ileana Marrero-Berrios for welcoming me when I joined the lab and always trying to help me when I had questions. I miss our coffee break with you guys! Thank you, Misaal Patel, for your generous support, advice, suggestion all the time. I always miss our small talk about anything! Thank you, Mollie Davis, for always giving me a big smile. I am so glad that we have made this journey together around the same time. I also want to thank my dear friend, Xiomara Isabel Perez, for making me laugh all the time in the lab. And my lab mate, friend, and research colleague, Nuozhou Chen - thank you, Noah, for always lending me your hands whenever I need some help. I got lucky to have you as a lab mate and a friend. Also, thank you for all the gifts from your trips.

Finally, I would have not made it without my family. Aeree, I can't thank you enough for your sacrifice to come to the U.S. with me and your patience throughout this journey. Thank you so much for trusting me and giving me your endless support and love. My parents and my little brother - without your support, I would not have come to the U.S., the opposite side of the globe from where you are. Thank you for always supporting me and praying for me – I'm very blessed to have your continuous support.

TABLE OF CONTENTS

LIST OF ILLUSTRATIONS

CHAPTER 1: INTRODUCTION

Note: This chapter is reproduced from the following publication written by **Hwan June Kang**:

Hwan June Kang, Nuozhou Chen, Biraja Dash, Henry Hsia, Francois Berthiaume, Self-assembled Nanomaterials for Chronic Skin Wound Healing, *Advances in Wound Care* (Published online ahead of print, June 2020).

1.1 Scope and significance

Chronic wounds often fail to progress through the normal wound healing process and thus do not heal in a timely and orderly manner for more than a month [1]. Some of the underlying molecular and cellular pathophysiological mechanisms include poor vascularization, excessive ECM degradation by proteases, decreased growth factor activity and bacterial infection. Several types of wound dressings and drug delivery systems have been developed to address these problems and have been discussed in other review articles [1-3]. Emerging technologies based on self-assembled nanomaterials, which will be discussed here, provide new opportunities for chronic wound healing applications, owing to their great biocompatibility, ECM-mimicking properties, drug delivery capabilities and easily tunable mechanics.

1.2 Translational relevance

Novel biomaterials are continuously being developed to enhance chronic wound healing; however, some limitations exist, such as their cost and complexity of manufacture. self-assembled nanomaterials may overcome some of these limitations, as they are cost-effective to produce, and can create complex and multifunctional structures via self-assembly [4]. Furthermore, the multi-functional aspects of self-assembled nanomaterials make them amenable to targeting multiple pathways in chronic wounds. Self-assembled nanomaterials may also be incorporated into existing wound dressings or used in combination with other technologies used for treating chronic wounds.

1.3 Clinical relevance

Chronic wounds severely burden the U.S. healthcare system, costing $31.7 billion/year and affecting an estimated 2.4-4.5 million people [5, 6]. Open wounds are prone to infection, which can lead to life-threatening sepsis or amputation of the affected limb [7]. Advanced methods to help wound healing, such as bioengineered skin substitutes, negative pressure therapy and hyperbaric oxygen therapy, often fail to achieve complete healing since wound size and location vary significantly among individuals, and these approaches only partially address the relevant biological mechanisms [5, 7]. Self-assembled nanomaterials may address a critical need to develop better treatments targeting multiple mechanisms in chronic wounds.

1.4 Overview

1.4.1 Wound Healing Targets for Self-Assembled Nanomaterials

Skin wound healing is an orderly multi-phase process consisting of four overlapping phases: hemostasis, inflammation, proliferation and remodeling [5]. However, chronic wounds are often stalled at the inflammatory phase [5, 7]. In chronic wounds, macrophages fail to switch from a pro-inflammatory M1 phenotype secreting high levels of inflammatory mediators to an anti-inflammatory or pro-resolution M2 phenotype [7]. The excessive inflammatory cytokine signaling increases the influx of neutrophils, which in turn release metalloproteinases and elastases. These abnormal conditions can impair wound healing through the following mechanisms, which can be potentially addressed by self-assembled nanomaterials (Figure 1.1): (1) loss of endogenous ECM, (2) impaired growth factor activity, and (3) bacterial infection.

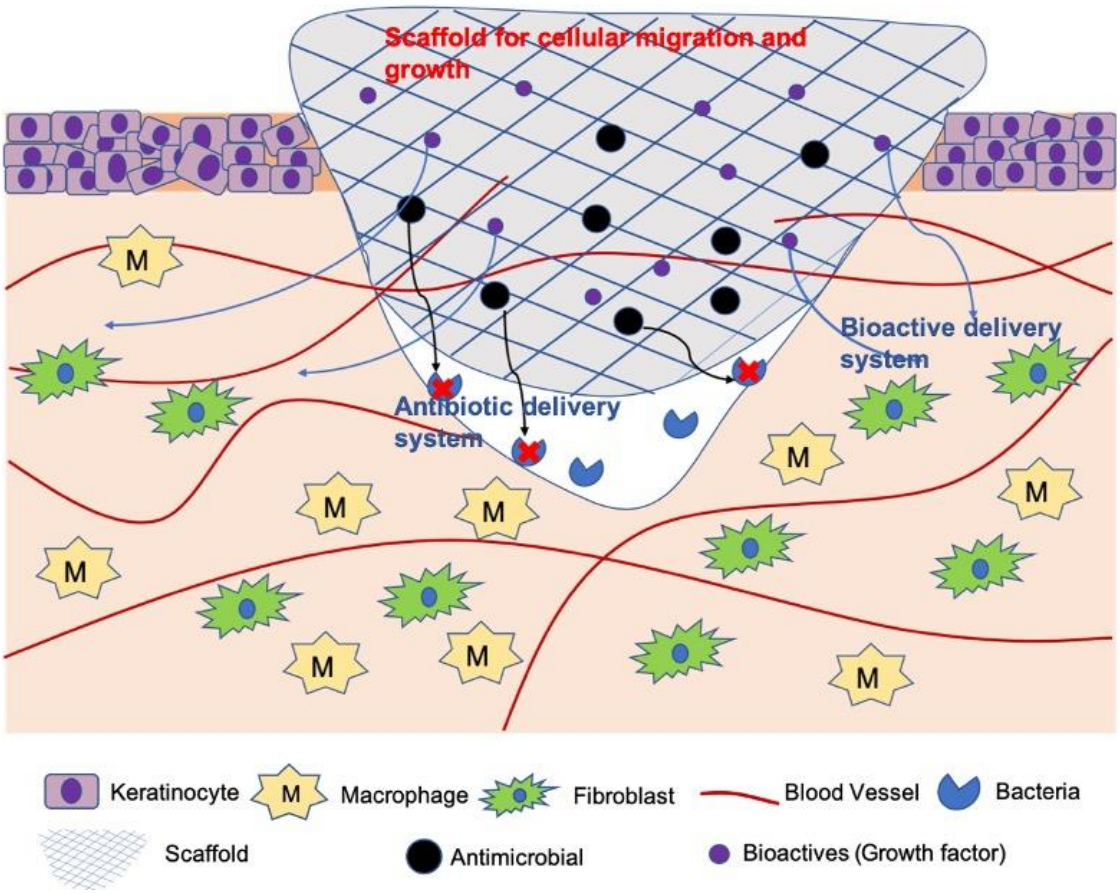

Figure 1.1 Schematic of self-assembled nanomaterials on skin wounds. Self-assembled nanomaterials can serve as (1) 3D scaffolds where cells can migrate and proliferate; (2) a delivery system where bioactive compounds such as growth factors can be encapsulated; (3) and an antibiotic delivery system to prevent bacterial colonization and infection. Self-assembled nanomaterials can be designed or combined to include multiple properties at the same time. 3D, three dimensional.

In the normal wound healing process, the temporary ECM constituted of fibrin of the granulation tissue is progressively invaded by endothelial cells and fibroblasts as it is being replaced by collagen to reconstitute damaged or lost tissue. However, elevated metalloproteinases and elastases in chronic wounds result in the continuous degradation of the ECM scaffold thus preventing cellular migration. Since many self-assembled nanomaterials are made of the same building blocks as natural peptides and mimic ECM

by incorporating specific amino acid sequences [4], they can provide a matrix that substitutes for the damaged or lost tissue in wounds.

Metalloproteinases also degrade endogenous growth factors and bioactive peptides, thus further impeding cellular proliferation, differentiation, and migration, responses that are associated with wound healing [5]. The activity of growth factors and cytokines may also be impaired due to the unusually high level of reactive oxygen species[8]. Exogenous topical growth factors are also susceptible to the same proteolytic processes, which may explain their limited success as therapeutics, with the exception of platelet-derived growth factor (PDGF; becaplermin) [9]. As will be discussed further below, self-assembled nanomaterials have been used as drug delivery vehicles that can shelter the bioactive compounds from degradation [10].

Chronic wounds are at high risk of bacterial infection and colonization, an increasing problem due to the emergence of antibiotic-resistant pathogens. Although systemic antibiotics are often used in cases of large wounds such as burns, topical application of antimicrobials has fewer systemic side effects and lower occurrence of antimicrobial resistance [11]. Self-assembled nanomaterial-based nanoparticles allow sustained and controlled release of antibiotics, thus minimizing the peak and trough variation in antibiotic levels that decreases effectiveness and increases the chance of antibiotic resistance.

1.4.2 Types of Self-assembled Materials

Self-assembled nanomaterials, especially synthetic self-assembled nanomaterials, are designed “from scratch” and thus are extremely versatile [12, 13]. Figure 1.2

summarizes the main types of synthetic self-assembling structures, which generally consist of peptides, polymers and metal-based structures.

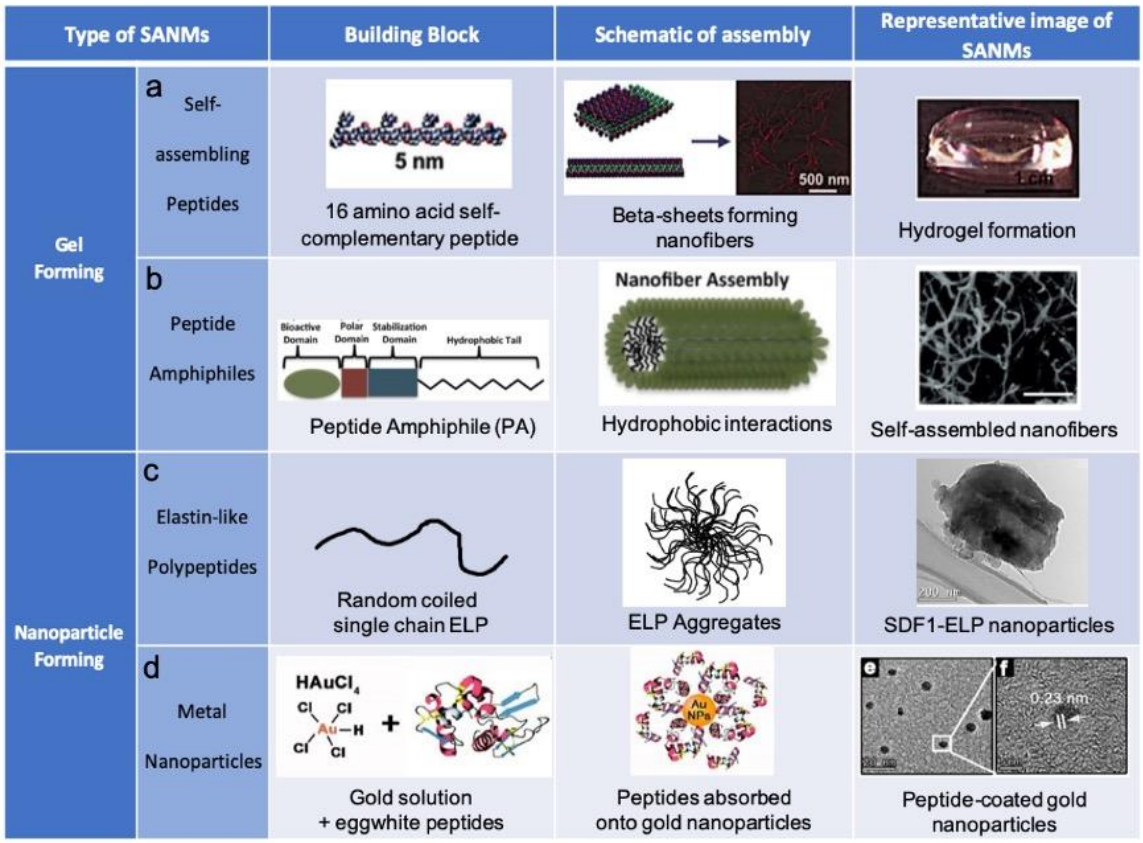

Figure 1.2 Major types of self-assembled nanomaterials used in wound healing studies. (a) The ionic self-complementary peptides form stable β-strand and β-sheet structures, which undergo self-assembly to form nanofibers. These nanofibers form interwoven matrices that further form a scaffold hydrogel with very high water content. Adapted from Ref. 13. (b) Peptide-amphiphiles contain four distinct engineered regions. Hydrophobic tails help cylindrical micelle assembly. The stabilization domain is often a β-sheet forming sequence of amino acids. The polar domain aids in solubility. A bioactive domain can be included to aid in cell adhesion, degradation, or growth factor presentation. Adapted from Ref. 12. (c) ELP exists as monomers below a transition temperature and undergoes nanoparticle formation above the transition temperature. Reprinted from Ref.41 with permission from Elsevier. (d) CEW was used to prepare the gold nanoparticles as a reducing and stabilizing agent. The MMT self-assemble on the surface of nanoparticles resulting in Au@CEW/MMT as an effective antibacterial agent. Adapted from Ref. 43 CEW, chicken egg white; ELP, elastin-like polypeptide; MMT, 2-mercapto-methylimidazole.

Self-assembling peptides

Self-assembling peptides (SAPs) consist of short amino acid chains that form nanofibrous hydrogels, nanoparticles and nanotubes [14]. Similar to the process of natural ECM formation, synthetic short peptide chains self-assemble via non-covalent interactions, such as hydrogen bonding, van der Waals forces, hydrophobic interactions and π-π stacking [12]. The fibrils can be further stabilized via cross-linking using physical or chemical methods [15]. The amino acid sequence governs the secondary structure of the peptide, usually an α-helix or a β-sheet. The β-sheet motif consists of alternating hydrophobic and hydrophilic amino acids, which stabilize into a β-sheet via hydrophobic interactions between the intermolecular hydrophobic interfaces and ionic interactions between hydrophilic interfaces. It is the most common mechanism of nanofiber assembly that results in peptide-based hydrogels. These hydrogels exhibit good injectability and tunable mechanical properties [15].

One of the simplest SAPs is diphenylalanine (FF), which self-assembles into hydrogels. Changing FF concentration can readily tune the hydrogel mechanics [15]. Another example of SAPs is EAK16-II (AEAEAKAKAEAEAKAK), which self-assembles to form hydrogen-bonded β-sheet nanofiber hydrogels [16]. Some of the most widely explored SAPs are RADA16-I (Ac-RADARADARADARADA-NH_2) and RADA16-II (Ac-RARADADARARADADA-NH_2) [17], which also form β-sheet structures in aqueous solutions. Recently, other types of SAPs, including crosslinked ultrashort peptides (LIVAGKC) [18], multidomain peptides consisting of 16-amino acids of $K_2(SL)_6K_2$ [19], and N-fluorenylmethyloxycarbonyl SAPs (Fmoc-SAPs) [20] have been used for wound healing.

Peptide Amphiphiles

Peptide amphiphiles contain four distinct domains: (1) a bioactive domain that binds specific receptors, thus promoting cell adhesion or other cellular responses, (2) a polar domain that confers solubility in aqueous environments, (3) a stabilization domain that is often a β-sheet forming sequence, and (4) a hydrophobic tail that enables micelle assembly [12]. Peptide amphiphiles self-assemble into nanofibers with a cylindrical geometry via intermolecular hydrogen bonding, which then forms a nanofibrous hydrogel that exhibits viscoelastic properties, topography and bioactive signaling reminiscent of native ECM [21]. The resulting 3D structure is easily tunable by changing the amino acid sequence.

Elastin-like Polypeptides

Another class of SAPs is elastin-like polypeptides (ELPs), which are derivatives of tropoelastin with pentapeptide repeats of Valine-Proline-Glycine-X-Glycine, where X can be any amino acid except proline [9, 22]. ELPs undergo a reversible thermal transition above a certain temperature, which is usually designed to be between 20°C and 70°C by adjusting the number of pentapeptide repeats, pH, ionic strength and the chosen X amino acid [23]. Above the transition temperature, ELPs fold into a β-spiral conformation and self-assemble via intrachain and interchain hydrophobic interactions. ELPs can also be engineered into fusion proteins incorporating bioactive peptides. The reversible self-assembly feature makes it possible to perform a relatively simple purification procedure, and also protects the bioactive molecule from proteolytic degradation when the fusion protein is in its nanoparticle form at physiological temperature.

1.4.3 Mechanisms of Nanomaterial Self-assembly

There are various mechanisms by which self-assembly can be achieved. Most widely used self-assembled nanomaterials that form peptide-based hydrogels self-assemble spontaneously in physiological conditions [12]. On the other hand, enzymes can also be used to aid the self-assembling process [15]. When stronger mechanical properties are required, physical or chemical crosslinking can be used [15]. In this section, we briefly overview some of the mechanisms that govern self-assembly (Figure 1.3).

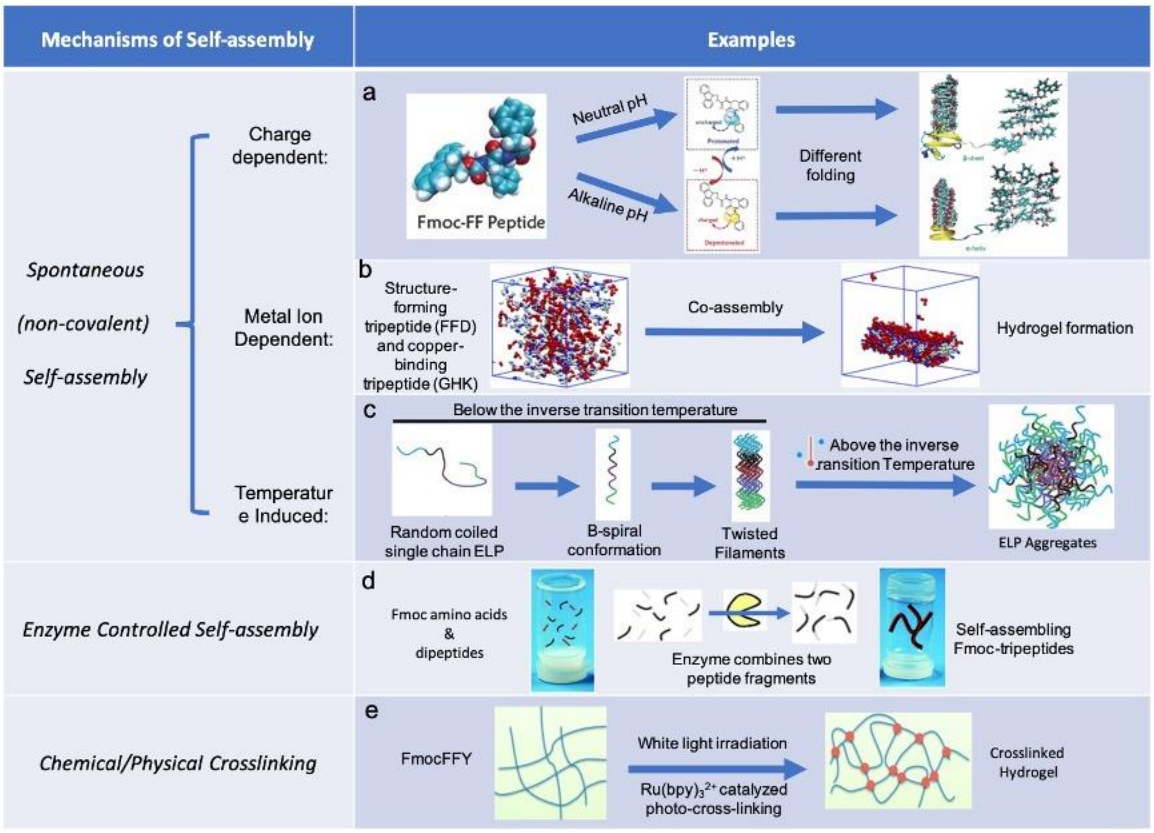

Figure 1.3 Representative mechanisms of self-assembly. (a) The Fmoc-FF monomers containing charged carboxyl groups can serve as a pH trigger for secondary structure transformation. The neutral Fmoc-FF dipeptide can form fibrous hydrogels, which consist of β-sheet structures. Adapted from Ref. 24. (b) Computational time course for the self-assembly of coassembled nanostructures. When introducing GHK into an FFD system, a coassembly is observed where GHK peptides are organized on the surface of the FFD structure. Adapted from Ref. 25. (c) Random coiled single ELP chains turn to a β-spiral

conformation, which stack up against each other to form ‘‘twisted filaments’’ as they reach their transition temperature. Above the transition temperature, the twisted filaments associate with each other to form insoluble aggregates. Adapted from Ref. 10. (d) Fmoc amino acids are enzymatically coupled to dipeptides to form Fmoc-tripeptides that self-assemble to higher order aggregates. Reprinted with permission from Ref. 26. Copyright (2006) American Chemical Society. (e) Hydrogelation and $Ru(bpy)_3^{2+}$ -mediated photocrosslinking enhance the mechanical stability of the FmocFFGGGY hydrogel. Reprinted with permission from Ref.29. Copyright (2013) American Chemical Society. FF, diphenylalanine; FFD, diphenylalanine-aspartic acid; GHK, glycine-histidine-lysine.

Spontaneous Self-assembly

Most self-assembled materials spontaneously form structures due to non-covalent interactions upon changing environmental conditions, including pH, metal ion concentration, salt concentration and temperature [12]. For example, adding Fmoc at the N-terminus of FF molecules, which themselves self-assemble into hydrogels, confers an additional level of control on the self-assembly process. The secondary structure formed from the modified peptides (Fmoc-FF) is dependent upon the charge on the molecules. By using a different pH at time of self-assembly, one can alter the protonation state of the carboxyl group at the C-terminus [24]. In acidic to neutral pH, Fmoc-FF molecules self-assemble into a nanofibrous β-sheet structure via amide-amide hydrogen bonding, which further forms a hydrogel via hydrogen bonding and π-π stacking. In contrast, when the carboxyl group is deprotonated at pH 8.5, the secondary structure of self-assembled Fmoc-FF is α-helical due to electrostatic repulsion between Fmoc-FF molecules, which yields a viscous solution and not a gel.

Metal ions can also be used to trigger self-assembly. Abul-Haija et al. used two different tripeptides, GHK, which itself is not a gelator but a copper-binding peptide, and FFD, which is a “structure-forming” peptide [25]. Although FFD peptides form hydrogels

at pH 5, FFD and GHK do not self-assemble at neutral pH; however, when copper ions were added to the mixture, GHK and FFD spontaneously formed hydrogels at neutral pH.

Temperature can also affect self-assembly of self-assembled nanomaterials. The best example of temperature sensitive materials are ELPs, which undergo spontaneous self-assembly above a certain "transition" temperature. Below that temperature, the ELPs exist largely as monomers, but when the temperature is increased above the transition temperature, ELPs fold into a β-spiral conformation and self-assemble via intrachain and interchain hydrophobic interactions to form nanoparticles [23].

Enzyme Catalyzed Self-assembly

Enzymes are biocompatible and offer mild reaction conditions (aqueous, pH 5-8, 37°C) to promote specific chemical reactions that can aid self-assembly, such as by reverse hydrolysis dephosphorylation [15, 26-28]. Toledano et al. used the protease thermolysin, which links nongelling Fmoc amino acids to dipeptides via reverse-hydrolysis to form amphiphilic Fmoc-tripeptides, which then self-assemble to form a hydrogel [26]. More recently, the same group developed Fmoc-protected dipeptide amphiphiles that self-assemble to form hydrogels. The self-assembly is triggered by adding alkaline phosphatase to dephosphorylate peptide precursors, which then form hydrogels, which also exhibit antimicrobial properties [27]. Another group, Gao et al., proposed the use of the oxidative enzyme tyrosinase to trigger the gel-solution phase transition of a small molecular hydrogel of Ac-YYYY-OMe via dephosphorylation of Ac-YYYpY-OMe [28].

Chemical/Physical Crosslinked Self-Assembly

Not all of SAPs have sufficient mechanical stability for in vivo use. Consequently, chemical and physical methods to promote intermolecular and/or intramolecular crosslinking have been investigated to enhance the mechanical strength of the resulting self-assembled structures. Ding et al. investigated a photo-cross-linking approach using $Ru(bpy)_3Cl_2$ to link two nearby tyrosine residues resulting in dityrosine adducts and showed 10^4-fold enhanced stiffness compared to non-crosslinked hydrogels [29]. In another study, the Chronopoulou group showed that genipin can crosslink the Fmoc-tripeptide, which itself self-assembles into a hydrogel, to enhance mechanical stiffness in a dose-dependent manner [30].

1.5 Discussion

Self-assembled nanomaterials have been widely used in tissue engineering and regenerative medicine applications. Below we discuss a few representative examples of the use of self-assembled nanomaterials for skin wound healing. We also address several important aspects that need to be considered in developing and designing self-assembled nanomaterials.

1.5.1 Self-assembled Nanomaterials as Wound Dressings and Scaffolds

Typical wound dressings are designed to physically protect wounds, maintain a moist environment, remove exudate and allow gas exchange with ambient air [2]. Skin scaffolds, on the other hand, provide a platform where cells migrate and proliferate to reconstitute the damaged or lost tissue. Several different types of injectable hydrogels using self-assembled nanomaterials have been developed as wound dressings and scaffolds as

the hydrogels exhibit high water content and allow cell proliferation in the 3D structure [31].

Seow and colleagues developed self-assembled hydrogel dressings using crosslinked ultrashort peptides (LIVAGKC) [18]. These peptides contain a hydrophobic tail with a string of amino acids that provide a gradient of hydrophobicity. The hydrophobic tail is followed by a hydrophilic headgroup to which cysteine is capped to allow disulfide crosslinking upon H_2O_2-mediated oxidation. The peptides self-assemble spontaneously in water to form hydrogels. Due to the disulfide-crosslinks, the resulting hydrogels were significantly stiffer than non-crosslinked gels. The hydrogels also improved re-epithelialization in a full-thickness injury mouse model with no obvious sign of allergenic effects [19]. Carrejo et al. developed another type of hydrogel from a different type of SAP. This group used "multidomain peptides" consisting of the 16-amino acid sequence $K_2(SL)_6K_2$, which self-assemble into a nanofibrous hydrogel. The hydrogels are syringe-deliverable and have predictable degradation at the wound sites. The multidomain peptide hydrogels facilitated 3D cell culture of fibroblasts when the cells were encapsulated. Fibroblasts grew in the 3D hydrogel and created extensive networks via cell-to-cell junctions. Additionally, when applied to diabetic mice with full-thickness wounds, granulation tissue and re-epithelialization formation, and wound closure were faster than groups treated with buffer only, or IntraSite, a commercially available hydrogel (Figure 1.4).

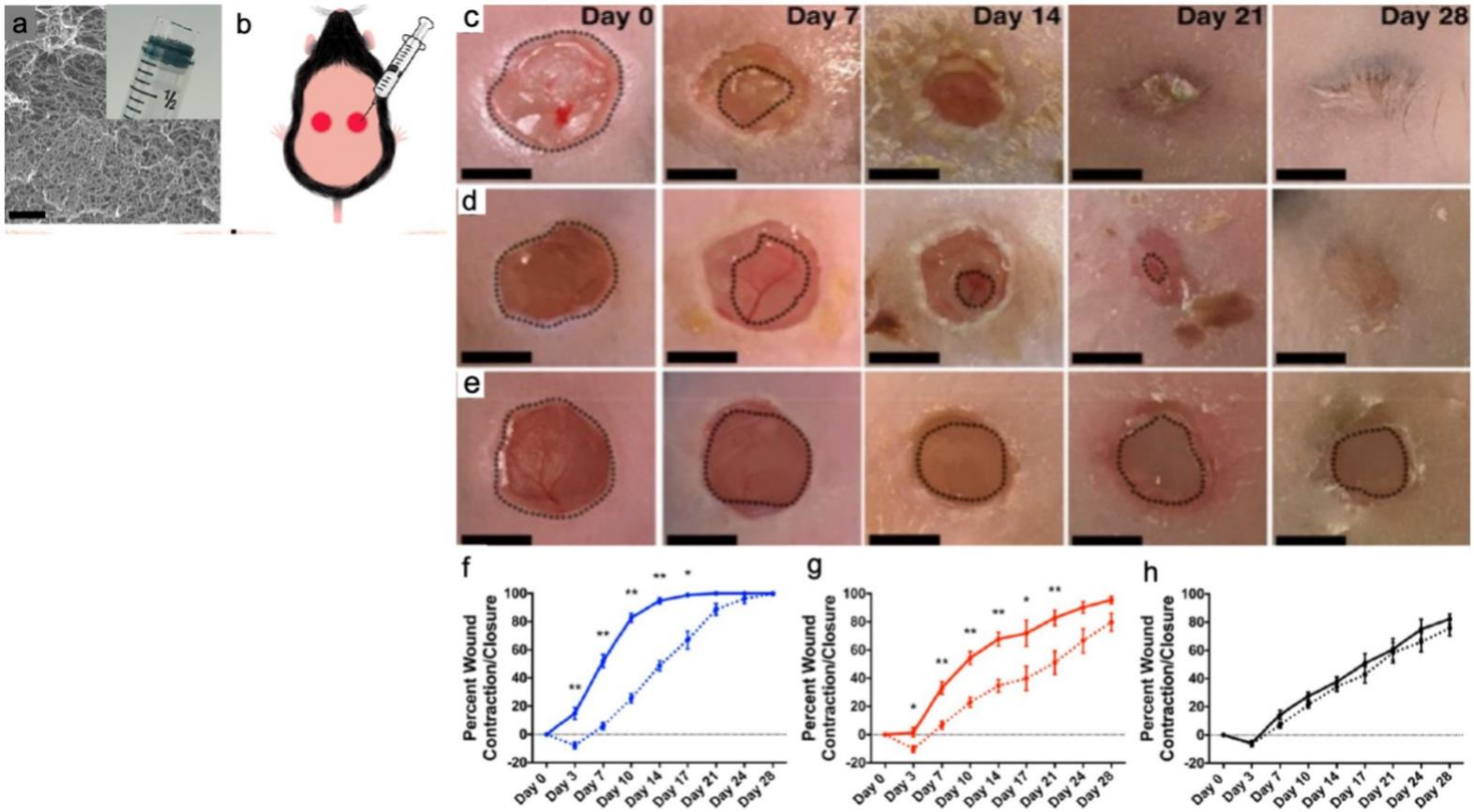

Figure 1.4 Effects of self-assembled multidomain peptides on full-thickness wounds in diabetic mice. (a) Nanofibers entangle and crosslink after the addition of multivalent salts, eventually forming a hydrogel (inset). Scale bar = 500 nm. (b) Because the hydrogel is syringe deliverable, it can be easily applied to wounds and conforms to their shape. (c) Multidomain peptide hydrogel, (d) IntraSite, and (e) buffer vehicle. Scale bars = 5 mm. Percent wound contraction (dashed lines) and percent wound closure (solid lines) for (f) multidomain peptide hydrogel, (g) IntraSite, and (h) buffer by normalizing to the wound area on day 0. Reprinted with permission from Ref.19. Copyright (2016) American Chemical Society.

Peptide amphiphiles have also been used to serve as wound dressings and scaffolds in combination with other molecules. One example is a heparin mimetic peptide nanofiber gel [32]. Yergoz et al. developed nanofiber networks formed by oppositely-charged peptide amphiphiles, heparin-mimetic peptide (HM-PA, lauryl-VVAGEGD(K-psb)S-Am) and K-PA (lauryl-VVAGK-Am) in 1:2 M ratio. The mixed peptide molecules self-assembled into fibrous networks that resemble ECM [32]. These hydrogels promoted faster wound closure of full-thickness burns in mice compared to wounds covered only by commercial Tegaderm™, and control nanofibers without the heparin-mimetic motifs. In another study, also in an acute wound model, HM-PA also showed increased re-epithelialization and granulation tissue formation in a full-thickness excisional wounds in rats [33]. Zhou et al. also used peptide amphiphile gels for burn wound healing[34]. The authors made several different types of peptide amphiphiles with a slight modification to include bioactive epitopes that mimic ECM. A cell proliferation assay was performed in thermally damaged fibroblasts and HUVECs and showed a higher level of proliferation in peptide amphiphile gel treated groups. Also, burn wounds in rats healed faster in the HM-PA treated group where the hydrogels were modified to contain Arg-Gly-Asp-Ser (RGDS) epitope, a well-known cell surface integrin-binding sequence.

Another interesting class of SAPs used as wound scaffolds is silk-elastin hydrogels. Silk-elastin contains repeats of silk fibroin (GAGAGS) and elastin-like (GVGVP) sequences that are recombinantly expressed [35, 36]. Kawabata et al. proposed silk-elastin hydrogels that absorb wound exudate at physiological temperature [35]. The authors reported larger areas of granulation in wounds covered by the silk-elastin hydrogels compared to the control polyurethane film.

1.5.2 Self-assembled Nanomaterials for Growth Factor Delivery

SAPs form stable hydrogels and are considered good candidates to serve as depots for delivery of bioactives to the wound. Several types of synthetic peptides have been developed and investigated to deliver growth factors and other bioactive molecules [10, 22, 37-40].

One of the most widely explored SAPs is self-complementary peptides with 16 amino acids, such as RAD16-I (RADARADARADARADA), RAD16-II (RARADADARARADADA) and their derivatives with a slight modification, which self-assemble into hydrogels. Several groups have reported slow and controlled release of molecules, growth factors, and cytokines from RADA-I nanofiber scaffolds [34, 37]. For example, Gelain et al. reported that designer SAP scaffolds made of RADA16-I and its derivatives (RADA16-DGE and RADA16-PFS) showed slow and sustained release of several cytokines [38]. In a study where the effects of the SAP hydrogels were investigated, Schneider et al. proposed to use SAP nanofibers containing EGF to accelerate wound healing [40]. They reported that EGF was preferentially released from the SAP hydrogels due to protease-mediated activity from cells in a wound created in a human skin equivalent in vitro. Wound closure was 3.5 fold faster and wound re-epithelialization was accelerated when treated with EGF-containing SAPs, compared to SAPs alone.

Another example is peptide amphiphiles that contain four distinct domains: (1) a bioactive molecule, (2) a polar domain that confers solubility, (3) a stabilization domain that is often a β-sheet forming sequence, and (4) a hydrophobic tail that enables cylindrical micelle self-assembly [12, 39]. Hosseinkhani and colleagues developed injectable 3D peptide amphiphile scaffolds with encapsulated bFGF for tissue regeneration [39]. Peptide

amphiphile aqueous solution was mixed with bFGF suspensions to produce injectable hydrogel scaffolds. When the bFGF and peptide amphiphile mixture was subcutaneously injected into the back of mice, a 3D hydrogel was formed in situ, and a significant angiogenic response was observed.

Koria et al. developed self-assembling peptides containing ELPs and KGF for chronic wound healing [9]. KGF was fused with 50 repeats of ELPs and the fusion proteins (KGF-ELP) were expressed in E. coli. KGF-ELP formed nanoparticles above the transition temperature. The authors confirmed the bioactivity of KGF in the nanoparticles in an in vitro proliferation assay using keratinocytes. Furthermore, when KGF-ELP nanoparticles were applied to full thickness wounds in diabetic mice, enhanced re-epithelialization and granulation were observed. More recently, Yeboah et al. developed another type of ELP fusion peptides containing stromal cell derived factor-1 (SDF-1) for chronic wound healing [22, 41]. The fusion protein, SDF1-ELP, self-assembled into nanoparticles at physiological temperature. When tested in vitro, SDF1-ELP promoted migration and vascularization of endothelial cells. Furthermore, SDF1-ELP remained intact after incubation in elastase for 12 days while free SDF1 was not detectable after incubation in the same condition (Figure 1.5 A-C). When SDF1-ELP in fibrin gel was applied onto in vivo diabetic wounds in mice, a higher number of vascular endothelial cells (CD31+ cells), faster wound closure, and much thicker epidermis and dermis were observed compared to free SDF1 and other control groups including empty ELP nanoparticles, and fibrin gel vehicle (Figure 1.5 D, E).

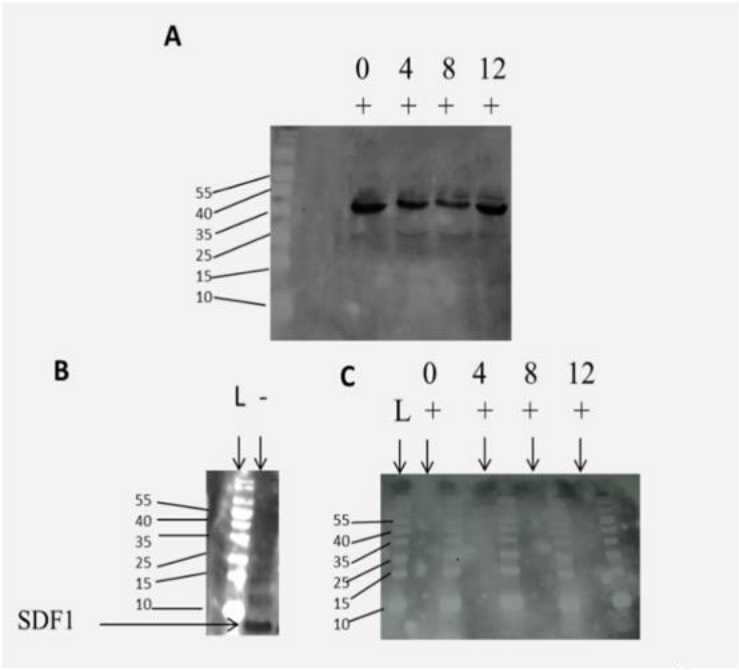
A
0 4 8 12
+ + + +
55
40
35
25
15
10
B
L -
55
40
35
25
15
10
SDF1
C
0 4 8 12
L + + + +
55
40
35
25
15
10

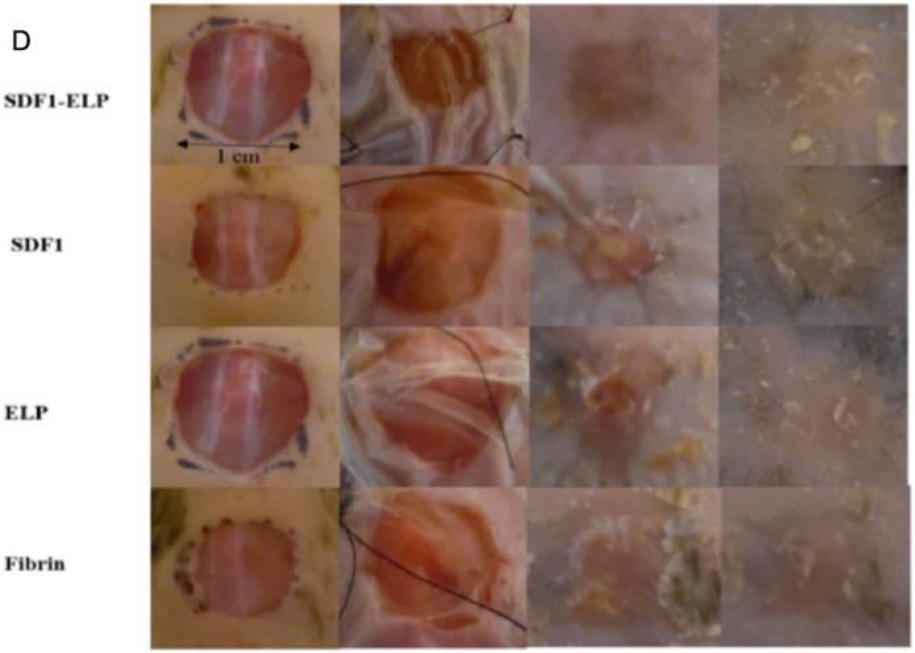
D
SDF1-ELP
1 cm
SDF1
ELP
Fibrin

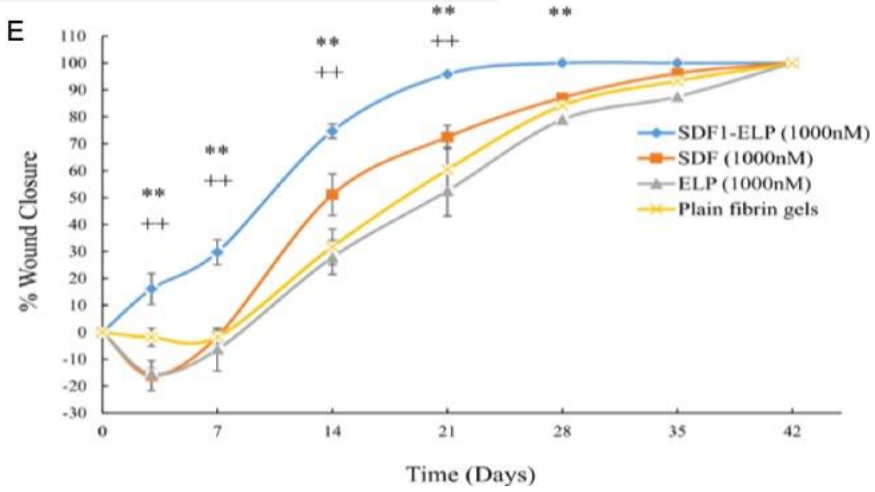
E
% Wound Closure
Time (Days)
SDF1-ELP (1000nM)
SDF (1000nM)
ELP (1000nM)
Plain fibrin gels
**
++

Figure 1.5 Stability of SDF1-ELP in elastase and effect of SDF1-ELP on wound healing in diabetic mice. Left: Degradation of SDF1-ELP or free SDF-1 by elastase. SDF1-ELP and SDF-1 were incubated in elastase over a 12-day period. Samples were pulled at 4-day intervals and subjected to Western blot analysis. (A) Representative blot of SDF1-ELP samples after incubation in elastase. (B) Lane 1, labeled L is the molecular weight ladder. Lane 2, labeled (-) is SDF-1 with no elastase. (C) Representative blot of SDF-1 samples in elastase. No SDF-positive bands are seen in any of the lanes. Right: Effect of SDF1-ELP on skin wound closure in diabetic mice. Full-thickness excisional wounds were treated with fibrin gel with SDF1-ELP particles, fibrin gel 75 containing free SDF-1, fibrin gel containing ELP particles, or plain fibrin gel (vehicle control). (D) Representative images of the wounds on different days. On postwounding day 28, the wound treated with SDF1-ELP was fully closed, while in the other groups it was still open, only fully closing by day 42. (E) Quantified wound closure as a function of time. n = 5 (**, ++: $p < 0.01$, one-way ANOVA, Fisher's LSD post-test; ++: SDF1-ELP compared with SDF1, **: SDF1-ELP compared with ELP or plain fibrin). Adapted from Ref. 41. SDF-1, stromal cell-derived factor-1.

1.5.3 Self-assembled Nanomaterials as Antimicrobials

A common complication that may make chronic wounds even more difficult to heal is bacterial infection [1]. Although conventional antimicrobial materials, such as silver, zinc oxide and copper oxide, have proven their potential, toxicity towards human cells limits dosage and duration of application [42]. Recently, researchers have explored and developed self-assembled nanomaterials as antimicrobial agents that may prevent wounds from developing biofilms.

Chen et al. developed antimicrobial peptides self-assembled on gold nanodots [42]. Gold nanomaterials in general have good stability and biocompatibility but by themselves have low antimicrobial activity. By co-immobilizing surfactin (SFT) and 1-dodecanethiol (DT), which self-assembled onto the gold nanoparticles, the group developed SFT-/DT-Au nanodots and demonstrated antimicrobial effectiveness towards a wide range of bacterial strains including multidrug-resistant bacteria. In another study, Lu and colleagues used gold nanoparticles coated with chicken egg white (CEW), onto which 2-mercapto-

methylimidazole (MMT) molecules were self-assembled [43]. The AU@CE/MMT nanoparticles showed antibacterial effects in vitro and accelerated healing of full-thickness skin wounds inoculated with Staphylococcus aureus in an in vivo rabbit model (Figure 1.6). In the course of these studies, they also established a maximum $HAuCl_4$:MMT ratio of 1:50 that exhibited no cytotoxicity towards skin fibroblasts.

Reithofer et al. used hydrogels made of self-assembled ultrashort peptides, Ac-LIVAGK-NH_2 (Ac-LK_6-NH_2), to serve as a matrix for in situ silver nanoparticle synthesis [44]. The resulting Ag-Ac-LK_6-NH_2 hydrogels showed sustained release of Ag nanoparticles for up to 14 days and inhibited gram-negative and gram-positive bacteria with no significant toxicity towards human dermal fibroblasts.

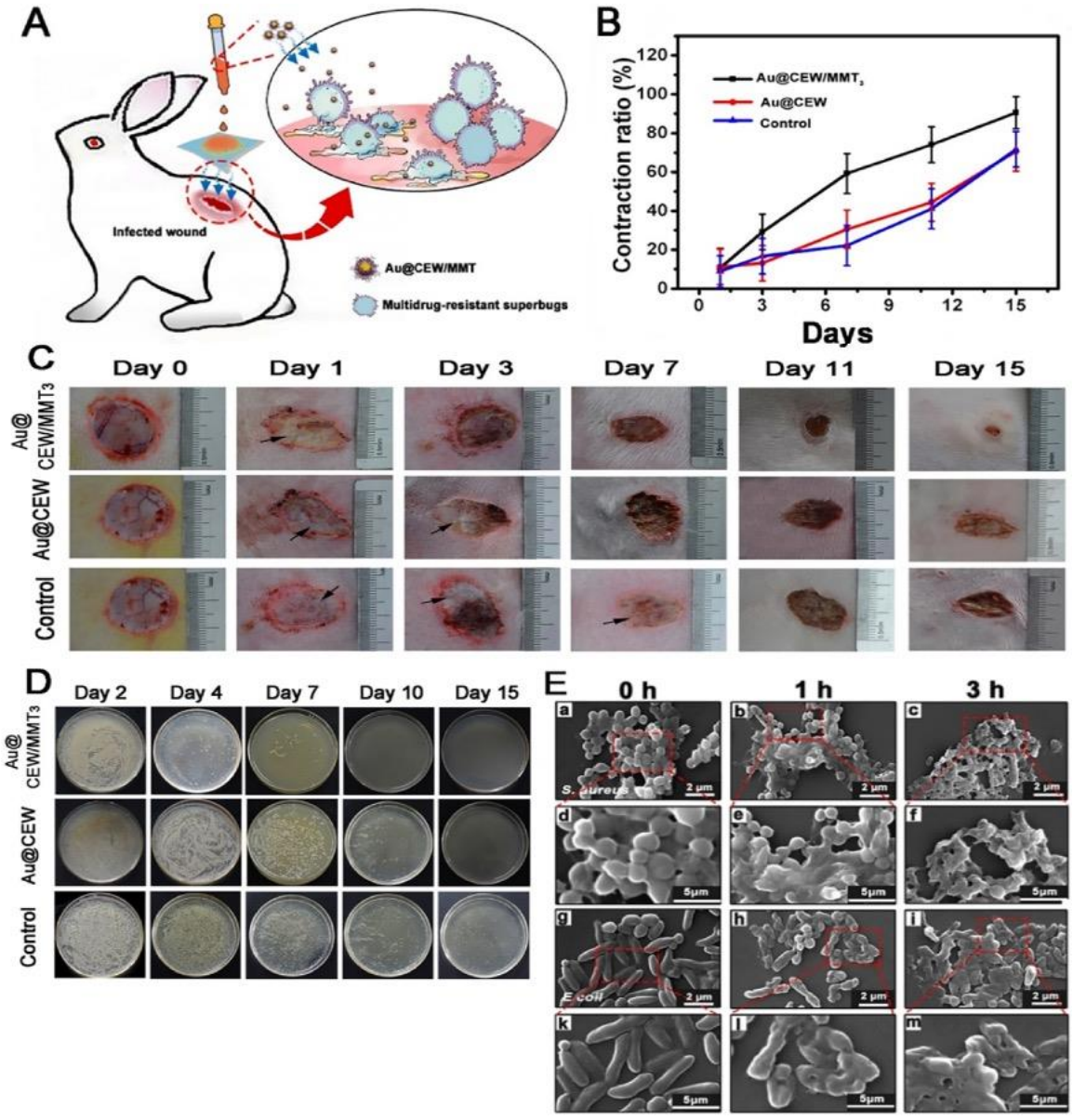

Figure 1.6 Antibacterial effects of Au@CEW/MMT on the healing of full-thickness wounds exposed to multidrug-resistant bacteria. (A) Schematics of experiments. (B) Wound contraction ratio versus time. Error bars denote the standard error of the mean (n = 3). (C) Photographs of MRSA-infected wounds, either untreated or treated with Au@CEW or Au@CEW/MMT3, taken on days 0, 1, 3, 7, 11, and 15. (D) Photographs of bacterial incubations from wounds that were untreated or treated with Au@CEW/MMT3 or Au@CEW/MMT4. (E) SEM images of (a–f) Staphylococcus aureus and (g–l) Escherichia coli after treatment for 0, 1, and 3 h. Cells at 0 h displayed the typical spherical shape with a smooth and intact membrane. After 1 h of treatment, most bacteria show a blurry membrane boundary and collapsed morphology. After 3 h, the bacterial structure was thoroughly destroyed and only their debris could be observed. Adapted from Ref. 43. SEM, scanning electron microscope.

Another interesting class of self-assembled nanomaterials is metallo-nucleoside hydrogels that can be self-assembled by mixing cytidine (C) with 0.5 equivalents each of $B(OH)_3$ and $AgNO_3$ (C-B-C•Ag^+) [31]. The C-B-C•Ag^+ hydrogels significantly inhibited gram-negative and gram-positive bacteria in vitro and promoted faster wound closure of mouse burn wounds (71.15% closure compared to 33.69% in non-treated group after 7 days of treatment).

Although not tested in vivo, Paladini et al. proposed silver-doped self-assembling di-phenylalanine hydrogels with high water content [45]. The group incorporated antimicrobial silver nanoparticles in di-phenylalanine (F_2)-9-fluorenylmethoxycarbonyl (Fmoc) peptides, which readily self-assemble to form hydrogels. They investigated the anti-bacterial effects of the hydrogels containing silver against Staphylococcus aureus and found good antibacterial capability with 0.1 wt% of silver.

1.6 Current Challenges and Future Directions

Self-assembled nanomaterials offer several advantages, including precise selectivity and multifunctionality that can address specific challenges and limitations in clinic. However, long-term stability of self-assembled nanomaterials, especially peptide-based nanomaterials, is critical to the success of wound healing therapies [46]. Proteases, such as metalloproteinases and elastase, whose levels are elevated in chronic wounds, may negatively impact on the stability of peptide-based self-assembled nanomaterials [5, 7]. Further efforts should be made to design protease-resistant self-assembled nanomaterials.

An alternative is to design self-assembled nanomaterials that can sequester these host proteases within the wound microenvironment during the remodeling phase.

The pH of the wound microenvironment should also be considered while designing self-assembled nanomaterials for chronic wounds. While the pH in acute wounds is slightly acidic (pH4.0 - pH6.3), the pH in chronic wounds is rather alkaline (pH7.15 - pH10.0) [47]. Therefore, development of self-assembled nanomaterials that maintain their structure even at these higher pH values is required for the treatment of chronic wounds. Understanding the impact of such environmental parameters on the ability of self-assembled nanomaterials to deliver bioactive molecules in a controlled and sustained manner, when such property is desired, is also critical.

Immunogenicity and toxicity are other major hurdles for the clinical translation of any nanomaterial. Although many of these therapies are to be used topically, the slow dynamics of chronic wound healing will likely require slow degradation and/or multiple applications thus causing prolonged exposure of the wound bed to the materials, and also the potential for significant systemic absorption. The field has progressed towards developing novel self-assembled nanomaterials with low acute toxicity; however, future studies should investigate the physicochemical properties of self-assembled nanomaterials that mitigate longer term cytotoxicity and immunoreactivity, especially in the context of skin, which is thought to be a highly immunogenic organ [48]. There is already a vast literature covering the impact of self-assembled material design on immunoreactivity, and there is considerable evidence suggesting a direct relationship between the physicochemical properties of nanomaterials and their negative effects on the immune system [49, 50]. Furthermore, in order to proceed to clinical trials in human subjects, more

relevant in vivo chronic wound models may be required. Currently, most in vivo studies rely on diabetic rodent models that exhibit delayed wound healing. Such models cannot address, in particular, the heterogeneity in human immune responses. Better animal models, perhaps such as humanized mice, may be used in the future to more thoroughly examine potential immune reactions to self-assembled nanomaterials.

Finally, self-assembled nanomaterials could help direct the remodeling phase to promote less scarring and more regenerative healing. For clinical use in humans, ideally these should eventually degrade, but the time scale of degradation should extend over several months to significantly impact remodeling. Future studies need to investigate the long-term impact of self-assembled nanomaterials on healing and scarring.

1.7 Summary

The pathophysiological mechanisms of chronic wounds are complex; therefore, multipronged approaches that address several different biological mechanisms are desirable. Self-assembled nanomaterials serve as physical scaffolds to support cell growth and migration, as well as growth factor and antimicrobial delivery systems. These nanomaterials are also relatively easy and inexpensive to manufacture and can be combined to target various aspects of the wound healing process. They can also be incorporated into existing wound dressings and combined with other treatment modalities. It should also be noted that some of the approaches reviewed in this article were so far investigated only in vitro, in which case future studies will need to establish their effectiveness in vivo, and that none so far have been investigated in human wounds, to the best of our knowledge.

1.8 References

1. Sen CK. Human Wounds and Its Burden: An Updated Compendium of Estimates. Adv Wound Care (New Rochelle). 2019;8(2):39-48.
2. Alberti T, Coelho DS, Voytena A, Pitz H, de Pra M, Mazzarino L, et al. Nanotechnology: A Promising Tool Towards Wound Healing. Curr Pharm Des. 2017;23(24):3515-28.
3. Rajendran NK, Kumar SSD, Houreld NN, Abrahamse H. A review on nanoparticle based treatment for wound healing. Journal of Drug Delivery Science and Technology. 2018;44:421-30.
4. Cui H, Webber MJ, Stupp SI. Self-Assembly of Peptide Amphiphiles: From Molecules to Nanostructures to Biomaterials. Biopolymers (Peptide Science). 2009;94(1):1-18.
5. Frykberg RG, Banks J. Challenges in the Treatment of Chronic Wounds. Adv Wound Care (New Rochelle). 2015;4(9):560-82.
6. Nussbaum SR, Carter MJ, Fife CE, DaVanzo J, Haught R, Nusgart M, et al. An Economic Evaluation of the Impact, Cost, and Medicare Policy Implications of Chronic Nonhealing Wounds. Value in Health. 2018;21(1):27-32.
7. Krzyszczyk P, Schloss R, Palmer A, Berthiaume F. The Role of Macrophages in Acute and Chronic Wound Healing and Interventions to Promote Pro-wound Healing Phenotypes. Front Physiol. 2018;9:419.
8. Garcia-Orue I, Pedraz JL, Hernandez RM, Igartua M. Nanotechnology-based delivery systems to release growth factors and other endogenous molecules for chronic wound healing. Journal of Drug Delivery Science and Technology. 2017;42:2-17.
9. Koria P, Yagi H, Kitagawa Y, Megeed Z, Nahmias Y, Sheridan R, et al. Self-assembling elastin-like peptides growth factor chimeric nanoparticles for the treatment of chronic wounds. Proc Natl Acad Sci U S A. 2011;108(3):1034-9.
10. Yeboah A, Cohen RI, Rabolli C, Yarmush ML, Berthiaume F. Elastin-like polypeptides: A strategic fusion partner for biologics. Biotechnol Bioeng. 2016;113(8):1617-27.
11. Dhivya S, Padma VV, Santhini E. Wound dressings - a review. Biomedicine (Taipei). 2015;5(4):22.
12. Wade RJ, Burdick JA. Advances in nanofibrous scaffolds for biomedical applications: From electrospinning to self-assembly. Nano Today. 2014;9(6):722-42.
13. Zhang S. Fabrication of novel biomaterials through molecular self-assembly. Nat Biotechnol. 2003;21(10):1171-8.
14. Hosseinkhani H, Hong PD, Yu DS. Self-assembled proteins and peptides for regenerative medicine. Chem Rev. 2013;113(7):4837-61.
15. Li J, Xing R, Bai S, Yan X. Recent advances of self-assembling peptide-based hydrogels for biomedical applications. Soft Matter. 2019;15(8):1704-15.
16. Luo Z, Zhao X, Zhang S. Self-organization of a chiral D-EAK16 designer peptide into a 3D nanofiber scaffold. Macromol Biosci. 2008;8(8):785-91.
17. Nune M, Kumaraswamy P, Krishnan UM, Sethuraman S. Self-Assembling Peptide Nanofibrous Scaffolds for Tissue Engineering: Novel Approaches and Strategies for Effective Functional Regeneration. Current Protein and Peptide Science. 2013;14(1):70-84.

18. Seow WY, Salgado G, Lane EB, Hauser CA. Transparent crosslinked ultrashort peptide hydrogel dressing with high shape-fidelity accelerates healing of full-thickness excision wounds. Sci Rep. 2016;6:32670.
19. Carrejo NC, Moore AN, Lopez Silva TL, Leach DG, Li IC, Walker DR, et al. Multidomain Peptide Hydrogel Accelerates Healing of Full-Thickness Wounds in Diabetic Mice. ACS Biomater Sci Eng. 2018;4(4):1386-96.
20. Rodriguez AL, Wang TY, Bruggeman KF, Horgan CC, Li R, Williams RJ, et al. In vivo assessment of grafted cortical neural progenitor cells and host response to functionalized self-assembling peptide hydrogels and the implications for tissue repair. J Mater Chem B. 2014;2(44):7771-8.
21. Loo Y, Goktas M, Tekinay AB, Guler MO, Hauser CA, Mitraki A. Self-Assembled Proteins and Peptides as Scaffolds for Tissue Regeneration. Adv Healthc Mater. 2015;4(16):2557-86.
22. Yeboah A, Maguire T, Schloss R, Berthiaume F, Yarmush ML. Stromal Cell-Derived Growth Factor-1 Alpha-Elastin Like Peptide Fusion Protein Promotes Cell Migration and Revascularization of Experimental Wounds in Diabetic Mice. Adv Wound Care (New Rochelle). 2017;6(1):10-22.
23. Christensen T, Hassouneh W, Trabbic-Carlson K, Chilkoti A. Predicting transition temperatures of elastin-like polypeptide fusion proteins. Biomacromolecules. 2013;14(5):1514-9.
24. Xing R, Yuan C, Li S, Song J, Li J, Yan X. Charge-Induced Secondary Structure Transformation of Amyloid-Derived Dipeptide Assemblies from beta-Sheet to alpha-Helix. Angew Chem Int Ed Engl. 2018;57(6):1537-42.
25. Abul-Haija YM, Scott GG, Sahoo JK, Tuttle T, Ulijn RV. Cooperative, ion-sensitive co-assembly of tripeptide hydrogels. Chem Commun (Camb). 2017;53(69):9562-5.
26. Toledano S, Williams RJ, Jayawarna V, Ulijn RV. Enzyme-Triggered Self-Assembly of Peptide Hydrogels via Reversed Hydrolysis. J AM CHEM SOC. 2006;128(4):1070-1.
27. Hughes M, Debnath S, Knapp CW, Ulijn RV. Antimicrobial properties of enzymatically triggered self-assembling aromatic peptide amphiphiles. Biomaterials Science. 2013;1(11).
28. Gao J, Zheng W, Kong D, Yang Z. Dual enzymes regulate the molecular self-assembly of tetra-peptide derivatives. Soft Matter. 2011;7(21).
29. Ding Y, Li Y, Qin M, Cao Y, Wang W. Photo-cross-linking approach to engineering small tyrosine-containing peptide hydrogels with enhanced mechanical stability. Langmuir. 2013;29(43):13299-306.
30. Chronopoulou L, Toumia Y, Cerroni B, Pandolfi D, Paradossi G, Palocci C. Biofabrication of genipin-crosslinked peptide hydrogels and their use in the controlled delivery of naproxen. N Biotechnol. 2017;37(Pt A):138-43.
31. Tang Q, Plank TN, Zhu T, Yu H, Ge Z, Li Q, et al. Self-Assembly of Metallo-Nucleoside Hydrogels for Injectable Materials That Promote Wound Closure. ACS Appl Mater Interfaces. 2019;11(22):19743-50.
32. Yergoz F, Hastar N, Cimenci CE, Ozkan AD, Tekinay T, Guler MO, et al. Heparin mimetic peptide nanofiber gel promotes regeneration of full thickness burn injury. Biomaterials. 2017;134:117-27.

33. Uzunalli G, Mammadov R, Yesildal F, Alhan D, Ozturk S, Ozgurtas T, et al. Angiogenic Heparin-Mimetic Peptide Nanofiber Gel Improves Regenerative Healing of Acute Wounds. ACS Biomaterials Science & Engineering. 2016;3(7):1296-303.
34. Zhou A, Chen S, He B, Zhao W, Chen X, Jiang D. Controlled release of TGF-beta 1 from RADA self-assembling peptide hydrogel scaffolds. Drug Des Devel Ther. 2016;10:3043-51.
35. Kawabata S, Kanda N, Hirasawa Y, Noda K, Matsuura Y, Suzuki S, et al. The Utility of Silk-elastin Hydrogel as a New Material for Wound Healing. Plast Reconstr Surg Glob Open. 2018;6(5):e1778.
36. Kawabata S, Kawai K, Somamoto S, Noda K, Matsuura Y, Nakamura Y, et al. The development of a novel wound healing material, silk-elastin sponge. J Biomater Sci Polym Ed. 2017;28(18):2143-53.
37. Davis ME, Motion JP, Narmoneva DA, Takahashi T, Hakuno D, Kamm RD, et al. Injectable self-assembling peptide nanofibers create intramyocardial microenvironments for endothelial cells. Circulation. 2005;111(4):442-50.
38. Gelain F, Unsworth LD, Zhang S. Slow and sustained release of active cytokines from self-assembling peptide scaffolds. J Control Release. 2010;145(3):231-9.
39. Hosseinkhani H, Hosseinkhani M, Khademhosseini A, Kobayashi H, Tabata Y. Enhanced angiogenesis through controlled release of basic fibroblast growth factor from peptide amphiphile for tissue regeneration. Biomaterials. 2006;27(34):5836-44.
40. Schneider A, Garlick JA, Egles C. Self-assembling peptide nanofiber scaffolds accelerate wound healing. PLoS One. 2008;3(1):e1410.
41. Yeboah A, Cohen RI, Faulknor R, Schloss R, Yarmush ML, Berthiaume F. The development and characterization of SDF1α-elastin-like-peptide nanoparticles for wound healing. Journal of Controlled Release. 2016;232:238-47.
42. Chen W-Y, Chang H-Y, Lu J-K, Huang Y-C, Harroun SG, Tseng Y-T, et al. Self-Assembly of Antimicrobial Peptides on Gold Nanodots: Against Multidrug-Resistant Bacteria and Wound-Healing Application. Advanced Functional Materials. 2015;25(46):7189-99.
43. Lu B, Lu F, Ran L, Yu K, Xiao Y, Li Z, et al. Self-assembly of natural protein and imidazole molecules on gold nanoparticles: Applications in wound healing against multi-drug resistant bacteria. Int J Biol Macromol. 2018;119:505-16.
44. Reithofer MR, Lakshmanan A, Ping AT, Chin JM, Hauser CA. In situ synthesis of size-controlled, stable silver nanoparticles within ultrashort peptide hydrogels and their anti-bacterial properties. Biomaterials. 2014;35(26):7535-42.
45. Paladini F, Meikle ST, Cooper IR, Lacey J, Perugini V, Santin M. Silver-doped self-assembling di-phenylalanine hydrogels as wound dressing biomaterials. J Mater Sci Mater Med. 2013;24(10):2461-72.
46. Acar H, Srivastava S, Chung EJ, Schnorenberg MR, Barrett JC, LaBelle JL, et al. Self-assembling peptide-based building blocks in medical applications. Adv Drug Deliv Rev. 2017;110-111:65-79.
47. Ono S, Imai R, Ida Y, Shibata D, Komiya T, Matsumura H. Increased wound pH as an indicator of local wound infection in second degree burns. Burns. 2015;41(4):820-4.

48. Hamuro L, Kijanka G, Kinderman F, Kropshofer H, Bu DX, Zepeda M, et al. Perspectives on Subcutaneous Route of Administration as an Immunogenicity Risk Factor for Therapeutic Proteins. J Pharm Sci. 2017;106(10):2946-54.
49. Engin AB, Hayes AW. The impact of immunotoxicity in evaluation of the nanomaterials safety. Toxicology Research and Application. 2018;2.
50. Halamoda-Kenzaoui B, Bremer-Hoffmann S. Main trends of immune effects triggered by nanomedicines in preclinical studies. Int J Nanomedicine. 2018;13:5419-31.

CHAPTER 2: SELF-ASSEMBLED ELASTIN-LIKE POLYPEPTIDE FUSION PROTEIN COACERVATES AS COMPETITIVE INHIBITORS OF ADVANCED GLYCATION END-PRODUCTS ENHANCE DIABETIC WOUND HEALING

Note: This chapter is reproduced from the following publication written by **Hwan June Kang**:

Hwan June Kang, Suneel Kumar, Arielle D'Elia, Biraja Dash, Vikas Nanda, Henry C. Hsia, Martin L. Yarmush, François Berthiaume. "Self-assembled Elastin-like Polypeptide Fusion Protein Coacervates as Competitive Inhibitors of Advanced Glycation End-Products Enhance Diabetic Wound Healing". *Journal of Controlled Release* (Submitted, 2020).

2.1 Introduction

Four to ten percent of diabetic patients develop a diabetic foot ulcer (DFU) each year [1] and total Medicare spending estimates for DFUs range between $6.2 and $18.7 billion yearly in the U.S. [2]. DFUs are chronic wounds in which the normal wound healing process is impaired due to diabetes-related mechanisms [3]. Protein glycation due to the diabetic hyperglycemic environment is potentially a major factor underlying the pathology of slow healing of diabetic wounds [3]. Protein glycation occurs when free amino groups of proteins react with carbonyl groups on reactive sugars leading to the formation of advanced glycation end-products (AGEs), which triggers pro-inflammatory signals that may inhibit the proliferative phase of wound healing [4, 5].

AGEs bind their cognate receptors (RAGEs) found on endothelial cells, macrophages, as well as mesangial cells [6]. AGE-RAGE binding induces intracellular generation of reactive oxygen species (ROS), which in turn results in the activation of the nuclear transcription factor, NF-κB, an inducer of pro-inflammatory gene expression [7, 8]. Among those are vascular cell adhesion molecule 1 (VCAM-1), intercellular adhesion molecule 1 (ICAM-1), tumor necrosis factor alpha (TNF-α) and metalloproteinases (MMPs) [9-11]. Furthermore, AGE-RAGE binding upregulates the expression of RAGE itself which then contributes to prolonged inflammation [4].

Soluble RAGEs (sRAGE) lacking the transmembrane and cytoplasmic domains of RAGEs could act as a competitive inhibitor of AGEs. In prior studies, application of sRAGE reduced pro-inflammatory gene expression, enhanced wound healing in diabetic animal models, and recovered the bioactivity of stromal cell derived factor 1 (SDF-1), which supports re-epithelialization during wound healing, in in vitro diabetic environments [11-13]. Among the five domains of RAGEs (V, C1, C2, transmembrane and cytoplasmic domains), the extracellular V domain is the one that binds AGEs [14, 15]. Several studies have found that an application of recombinant V domain of RAGE (vRAGE) blocked AGE-RAGE binding in vitro [10, 16]. While sRAGE and vRAGE could be used as potential therapeutic peptides, they are subject to degradation in the presence of proteases. In fact, higher levels of MMPs have been reported in chronic wounds compared to acute wounds, and specifically in diabetic wounds, high levels of MMP-2 and MMP-9 have been found [17]. Topical application of growth factors is under consideration to compensate for decreased activities of growth factors in chronic wounds [18]. However, exogenous growth factors have not been very successful as therapeutic agents, presumably due to their rapid

degradation in the highly proteolytic chronic wound environment, which similarly affect other bioactive peptides [18].

Elastin-like polypeptides (ELPs) that can be expressed as a fusion protein with various bioactive peptides to create coacervates have been shown to serve as "shields" from exposure to the highly proteolytic environment [19-23]. ELPs are derivatives of tropoelastin consisting of pentapeptides repeats of Valine-Proline-Glycine-Xaa-Glycine, where Xaa can be any amino acids except Proline [24, 25]. ELPs are thermally responsive and reversibly self-assemble into coacervates above a transition temperature [26]. In the present study, we have developed a self-assembled coacervate system containing a fusion of vRAGE and ELPs (vRAGE-ELP) that effectively blocks AGE-RAGE-mediated signaling, thus improving diabetic wound healing.

2.2 Materials and Methods

2.2.1 Design and cloning of a vRAGE-ELP expression vector

DNA encoding the V domain (residues 23-123)[15] of RAGE that contains XbaI and NdeI restriction enzyme sites and a short linker sequence of three repeats of four glycines and one serine was synthesized and ordered from GenScript Biotech (Piscataway, NJ, USA). Previously, a pET25B+ plasmid encoding 50 pentapeptide repeats of ELP and a 6-histidine tag was used to develop a fusion protein containing SDF1 and ELP [23, 27]. The same pET25B+ plasmid with ELP repeats was used to subclone the V domain genes into the ELP expression vector using the two restriction enzyme sites, XbaI and NdeI. The subcloning of vRAGE-ELP expression vector and sequencing of the ligation areas were

performed by GenScript to ensure a successful cloning of the vRAGE-ELP expression vector.

2.2.2 Expression of vRAGE-ELP fusion protein and empty ELP protein

E. coli (One Shot™ BL21 Star™ (DE3) Chemically Competent, Invitrogen™) was purchased from Thermo Fisher Scientific (USA). The bacterial cells were transformed with the vRAGE-ELP expression vector by following the manufacturer's instructions. The transformation reaction was plated onto LB agar plate containing 100 μg/mL of carbenicillin and incubated overnight at 37°C. Next day, a single, isolated colony was picked. The colony was then inoculated in 25 mL of LB medium containing 100 μg/mL of carbenicillin by shaking overnight at 220 rpm at 37°C. The 25 mL overnight culture was then transferred to 1 L of TB medium containing 100 μg/mL of carbenicillin, and the culture was grown by shaking at 220 rpm at 37°C until the optical density (OD) reached 0.6-0.8. When the OD reached 0.6-0.8, 1 mM of isopropyl β-d-1-thiogalactopyranoside (IPTG, Gold Biotechnology, USA) was added to induce protein expression and the culture was left overnight at 37°C by shaking at 220 rpm. Next day, the overnight culture was collected in four 250 mL bottles and centrifuged at 3,000 g for 20 minutes at 4°C. The supernatant was discarded, and the bacterial pellets were stored at -80°C until ready for purification. Similarly, empty ELP proteins without the vRAGE insert were expressed to be used as a vehicle control.

2.2.3 Purification of vRAGE-ELP fusion protein and empty ELP protein

The thermally responsive property of ELP was used to purify the proteins as previously described [22, 23, 25]. Briefly, the bacterial pellets from the 1 L culture were resuspended in a total of 28 mL of cold phosphate buffered saline (PBS) and sonicated on ice for 3 minutes (5 seconds ON, 25 seconds OFF cycle) twice. Poly(ethyleneimine) (PEI) solution (MilliporeSigma, USA) at a final concentration of 0.5% w/v was added to the cell lysate to remove negatively charged residual DNA. The cell lysate was then centrifuged at 18,000 g for 15 minutes at 4°C and the supernatant containing the fusion proteins was collected in a new 50 mL conical tube. 0.3 M of sodium citrate (MilliporeSigma, USA) was added to the protein solution to induce coacervate formation followed by incubating in a 35°C water bath for 10 minutes. The protein sample was centrifuged at 16,000 g for 10 minutes at 35°C (1st "hot spin"). 20 μL of supernatant containing soluble contaminants were collected for SDS-PAGE analysis, and the protein pellet containing the vRAGE-ELP fusion protein was resuspended in ~5 mL of icy cold PBS to resolubilize the fusion protein. The tube was placed on ice and occasionally vortexed until the pellet was completely dissolved. The tube was then centrifuged at 16,000 g for 10 minutes at 4°C (1st "cold spin"). 20 μL of the supernatant containing soluble vRAGE-ELP fusion proteins were saved for SDS-PAGE analysis and a pellet containing insoluble contaminants was discarded. The procedures of "hot spin" and "cold spin" were repeated three times to obtain pure vRAGE-ELP fusion proteins at the end of process. Empty ELP proteins were purified using similar methods.

2.2.4 Physical characterization

2.2.4.1 SDS-PAGE and Western Blot

The samples collected after each hot and cold spin during the purification process were run on SDS-PAGE using 4-20% precast gel and Tris/Glycine/SDS buffer (Bio-Rad Laboratories, USA) to separate proteins by size. The gel was stained with SimplyBlue™ SafeStain solution (Thermo Fisher Scientific) for 1 hour to visualize protein bands followed by washing in distilled water for 1 hour. In a separate experiment, an SDS-PAGE gel was transferred onto a nitrocellulose membrane (0.2 μm pore size, Bio-Rad Laboratories) for Western blotting. The membrane was then blocked with 1X TBS 1X casein blocker (Bio-Rad Laboratories) for one hour. After the blocking step, the membrane was incubated with anti-RAGE antibody (ab37647, Abcam, USA) overnight at 4°C. Next day, the membrane was washed three times with PBS containing 0.05% Tween 20 (PBST) for 5 minutes each. The membrane was then incubated with HRP conjugated secondary antibody (Goat Anti-Rabbit IgG, (H+L), HRP conjugated, Thermo Fisher Scientific) for 1 hour at room temperature. The membrane was washed with PBST three times and exposed to TMB substrate solution (1-Step™ Ultra TMB-Blotting Solution, Thermo Fisher Scientific).

2.2.4.2 Quantification of bacterial endotoxin level

To quantify bacterial endotoxin levels in the purified fusion protein, a chromogenic limulus amebocyte lysate (LAL) assay (ToxinSensor™ Chromogenic LAL Endotoxin Assay Kit, GenScript) was used according to the manufacturer's protocol.

2.2.4.3 Measurement of Solution Turbidity

25 μM of purified vRAGE-ELP fusion proteins in PBS (100 μL total volume) were prepared in a 96-well plate. The plate was placed in a plate reader to measure the turbidity of the protein solution as the temperature of the instrument was increased from an initial temperature of 22°C to a final temperature of 40°C in 1°C increments. Solution turbidity, which indicates the formation of coacervates above the transition temperature, was determined by measuring the absorbance of the samples at 350 nm.

2.2.4.4 Size of coacervates

Three different concentrations of vRAGE-ELP fusion proteins (5 μM, 10 μM and 25 μM) in 25 μL of PBS were prepared to measure the sizes of coacervates. The size was measured at 4°C, 30°C, and 37°C by dynamic light scattering using a Zetasizer Nano S (Malvern Panalytical, USA). The size of coacervates over time was also monitored by incubating vRAGE-ELP at 5μM at 37°C and collecting samples at days 0, 1, 3, 5 and 7. The size of each sample was measured by dynamic light scattering.

2.2.4.5 Binding activity of vRAGE-ELP to AGE

A commercially available AGE-RAGE in vitro binding assay kit (CircuLex AGE-RAGE in vitro Binding Assay Kit, MBL International Corporation, USA) was used to investigate the binding ability of vRAGE-ELP to AGE according to the manufacturer's protocol with a slight modification. Briefly, vRAGE-ELP fusion proteins, recombinant sRAGE, and empty ELP, all of which contain a 6-histidine tag, were prepared in reaction buffer at various concentrations. vRAGE-ELP, sRAGE or ELP was then added to an AGE (glycated BSA)-coated well in a 96-well plate or a BSA-coated well in a 96-well plate as

a control. The plates were incubated for 60 minutes at room temperature after which the wells were washed with wash buffer four times. After washing, HRP conjugated anti-His-tag antibody was added and the plates were incubated for 60 minutes. The plates were then washed four times with wash buffer. Substrate reagent was then added to each well and the plates were incubated for 10 minutes after which stop solution was added. The absorbance was measured at 450 nm.

2.2.4.6 vRAGE-ELP monomer release from coacervates

25 μM of vRAGE-ELP fusion protein (500 μL total volume) were prepared in each of six centrifugal tubes with 10 nm pore membranes (Nanosep® with Omega^{TM} 100K, Pall Corporation, USA). The tubes were equilibrated at 37°C for 10 minutes to initiate coacervate formation. Subsequently, tubes were retrieved from incubation after 0, 1, 2, 4, 6 and 24 hours of further incubation and immediately centrifuged at 5,000 g for 5 minutes at 37°C to separate protein monomers in filtrate from coacervates remaining on the membrane. The filtrate was collected in a new tube and the proteins in filtrate was quantified using a bicinchoninic acid (BCA) assay (Thermo Fisher Scientific).

2.2.5 In vitro bioactivity

2.2.5.1 Cell culture

Primary human umbilical vein endothelial cells (HUVECs) were purchased from Thermo Fisher Scientific. Cells were maintained in M200 media supplemented with low serum growth supplement (LSGS) kit (Thermo Fisher Scientific).

2.2.5.2 HUVEC viable number assay

HUVECs were plated in a 96-well plate at a density of 2,000 cells/well. Cells were grown in M200 media supplemented with LSGS kit overnight to allow for cell attachment. Next day, one group of cells was exposed to 100 μg/mL of bovine serum albumin (BSA, MilliporeSigma) as a control. Another group was stimulated with 100 μg/mL of commercially available AGEs consisting of glycated BSA (Advanced Glycation End Product-BSA, MilliporeSigma) to mimic a diabetic condition [9]. As previously done in the literature [10, 28], for the treatment groups, 100 μg/mL of AGEs were pre-incubated with various concentrations of vRAGE-ELPs (300 μg/mL, 500 μg/mL or 1 mg/mL) or empty ELPs (300 μg/mL, 500 μg/mL or 1 mg/mL) for at least 30 minutes at 37°C to allow enough time for the vRAGE-ELP coacervates to react with AGEs. Each mixture of AGEs and vRAGE-ELP coacervates was then added to cells in growth media. In the other group, cells were stimulated with AGEs and co-treated with 30 mM of N-acetylcysteine (NAC) as a treatment control. All groups were incubated for 24 hours at 37°C. Viable cell number per well was measured using a 3-(4,5-dimethylthiazol-2-yl)-2,5-diphenyl-2H-tetrazolium bromide (MTT) assay (Vybrant MTT cell proliferation assay kit, Thermo Fisher Scientific).

2.2.5.3 ROS measurements

HUVECs were plated in a 96-well plate at a density of 5,000 cells/well in M200 media supplemented with LSGS kit and grown at 37°C for 24 hours. Cells were then treated with BSA (100 μg/mL), AGE (100 μg/mL) only, AGE (100 μg/mL) + vRAGE-ELP (1 mg/mL) (pre-incubated for 30 minutes), AGE (100 μg/mL) + ELP (1 mg/mL) (pre-

incubated for 30 minutes), or AGE (100 μg/mL) + NAC (30 mM) and incubated at 37°C for 24 hours. To visualize the generation of intracellular ROS, CellRox® Green Reagent (Thermo Fisher Scientific) was used. Briefly, after 24 hours of treatment, cells were washed with growth media twice to remove vRAGE-ELP coacervates from the well. CellRox® Green Reagent was then added to the cells in growth media at a final concentration of 5 μM and incubated at 37°C. After 30 minutes, cells were washed three times with PBS. The intracellular ROS was visualized under the fluorescent microscope (Olympus IX81) and the images were captured.

2.2.5.4 Measurements of ICAM-1 expression

Immunocytochemistry

8 mm cover glasses (Electron Microscopy Sciences, USA) were placed in a 48-well plate and coated with 0.1% gelatin in deionized water (MilliporeSigma) for 10 minutes at room temperature. The gelatin solution was removed, and the cover glasses were air-dried for 15 minutes before use. HUVECs were seeded onto cover glasses at a density of 5,000 cells/well and grown in growth media. When cells became confluent, cells were treated with BSA (100 μg/mL), AGE (100 μg/mL) only, AGE (100 μg/mL) + vRAGE-ELP (1 mg/mL) (pre-incubated for 30 minutes), AGE (100 μg/mL) + ELP (1 mg/mL) (pre-incubated for 30 minutes), or AGE (100 μg/mL) + NAC (30 mM) and incubated at 37°C for 6 hours. Cells were then washed with fresh media twice and fixed in 2% paraformaldehyde in PBS for 20 minutes at room temperature. Fixed cells were washed twice in wash buffer (0.1% BSA in PBS). Cells were then blocked with blocking buffer

(10% normal donkey serum, 0.3% Triton X-100, MilliporeSigma) for 45 minutes at room temperature. After blocking, cells were incubated with human ICAM-1/CD54 antibody (R&D Systems, Catalog #BBA3) at a final concentration of 25 μg/mL for 1 hour at room temperature. Cells were washed twice with wash buffer and incubated again with secondary antibody (Alexa Flour 647 donkey anti-mouse secondary antibody, Invitrogen # A-31571) for 1 hour at room temperature. Cells were washed twice with wash buffer and a drop of antifade mounting medium containing DAPI (ProLong Diamond Antifade Mountant with DAPI, Invitrogen™) was added to each cover glass. Cover glasses were taken out of the well plate carefully using a tweezer and placed on glass slides. The expression of ICAM-1 was visualized by fluorescence microscopy (Olympus IX81) and the images were captured.

Cell-based ELISA

HUVECs were plated in a 96-well plate at a density of 5,000 cells/well and grown in growth media for 48 hours or until confluence. When cells became confluent, cells were treated with BSA (100 μg/mL), AGE (100 μg/mL) only, AGE (100 μg/mL) + vRAGE-ELP (1 mg/mL) (pre-incubated for 30 minutes), AGE (100 μg/mL) + ELP (1 mg/mL) (pre-incubated for 30 minutes), AGE (100 μg/mL) + NAC (30 mM) or AGE (100 μg/mL) + Human RAGE antibody (10 μg/mL, R&D Systems, MAB11451) and incubated at 37°C for 6 hours. Cells were then washed with fresh media twice and fixed in 2% paraformaldehyde in PBS for 20 minutes at room temperature. Fixed cells were washed twice with PBS. Unspecific binding sites were blocked by incubating cells with blocking buffer containing 2% BSA and 4% non-fat dry milk for 30 min at room temperature. Cells

were then incubated with anti-ICAM1 monoclonal antibody (Thermo Fisher Scientific, #MEM-111) diluted in blocking buffer for 2 hours at 37°C and washed four times with PBS. Cells were incubated with rabbit anti-mouse IgG HRP (Abcam, #ab6728) for 1 hour at 37°C and washed 5 times with PBS. After washing, TMB substrate (1-Step™ Ultra TMB-ELISA Substrate Solution, Thermo Fisher Scientific) was added to each well and colors were developed for 10 minutes at room temperature after which stop solution (Thermo Fisher Scientific, #N600) was added. Absorbance at 450 nm was measured to quantify the expression of ICAM-1.

2.2.5.5 Stability test in the presence of elastase in vitro

To investigate whether vRAGE-ELP remains stable in the presence of elastase (MilliporeSigma), we incubated 5μM of vRAGE-ELP or free sRAGE in 1 μM of elastase or in PBS without elastase as a control at 37°C for 1, 3, 5, and 7 days. Samples collected at each time point were stored in -80°C until running on Western blot using the same method described above.

2.2.6 In vivo bioactivity: effects on wound healing in diabetic mice

2.2.6.1 Wound closure study

Animal studies were conducted in accordance with a protocol approved by the Institutional Animal Care and Use Committee (IACUC) at Rutgers University. Genetically modified diabetic mice (BKS. Cg-Dock7^{m}+/+ Lepr^{db}/J, 3 females, 5 males) were purchased from the Jackson Laboratory (Bar Harbor, ME, USA) and used at the age of 10 weeks. A

day before surgery, mice were anesthetized by isoflurane (Henry Schein, USA) inhalation. The dorsum was shaved using a clipper, and Nair™ cream was applied to remove residual hair. On the day of surgery, a 1 cm by 1 cm excisional skin wound was created on the back of mice. Briefly, the mice were anesthetized, and betadine scrub and 70% ethanol were applied alternatively on the back three times. Full thickness skin was then excised by using a 1 cm by 1 cm template and surgical scissors. In order to apply treatments (vehicle control, empty ELP, native sRAGE, and vRAGE-ELP), fibrin gels were prepared. Briefly, 5 μM of empty ELP, native sRAGE or vRAGE-ELP were mixed in 80 μL of fibrinogen solution, which was prepared by dissolving human fibrinogen (MilliporeSigma) in deionized water at a final concentration of 6.25 mg/mL. The empty ELP and vRAGE-ELP in fibrinogen were then placed in a 37ºC water bath to initiate coacervate formation. The coacervates in fibrinogen solution were then mixed with 20 μL of thrombin at 12.5 U/mL (MilliporeSigma). The mixture was immediately applied onto the wound by pipetting and allowed to rest for 2 minutes to form a gel. The wound area was then covered with Tegarderm™ (3M, USA) and photographed on days 1, 3, 7 and weekly thereafter over a period of 35 days. The percent wound closure at each time point compared to the initial wound area was analyzed using Image J software (NIH) and calculated as $\left(1 - \frac{\text{remaining wound area}}{\text{initial wound area}}\right) \times 100$.

2.2.6.2 Wound tissue histology and epidermal thickness

On post-wounding day 35, wounded skin samples were collected and fixed in 10% formalin for at least 24 hours before processing for histology at Rutgers Research Pathology Services. Tissue samples were paraffin-embedded and thin sections (5 μm) were

stained with hematoxylin and eosin (H&E) to visualize tissue morphology. Pictures of stained tissue samples on glass slides were taken using a light microscope and a microscope camera (Olympus CKX41 and Infinity 2, Lumenera). Epidermal thickness and dermal thickness were measured using ImageJ.

2.2.7 Statistical analysis

GraphPad Prism 8 software (GraphPad Software Inc., San Diego, CA, USA) was used for statistical analysis. The p value was calculated by using ANOVA followed by post-hoc analysis with Tukey's test to identify differences among groups at specific time points. A value of $p < 0.05$ was considered statistically significant. Results are expressed as mean ± SEM. Additionally, Kaplan Meier endpoint analysis was performed to compare the effects of empty ELP, free sRAGE and vRAGE-ELP on in vivo wound healing.

2.3 Results

2.3.1 vRAGE-ELP expression vector design

The design of vRAGE-ELP fusion protein is shown in Figure 2.1A. The linker consisting of three repeats of four glycines and one serine, $(GGGGS)_3$ was chosen as this specific type of linker provides flexibility while allowing for mobility of the bioactive domain [29]. Genes encoding the V domain of RAGE (residues 23-123) and the linker sequence were synthesized and subcloned into ELP plasmids containing 50 pentapeptide repeats (V40C2, where V = VPGVG and C = VPGVGVPGVGVPGCGVPGVGVPGVG) using two restriction enzyme sites, XbaI and NdeI (Figure 2.1B). The predicted molecular

weight of vRAGE-ELP fusion protein is 35.8 kD. The entire amino acids sequence of vRAGE-ELP fusion protein is as follows:

MAQNITARIGEPLVLKCKGAPKKPPQRLEWKLNTGRTEAWKVLSPQGGGPWDS
VARVLPNGSLFLPAVGIQDEGIFRCQAMNRNGKETKSNYRVRVYQIPGGGGSGG
GGSGGGGSHMGPGVGVPGVGVPGVGVPGVGVPGVGVPGVGVPGVGVPGVGVPGVGVP
GVGVPGVGVPGVGVPGVGVPGVGVPGVGVPGVGVPGVGVPGVGVPGVGVPGVGVPGV
GVPGVGVPGVGVPGVGVPGVGVPGVGVPGVGVPGVGVPGVGVPGVGVPGVGVPGVGV
PGVGVPGVGVPGVGVPGVGVPGVGVPGVGVPGVGVPGVGVPGVGVPGVGVPGVGVPG
VGVPGVGVPGVGVPGVGVPGCGVPGVGVPGVGVPGVGVPGVGVPGCGVPGVG
VPGWPTSQPELAPEDPEDVEHHHHHH

2.3.2 Physical Characteristics of vRAGE-ELP

2.3.2.1 Purification and identification of vRAGE-ELP fusion protein

Samples collected at the end of each purification step were run on SDS-PAGE to confirm the protein molecular weight in the final product. The gel stained with Coomassie G-250 shows a single band in the final product (Figure 2.1C, Lane 8), which closely aligned with the 37 kD band of the protein standard ladder, indicating the size of the purified protein was close to that predicted for vRAGE-ELP (35.8 kD). To further confirm that the purified protein was indeed vRAGE-ELP, we performed Western blotting using a polyclonal anti-RAGE antibody that binds an epitope in the V domain of RAGE. The results showed a single clear band in the final product confirming that the purified protein is vRAGE-ELP (Figure 2.1D). Furthermore, the LAL assay measured bacterial endotoxin

concentration at 0.0168 EU per 1 ug of vRAGE-ELP, which is significantly lower compared to those of commercially available recombinant proteins and acceptable levels of endotoxin in vaccine formulation during preclinic research [30, 31].

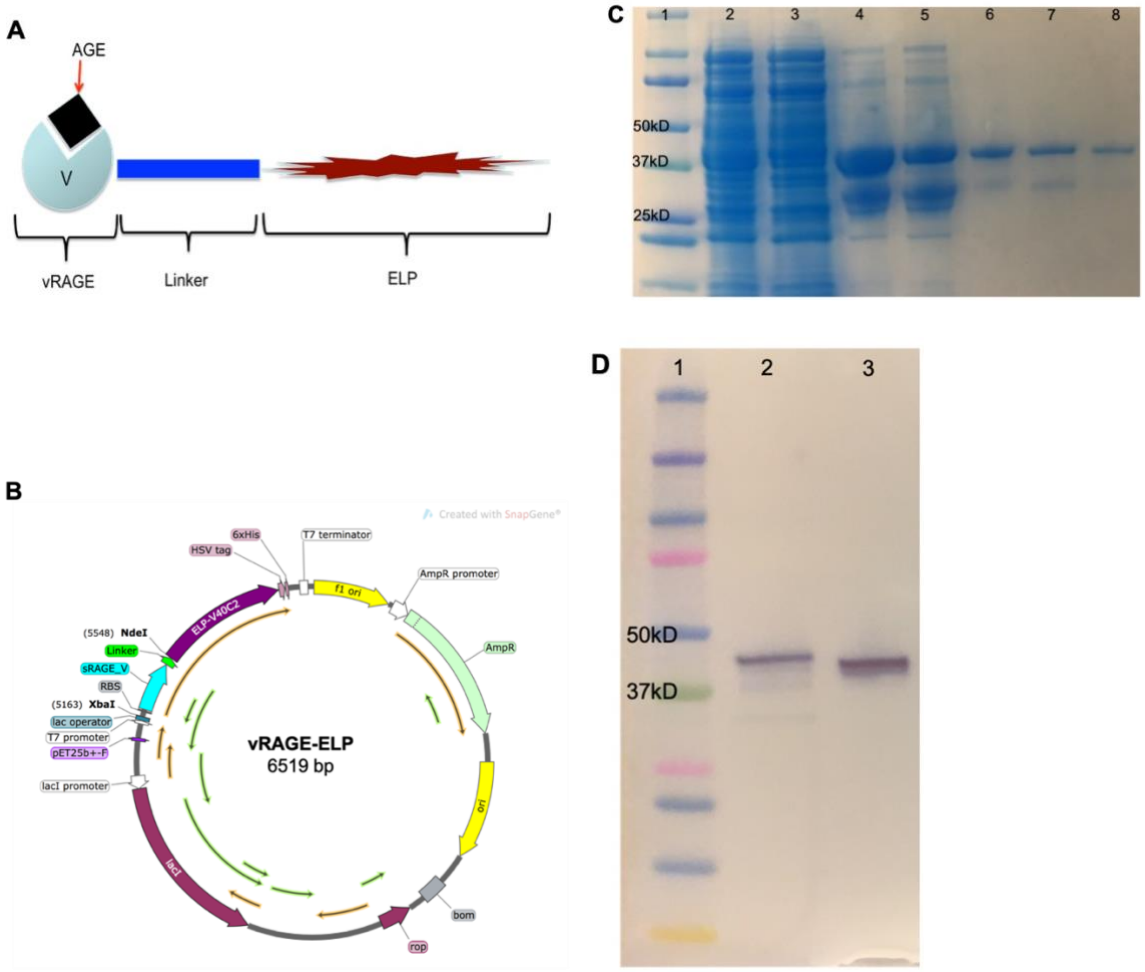

Figure 2.1 Expression and Purification of vRAGE-ELP. (A) Design of vRAGE-ELP fusion protein. The V domain of RAGE was fused to 50 repeats of ELP via a 15-amino acid linker. (B) Plasmid map of vRAGE-ELP expression vector. Genes encoding the V domain of RAGE and the linker were subcloned into the ELP plasmid using XbaI and NdeI restriction enzymes. The plasmid map was created using SnapGene software (from Insightful Science; available at snapgene.com). (C) SDS-PAGE of product after each purification step. A clear band in the final product was observed (lane 8). Lane 1: Protein standard, Lane 2: Total lysate, Lane 3: Supernatant collected after the 1st hot spin, Lane 4: Supernatant collected after the 1st cold spin, Lane 5: Supernatant collected after the 2nd hot spin, Lane 6: Supernatant collected after the 2nd cold spin, Lane 7: Supernatant collected after the 3rd hot spin, Lane 8: Supernatant collected after the 3rd cold spin, which is the final product. (D) Western blot analysis of final product. Lane 1: Protein standard ladder, Lane 2: Native sRAGE as a control, Lane 3: vRAGE-ELP final product

2.3.2.2 Determination of the transition temperature and size of vRAGE-ELP coacervate

In previous studies where the same type and number of ELP repeats were used to manufacture KGF-ELP and SDF1-ELP, coacervates formed around 30ºC and 35ºC, respectively [21-23]. The transition temperature of ELP fusion proteins is determined by several factors such as ELP concentration, the composition and the length of ELPs, and the composition of fused peptides [32]. Since the size of vRAGE-ELP is close to that of KGF-ELP or SDF1-ELP, we expected the vRAGE-ELP fusion proteins to have a similar transition temperature. To determine the transition temperature of vRAGE-ELP, we monitored solution turbidity of vRAGE-ELP while increasing temperature. Figure 2.2A shows a sharp increase in solution turbidity right above 30ºC indicating that vRAGE-ELP form coacervates at around 30-31ºC.

Next, we studied the effect of temperature and protein concentration on the size of coacervates. We prepared vRAGE-ELP fusion proteins at three different concentrations, 5 μM, 10 μM and 25 μM, and measured the size of coacervates at each concentration for three different temperatures, 4ºC, 30ºC, and 37ºC. Figure 2.2B shows representative size scans for vRAGE-ELP at 5 μM (data for 10 μM and 25 μM not shown). At 4ºC, the majority of vRAGE-ELP proteins exist in monomeric form as evidenced by a dominant peak around 10 nm in the volume fraction plot obtained by dynamic light scattering, suggesting little coacervate formation. In contrast, a clear signal with a single peak was shifted rightwards at 30ºC and 37ºC, thereby confirming the formation of coacervates at these temperatures. Autocorrelation analyses of the light scattering time series (Figure 2.2C) show y-intercepts

near one, indicating low noise from multiple scattering. Sharp transitions in the correlation coefficient track with particle size and are consistent with low polydispersity, particularly at 30ºC and 37ºC. Interestingly, the size distribution at 30ºC was broader indicating the coacervates have just begun to form. We also monitored the size of coacervates over a 7-day period and the size at 5 μM did not significantly change (S.I. Figure 2.1).

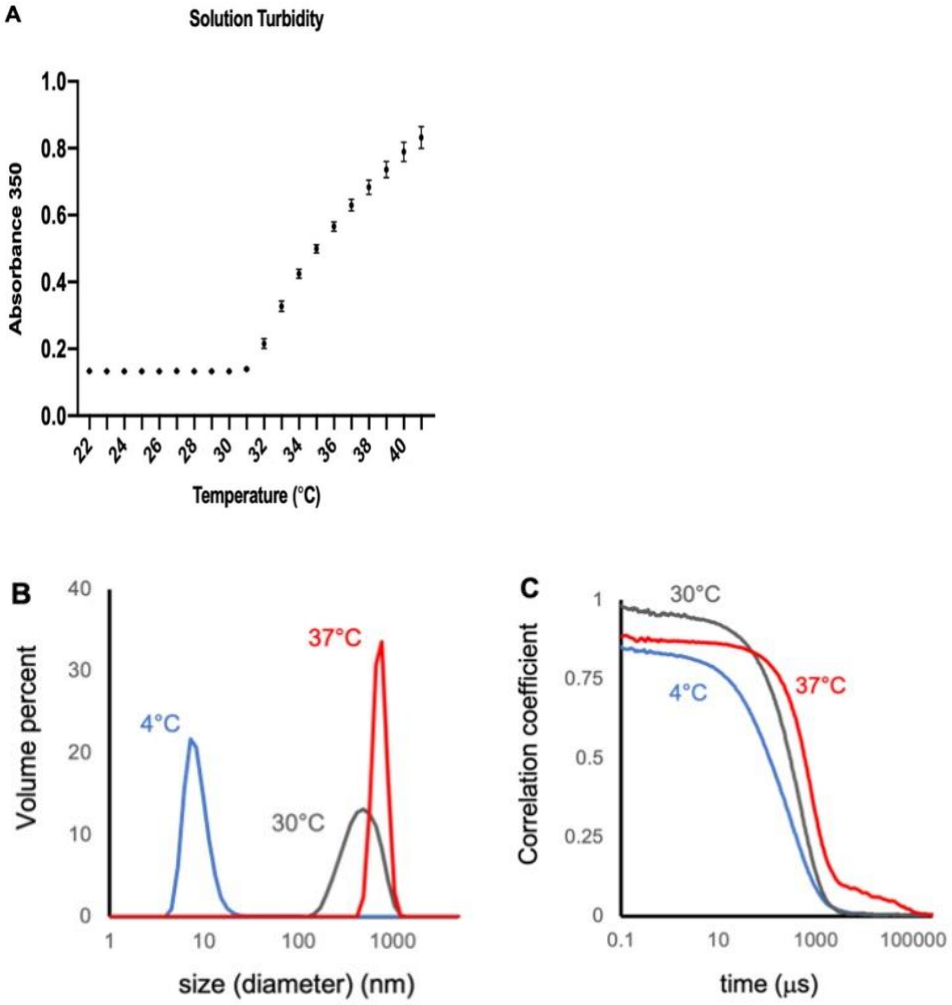

Figure 2.2 Transition temperature and size of coacervates. (A) Solution turbidity of vRAGE-ELP fusion proteins. The solution turbidity increases after around 30ºC indicating the formation of coacervates. N=5. (B) Size of vRAGE-ELP coacervates at 5 μM. The size of coacervates significantly increased as temperature increased from 4ºC to 30ºC and 37ºC. (C) Correlogram. Autocorrelation analyses of the light scattering time series show y-intercepts near one, indicating low noise from multiple scattering. Sharp transitions in the correlation coefficient track with particle size and are consistent with low polydispersity, particularly at 30ºC and 37ºC.

2.3.2.3 Binding of vRAGE-ELP to AGEs

Quantification of the vRAGE-ELP binding curve showed that both vRAGE-ELP and free sRAGE bind to AGE (glycated BSA) in a similar fashion; in contrast, empty ELP did not bind AGEs. Thus, it is the vRAGE portion of vRAGE-ELP that is responsible for binding (Figure 2.3A). None of vRAGE-ELP, free sRAGE or empty ELP showed noticeable binding to BSA-coated wells used as a control (Figure 2.3B).

2.3.2.4 Release of vRAGE-ELP monomers from coacervates

A previous study on SDF1-ELP suggested that fusion protein-ELP coacervates co-exist with monomers at equilibrium [23, 27]. Therefore, we next questioned whether the coacervate form of vRAGE-ELP releases vRAGE-ELP monomers over time, and what is the equilibrium point between monomers and coacervates. vRAGE-ELP (25 mM) was incubated at 37°C and the fraction of vRAGE-ELP monomers released was measured over time. As shown in Figure 2.3C, the percentage of vRAGE-ELP monomers released from the coacervates was around 17% after a 2-hour incubation and this fraction for the remainder of the time course of 72 hours oscillated between 18% and 21%. This suggests that, at equilibrium, 18-21% of vRAGE-ELP monomers is with coacervates.

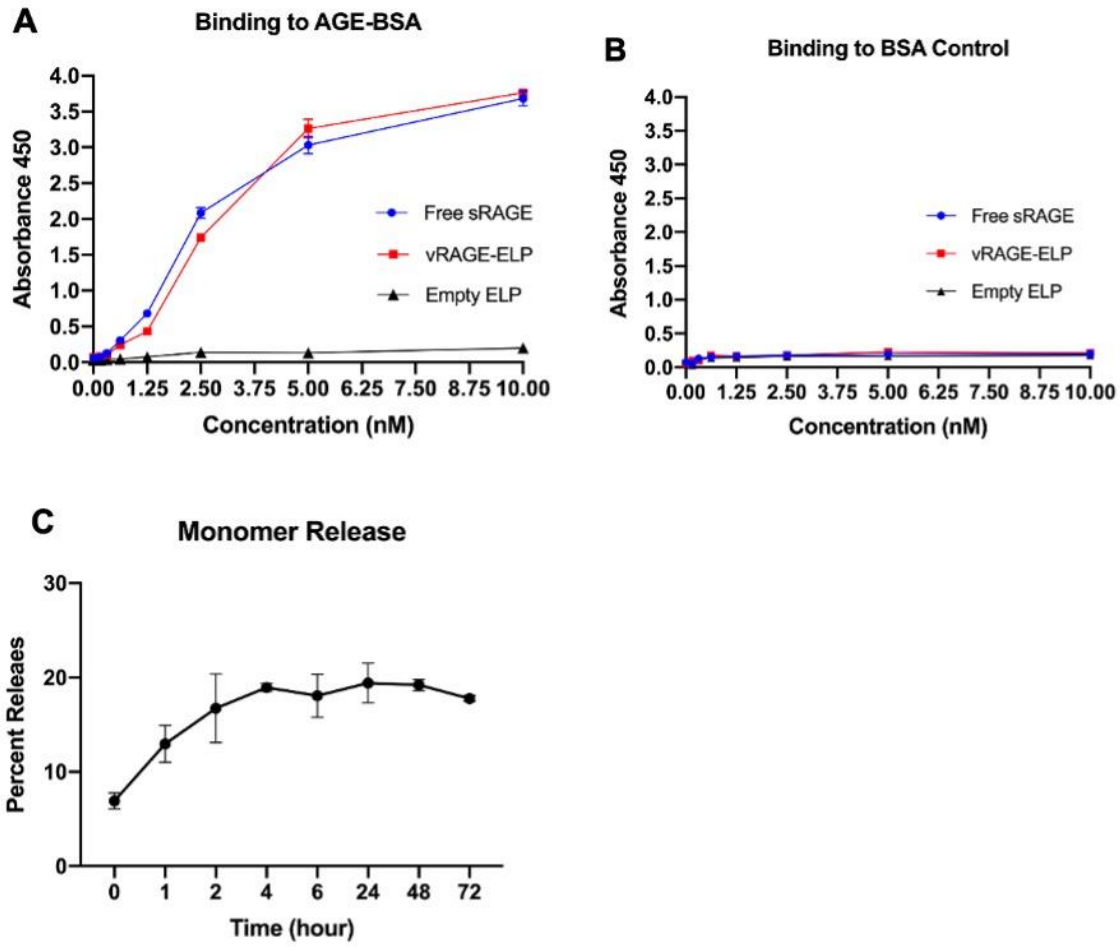

Figure 2.3 Binding activity of vRAGE-ELP to AGE (A, B) and release of vRAGE-ELP monomers from vRAGE-ELP coacervates (C). (A) Binding to AGE. vRAGE-ELP and sRAGE showed similar binding activities to AGE while empty ELP did not bind to AGE. (B) Binding to BSA as a control. None of vRAGE-ELP, free sRAGE or empty ELP showed noticeable binding to BSA control. (C) Release of vRAGE-ELP monomers from coacervates over time. Monomers were separated from coacervates using a 300-900 kD ultrafiltration membrane after incubation up to 72 hours. The concentration in filtrate (monomers) was quantified using a BCA assay. Beyond 2 hours of incubation, the percentage of vRAGE-ELP monomers released from the coacervates remained between 18% and 21%. N=4.

2.3.3 In vitro bioactivity

In order to investigate the bioactivity of vRAGE-ELP in an in vitro simulated diabetic condition, we used cultured HUVECs, which express RAGEs [10, 33, 34], thus

allowing the study of blockade effects of vRAGE-ELP in the presence of AGEs. In previous studies, AGE-stimulated HUVECs showed a decrease in proliferation [33], an increase in pro-inflammatory marker expression [9], and inhibition of migration [33]. Furthermore, endothelial cells are known to be involved in angiogenesis and cell proliferation during wound healing [27]. Therefore, we investigated whether vRAGE-ELP could block AGE-RAGE interaction in AGE-stimulated HUVECs.

2.3.3.1 HUVEC viable number

We stimulated HUVECs with commercially available AGEs, consisting of glycated BSA. We used 100 μg/mL of AGEs, a concentration previously shown to decrease cell proliferation and increase pro-inflammatory marker expression [9, 33]. To investigate whether vRAGE-ELP could recover the proliferation of AGE-stimulated HUVECs, we added pre-mixed AGEs with vRAGE-ELP to the cells. We also investigated dose-dependent effects of vRAGE-ELP by varying the concentration of vRAGE-ELP. Figure 2.4A shows that 100 μg/mL of AGEs alone reduced the number of HUVECs to 70% of the group treated with 100 μg/mL non-modified BSA. When 300 μg/mL of vRAGE-ELP were applied, cell number was slightly increased although not statistically significant. When cells were treated with 500 μg/mL of VRAGE-ELP, cell number significantly increased compared to the AGE-stimulated group ($p<0.01$), and the effect was even more significant at 1 mg/mL of vRAGE-ELP ($p<0.001$), consistent with a dose-dependent effect of vRAGE-ELP. Therefore, we used 1 mg/mL of vRAGE-ELP in subsequent experiments. The vehicle control consisting of empty ELP did not restore cell number, which confirms that the V-domain of RAGE was responsible for the bioactivity of vRAGE-ELP. As an additional

treatment control, we tested the ability of the antioxidant N-acetylcysteine (NAC) to knock down the AGE-mediated response [9]. Interestingly, NAC restored cell number similarly to vRAGE-ELP, suggesting that the reduced cell number in AGE-stimulated cells is a result of downstream intracellular ROS generation.

2.3.3.2 ROS measurement

As both vRAGE-ELP and NAC protected HUVECs from AGEs, we next investigated whether vRAGE-ELP reduces ROS generation in AGE-stimulated cells. There was an increase in ROS levels when HUVECs were stimulated with AGEs alone (Figure 2.4B). In contrast, both vRAGE-ELP (1 mg/mL) and NAC (30 mM) decreased ROS levels in AGE-stimulated HUVECs. A vehicle control (empty ELP) did not reduce AGE-induced ROS levels, indicating that the vRAGE portion of the fusion protein is required to inhibit AGE-mediated ROS generation.

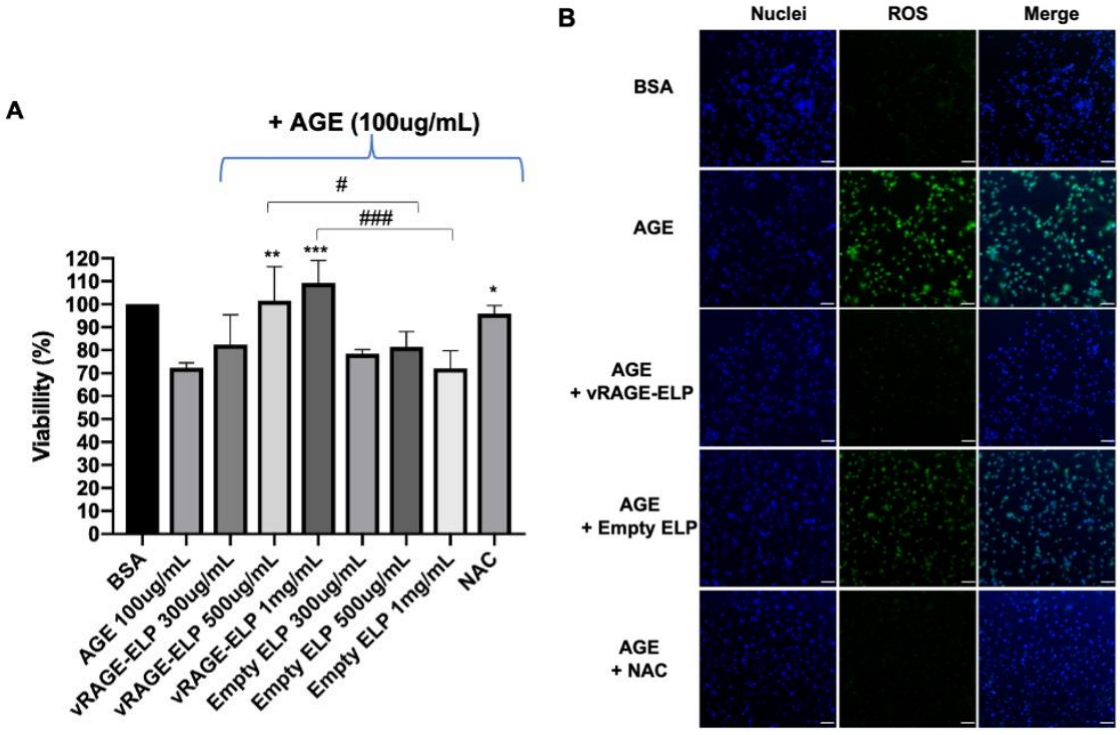

Figure 2.4 Effect of AGEs and RAGEs inhibitors on HUVEC number and ROS generation. (A) Viable cell number. Viable cell number was measured after 24 hours of incubation in each condition and normalized to the BSA control = 100%. AGEs alone significantly decreased cell number ($p=0.0147$). vRAGE-ELP, but not empty ELP, restored cell viability in a dose-dependent manner. NAC, an antioxidant, also recovered cell viability. N=6. Statistics: One-way ANOVA followed by Tukey's test: #$p<0.05$, ### $p< 0.001$, * $p<0.05$, ** $p<0.01$, *** $p<0.001$. Asterisks indicate comparisons with AGE group. (B) ROS levels. AGE stimulation increased ROS generation in HUVECs. The ROS level significantly decreased when cells were treated vRAGE-ELP or NAC, while empty ELPs had no effect. AGE = 100 μg/mL, vRAGE-ELP = 1 mg/mL, ELP = 1 mg/mL, NAC = 30 mM. Blue: Nuclei, Green: ROS. Scale bar = 200 μm.

2.3.3.3 Surface ICAM-1 expression

One of the downstream cellular events resulting from AGE-RAGE binding is the upregulation of pro-inflammatory markers, including ICAM-1 [3, 28]. Basal expression of ICAM-1 is low on endothelial cells, but the expression is significantly up-regulated in inflammation [35]. We investigated whether vRAGE-ELP could suppress the expression of ICAM-1. AGE-stimulated HUVECs exhibited an increased level of ICAM-1, compared to those treated with regular BSA, as seen by immunocytochemistry using anti-ICAM1 antibodies (Figure 2.5A). vRAGE-ELP as well as NAC reversed the effect of AGE stimulation. As expected, vehicle control consisting of empty ELP did not have much effect on ICAM-1 levels. To quantify ICAM-1 surface expression, we also performed a cell-based ELISA (Figure 2.5B). Consistent with Figure 2.5A, AGEs increased ICAM-1 expression. Furthermore, when HUVECs were pre-treated with a polyclonal anti-RAGE antibody, AGEs failed to induce ICAM-1 expression, indicating that the ICAM-1 response reflects an interaction of AGEs with RAGEs on the HUVEC surface. Both the fusion protein vRAGE-ELP and NAC inhibited AGE-mediated ICAM-1 expression. There was a statistically significant difference between the AGE-stimulated and vRAGE-treated groups ($p<0.0001$), while the empty ELP, used as vehicle control, did not show much effect. Thus

the inhibitory effect of vRAGE-ELP on AGE-RAGE signaling is very similar to that of the anti-RAGE blocking antibody and NAC.

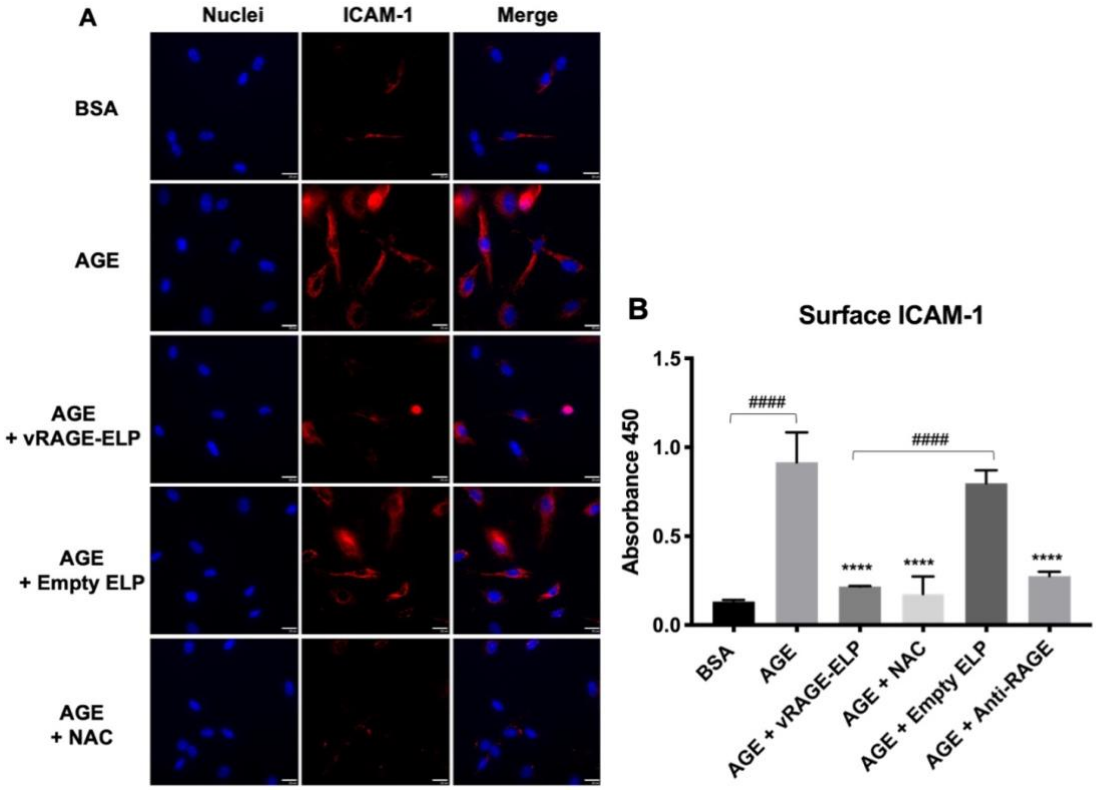

Figure 2.5 Effect of AGEs and inhibitors on surface ICAM-1 expression. (A) Images of immunostaining. vRAGE-ELP coacervates suppressed ICAM-1 expression in AGE-stimulated cells. Blue: DAPI-stained nuclei. Red: antibody-stained ICAM-1. Scale bar = 20 μm. (B) Cell-based ELISA. vRAGE-ELP significantly reduced the expression of ICAM-1 ($p<0.0001$). N=6. Statistics: One-way ANOVA, Tukey's test. #### $p<0.0001$, **** $p<0.0001$. Asterisks indicate comparisons with AGE group. BSA = 100 μg/mL. AGE = 100 μg/mL. vRAGE-ELP = 1 mg/mL. Empty ELP = 1 mg/mL. NAC = 30 mM. Anti-RAGE antibody = 10 μg/mL.

2.3.3.4 Stability in elastase in vitro

While a previous study reported instability of some ELP constructs in elastase, one of the proteases found in diabetic wounds, a recent study, where the same ELP construct was used to develop SDF1-ELP, showed that SDF1-ELP remained intact up to 7 days in the presence of 1 μM elastase [23, 36]. Therefore, to ensure that vRAGE-ELP would also

remain intact in elastase, we conducted a stability test by incubating vRAGE-ELP or free sRAGE in elastase or in PBS without elastase at 37ºC for up to 7 days. The results shown in Figure 2.6A and 6B indicate that vRAGE-ELP remained intact in the presence of elastase while free sRAGE degraded after 3 days. Interestingly, free sRAGE incubated in PBS without elastase showed a weaker band on days 5 and 7 on the Western blot while vRAGE-ELP remained intact.

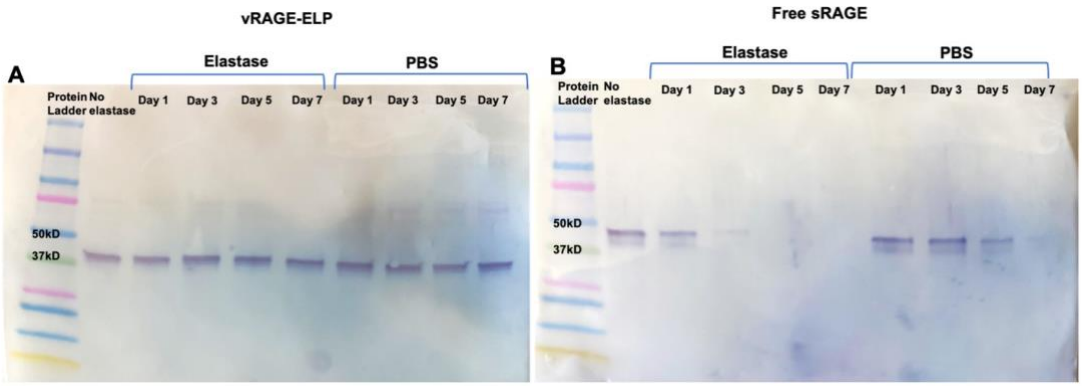

Figure 2.6 Stability of vRAGE-ELP in elastase. (A) Western blot image of vRAGE-ELP incubated in PBS with or without elastase. vRAGE-ELP remained intact in elastase or in PBS without elastase for 7 days. (B) Western blot image of free sRAGE incubated in PBS with or without elastase. Free sRAGE showed a faint band on day 3 and no visible band on day 7 in elastase. Free sRAGE incubated in PBS also showed weaker bands after day 5.

2.3.4 In vivo bioactivity: Effects of vRAGE-ELP on wound healing in diabetic mice

To investigate the effects of vRAGE-ELP coacervates in vivo, we created 1 cm by 1 cm excisional wounds in diabetic mice and treated them once topically with fibrin gel, empty ELP, native sRAGE, or vRAGE-ELP. We used 5 µM (corresponding to 20 µg/100 µL) of sRAGE or vRAGE-ELP, which is the dose reported in the literature where multiple doses of native sRAGE were found to improve diabetic wound healing in mice [11, 12]. Figure 2.7A shows images of wounded areas taken at regular time points. Wounds treated

with vRAGE-ELP closed faster than any other group; this difference was especially evident starting on day 21. We quantified the percent wound closure throughout the wound healing process by taking one minus the ratio of the remaining open wound area compared to the initial wound area. As shown in Figure 2.7B, mice treated with vRAGE-ELP showed significantly faster wound closure starting on day 7, with over 90% wound closure on day 28, whereas wounds in other groups were only about 60-78% closed on day 28. Although native sRAGE caused more rapid wound closure compared to the control groups, native sRAGE was generally less effective than vRAGE-ELP. Furthermore, Kaplan Meier endpoint analysis was performed to compare the effects of empty ELP, free sRAGE and vRAGE-ELP (S.I. Figure 2.2). When the time at which mice achieved 50% wound closure was set in the analysis, there was a statistically significant difference between vRAGE-ELP and empty ELP (S.I. Figure 2.2A). When the time at which mice achieved 70% wound closure was set, there was a statistically significant difference between empty ELP and free sRAGE, empty ELP and vRAGE-ELP, and free sRAGE and vRAGE-ELP (S.I. Figure 2.2B). Additionally, when the time at which mice achieved 80% wound closure was set, there was a statistically significant difference between vRAGE-ELP and empty ELP, and vRAGE-ELP and free sRAGE (S.I. Figure 2.2C).

On day 35 post-wounding, we collected skin wound tissues for histology analysis. H&E staining results show that the epidermal layer in mice treated with vRAGE-ELP was continuous throughout the section and was thicker than in the other groups (Figure 2.8A). In contrast, there was no distinguishable epidermis in the middle of the wound in the fibrin-treated or vehicle control group (red arrows) confirming incomplete wound closure on day 35. Although there was visible epidermis in the native sRAGE groups, the skin layer was

relatively thinner compared to the vRAGE-ELP group. We also quantified the thicknesses of epidermis and dermis in each group by randomly selecting a few spots throughout sections. Both epidermis and dermis were thicker in mice treated with vRAGE-ELP compared to the other groups (Figure 2.8B-C). Mice treated with native sRAGE also showed a thicker epidermis compared to the fibrin-treated group. There was no significant difference in dermal thickness among the groups treated with fibrin, empty ELP and native sRAGE.

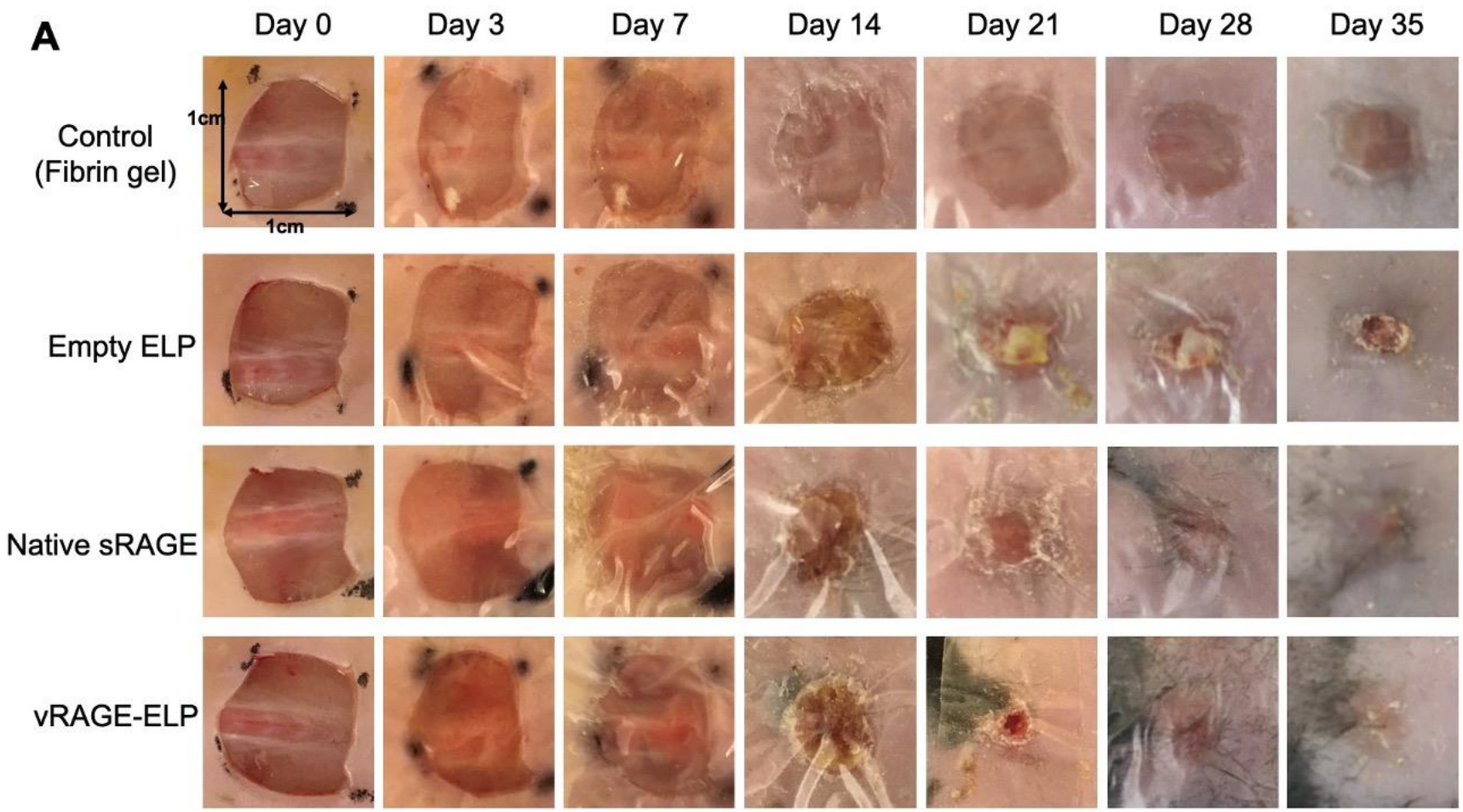
A
Day 0
Day 3
Day 7
Day 14
Day 21
Day 28
Day 35
Control
(Fibrin gel)
1cm
1cm
Empty ELP
Native sRAGE
vRAGE-ELP

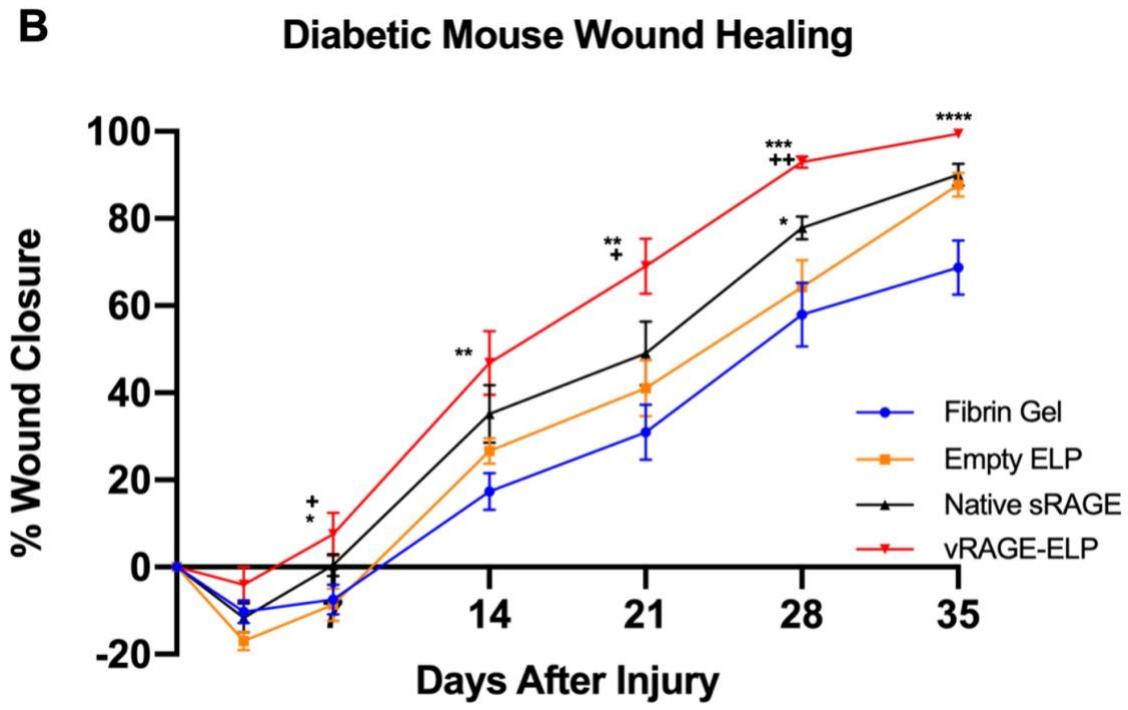

Figure 2.7 Effect of vRAGE-ELP on skin wound closure in diabetic mice. (A) Photos of wounded areas over time. (B) Percent wound closure analyzed by comparing remaining wound areas with initial wound areas. Diabetic mice treated with vRAGE-ELP showed significantly faster wound closure compared to other groups. N=8. Statistics: One-way ANOVA followed by Tukey's test. Asterisks (*) indicate comparisons with fibrin gel control. Plus (+) marks indicate comparisons with vehicle (empty ELP) control. Day 7, * $p<0.05$, + $p<0.05$. Day 14, ** $p<0.01$. Day 21, ** $p<0.01$, + $p<0.05$. Day 28, * $p<0.05$, *** $p<0.001$, ++ $p<0.01$. Day 35, **** $p<0.0001$.

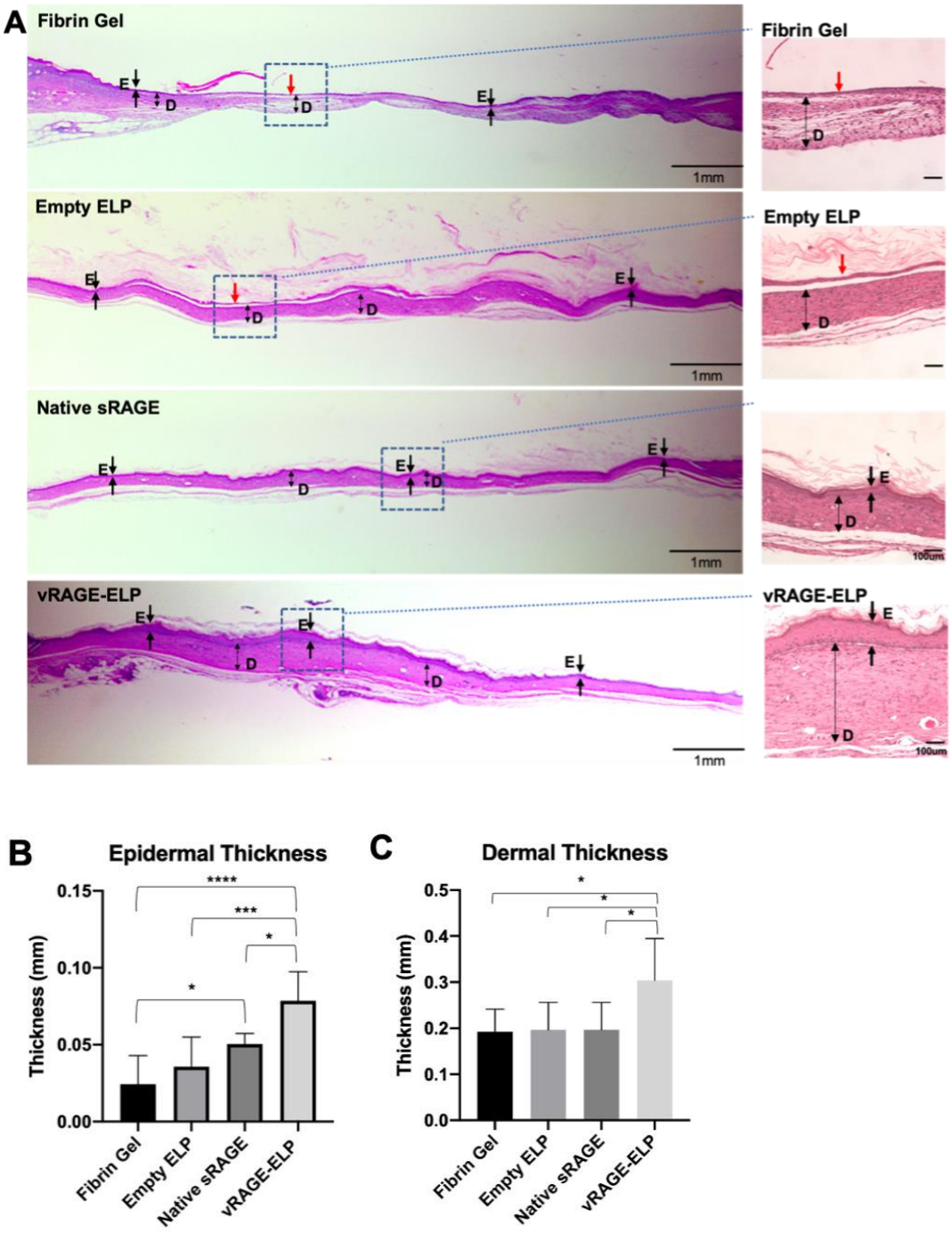

Figure 2.8 Histology of wounded areas collected on post-wounding day 35. (A) Images from H&E staining. Single-headed arrows indicate epidermis. Double-headed arrows represent dermis. A red arrow indicates an area where no visible epidermis is observed. D: Dermis. E: Epidermis. (B) Thickness of epidermis. Values are averages of 6 randomly selected areas from two different sections per group. (C) Thickness of dermis. Values are averages of 6 randomly selected areas from two different sections per group. Statistics: One-way ANOVA followed by Tukey's test. *p<0.05, ***p<0.001, ****p<0.0001.

2.4 Discussion

The majority of therapeutic options used to improve the metabolism of chronic wounds involve enhancing the delivery of oxygen to tissue. There are no available treatments that address the impact of AGE-mediated signaling on the biological mechanisms of impaired healing in diabetes. Although sRAGE was previously reported to be effective in blocking AGE-RAGE-mediated signaling and in enhancing diabetic wound healing in experimental animals [11], potential therapeutic peptides have limited ability to survive in the presence of the high levels of proteases [11, 12, 22, 23]. To circumvent this issue, the peptide may be administered frequently and multiple times, such as in the case of sRAGE in a mouse model, which was given daily on post-wounding days 3-10 [11]. This, however, would be costly and impractical in clinical settings. ELP-based coacervates have shown promise as delivery systems for peptide growth factors in prior studies both in vitro and in vivo [22, 23, 27]. Herein, we took advantage of the ELP delivery system to develop a wound protease-resistant fusion protein containing vRAGE that inhibits the binding of AGEs to RAGEs on the surface of endothelial cells, thus knocking down ROS generation and ICAM-1 expression induced by AGEs, as well as reversing the decrease in viability caused by AGEs.

The mechanism of protection from proteolysis is not well understood; our results showed that at 37°C, which is well above the recorded transition temperature of 30-31°C, approximately 80% of the vRAGE-ELP protein was in coacervate form and 20% was in monomeric form (or small assemblies < 900 kD molecular weight cutoff of the membrane separator). It is possible that the coacervate configuration decreases the contact surface area between vRAGE and surrounding proteases; however, we cannot exclude that even

monomeric vRAGE-ELP itself may be more protease-resistant. vRAGE-ELP may also be more inherently stable as it was noted that native sRAGE was lost at 37ºC even in the absence of exogenous proteases in vitro (Figure 2.6). We chose a 7-day incubation period to evaluate stability in elastases as wound dressings are often replaced on a weekly basis; thus, vRAGE-ELP would not be expected to lose activity in-between dressing changes. Although the diabetic wound fluid generally exhibits significant levels of MMP-2, MMP-9 and elastase, the levels of proteases may vary depending on wound etiology, healing stage and bacterial colonization. A wider range of wound fluid samples would be necessary to fully assess the stability of vRAGE-ELP in the wound environment.

vRAGE-ELP reversed the effect of AGEs on three different responses in HUVECs: (1) increased ROS levels, (2) increased ICAM-1 expression, and (3) decreased viability. The vehicle control consisting of empty ELPs showed no effect confirming it is vRAGE that retains the biological effect of the molecule. A dose-dependent effect of vRAGE-ELP was observed, with a return to baseline level using 1 mg/mL vRAGE-ELP (~28 mM) in the viability/proliferation assay in presence of 100 mg/mL AGEs (~1.4 mM) while 300 mg/mL vRAGE-ELP (~8.4 mM) did not show a significant difference, suggesting there may be a minimal amount of vRAGE-ELP required to be effective as a competitive inhibitor. This finding is also consistent with previous findings where 30 times molar excess of sRAGE were used to study the blockade effects of sRAGE when AGEs were present [9]. Furthermore, the antioxidant NAC mimicked the effect of vRAGE-ELP based on these three metrics. Previous studies have shown that NAC can inhibit inflammation in vitro and improve wound healing in diabetic mice [37, 38]; while NAC is widely available, it is not used in clinical settings for treating wounds. NAC is not a specific antioxidant, and

it is unclear whether it would still be beneficial in a typical wound environment where ROS are potentially important for signaling immune cell recruitment and in mechanisms to kill pathogens [39]. The use of anti-RAGE antibodies in the ICAM-1 expression studies also suggests that blocking RAGEs is a potential alternative to prevent binding AGEs (Figure 2.5B). A prior study showed that anti-RAGE antibody-applied wounds in diabetic mice healed faster compared with a control group [40]. However, in that study, anti-RAGE antibodies were applied every two days until post-wounding day 10 implying the in vivo use of antibodies may be costly, and their effectiveness may be compromised by wound proteases.

We used a genetically induced diabetic mouse model to investigate the bioactivity of vRAGE-ELP in vivo. Although the time scale of onset of diabetes in these animals is on the order of weeks as compared to years and decades in humans, wounds in diabetic mice are widely used to study diabetic impaired wound healing [41, 42], as well as to carry out initial evaluations of potential therapeutics such as sRAGE and other ELP fusion proteins[11, 21-23, 27]. Furthermore, high levels of AGEs are found in diabetic mice [41], and RAGE expression is down-regulated in wounds of diabetic mice treated by sRAGE [11], thus making it an ideal system to study the impact of AGE-mediated signaling, and its inhibition thereof, on wound healing. Mice treated with a single dose of vRAGE-ELP closed excisional skin wounds faster than any other group, including those treated with native sRAGE, as well as the control groups treated with fibrin or vehicle (empty ELP) (Figure 2.7). Wound closure in the vRAGE-ELP-treated group appeared to be one week ahead compared to the sRAGE-treated group, and two weeks ahead compared to the vehicle control. Consistent with this observation, vRAGE-ELP treatment also resulted in

thicker epidermis and dermis, suggesting a more mature scar (Figure 2.8). Prior studies with sRAGE have suggested that inhibiting AGE-mediated signaling decreases the levels of inflammatory markers in mouse diabetic wounds [9, 11]. Based on the in vitro data included herein, a similar mechanism is potentially involved with vRAGE-ELP but it would have to be explored in vivo in the future.

2.5 Conclusions

In conclusion, we report that a novel vRAGE-ELP fusion protein inhibits AGE-RAGE mediated signaling and enhances wound healing in diabetic mice. vRAGE-ELP reversibly form coacervates ranging in size from 500-1600 nm. To our knowledge, this is the first study where a competitive inhibitor of AGE, namely vRAGE, was engineered in the form of fusion proteins, which provide a stable form of delivery method for vRAGE in the highly proteolytic wound environment. Our results suggest that vRAGE-ELP reversed the effects of AGE-RAGE-mediated signaling in vitro and that one dose of vRAGE-ELP treatment was effective to accelerate wound healing in diabetic mice, compared to control vehicle groups. Furthermore, the small size of vRAGE-ELP coacervates would make it possible to incorporate them into already existing microporous skin substitutes and hydrogels currently used clinically.

2.6 Supporting information

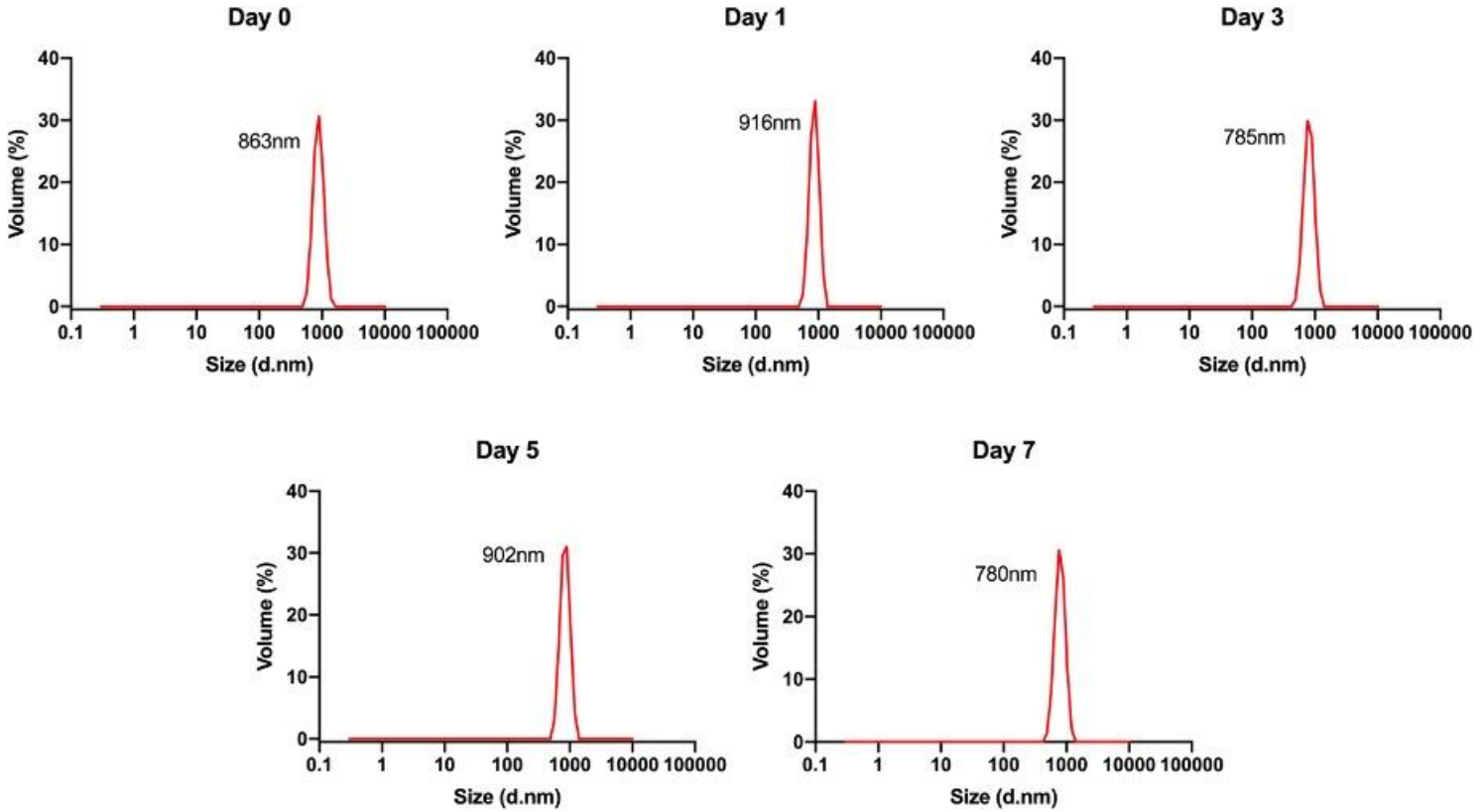

S.I. Figure 2.1 Size of vRAGE-ELP coacervates over time. 5 samples of vRAGE-ELP at 5 μM were incubated at 37 ºC for 0, 1, 3, 5, and 7 days. Size of nanoparticles at each time point was measured using dynamic light scattering.

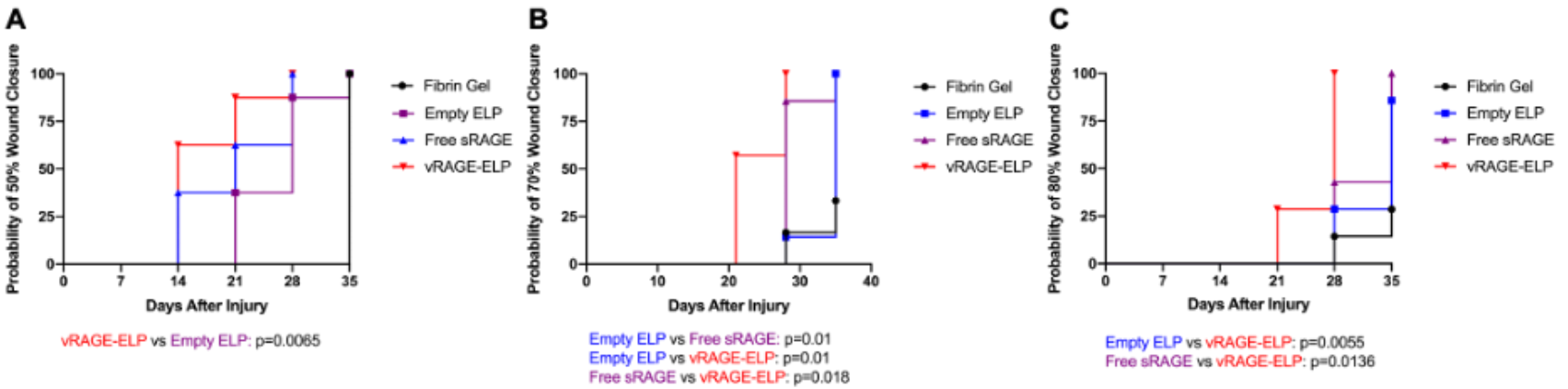

S.I. Figure 2.2 Effect of vRAGE-ELP on skin wound closure in diabetic mice. Kaplan Meier Endpoint Analysis was performed to compare between the effects of empty ELP, free sRAGE and vRAGE-ELP. When the time at which mice achieved 50% wound closure was set, there was a statistically significant difference between vRAGE-ELP and empty ELP. When the time at which mice achieved 70% wound closure was set, there was a statistically significant difference between empty ELP and free sRAGE, empty ELP and vRAGE-ELP, and free sRAGE and vRAGE-ELP. When the time at which mice achieved 80% wound closure was set, there was a statistically significant difference between vRAGE-ELP and empty ELP, and vRAGE-ELP and free sRAGE.

2.7 References

1. Sen CK. Human Wounds and Its Burden: An Updated Compendium of Estimates. Adv Wound Care (New Rochelle). 2019;8(2):39-48.
2. Nussbaum SR, Carter MJ, Fife CE, DaVanzo J, Haught R, Nusgart M, et al. An Economic Evaluation of the Impact, Cost, and Medicare Policy Implications of Chronic Nonhealing Wounds. Value Health. 2018;21(1):27-32.
3. Ahmed N. Advanced glycation endproducts--role in pathology of diabetic complications. Diabetes Res Clin Pract. 2005;67(1):3-21.
4. Goldin A, Beckman JA, Schmidt AM, Creager MA. Advanced glycation end products: sparking the development of diabetic vascular injury. Circulation. 2006;114(6):597-605.
5. Hu SC, Lan CE. High-glucose environment disturbs the physiologic functions of keratinocytes: Focusing on diabetic wound healing. J Dermatol Sci. 2016;84(2):121-7.
6. Brownlee M. Biochemistry and molecular cell biology of diabetic complications. Nature. 2001;414:813-20.
7. Barnes P, Karin M. Nuclear Factor-kB - a pivotal transcription factor in chronic inflammatory disease. The New England Journal of Medicine. 1997;336(15):1066-71.
8. Liu T, Zhang L, Joo D, Sun SC. NF-kappaB signaling in inflammation. Signal Transduct Target Ther. 2017;2.
9. Schmidt AMH, O.; Chen J. X.; Li, J. F.; Crandall, J.; Zhang, J.; Cao, R.; Yan, S. D.; Brett, J.; Stern, D. Advanced Glycation Endproducts Interacting with Their Endothelial Receptor Induce Expression of Vascular Cell Adhesion Molecule-1 (VCAM-1) in Cultured Human Endothelial Cells and in Mice. J Clin Invest. 1995;96:1395-403.
10. Kislinger TF, C.; Huber, B.; Qu, W.; Taguchi, A.; Yan, S.; Hofmann, M.; Yan, S.; Pischetsrieder, M.; Stern, D.; Schmidt A. Ne-(Carboxymethyl)Lysine Adducts of Proteins Are Ligands for Receptor for Advanced Glycation End Products That Activate Cell Signaling Pathways and Modulate Gene Expression. The Journal of Biological Chemistry. 1999;274(44):31740-9.
11. Goova MT, Li J, Kislinger T, Qu W, Lu Y, Bucciarelli LG, et al. Blockade of Receptor for Advanced Glycation End-Products Restores Effective Wound Healing in Diabetic Mice. The American Journal of Pathology. 2001;159(2):513-25.
12. Olekson MP, Faulknor RA, Hsia HC, Schmidt AM, Berthiaume F. Soluble Receptor for Advanced Glycation End Products Improves Stromal Cell-Derived Factor-1 Activity in Model Diabetic Environments. Adv Wound Care (New Rochelle). 2016;5(12):527-38.
13. Schmidt AMSDM. RAGE: A New Target for the Prevention and Treatment of the Vascular and Inflammatory Complications of Diabetes. TEM. 2000;11(9):368-75.
14. Bongarzone S, Savickas V, Luzi F, Gee AD. Targeting the Receptor for Advanced Glycation Endproducts (RAGE): A Medicinal Chemistry Perspective. J Med Chem. 2017;60(17):7213-32.
15. Xue J, Rai V, Singer D, Chabierski S, Xie J, Reverdatto S, et al. Advanced glycation end product recognition by the receptor for AGEs. Structure. 2011;19(5):722-32.
16. Matsumoto SY, T.; Murata, H.; Harada, S.; Fujita, N.; Nakamura, S.; Yamamoto, Y.; Watanabe, T.; Yonekura, H.; Yamamoto, H.; Ohkubo, T.; Kobayashi, Y. Solution

Structure of the Variable-Type Domain of the Receptor for Advanced Glycation End Products: New Insight into AGE-RAGE Interaction. Biochemistry. 2008;47:12299-311.
17. Tardaguila-Garcia A, Garcia-Morales E, Garcia-Alamino JM, Alvaro-Afonso FJ, Molines-Barroso RJ, Lazaro-Martinez JL. Metalloproteinases in chronic and acute wounds: A systematic review and meta-analysis. Wound Repair Regen. 2019;27(4):415-20.
18. Guo S, Dipietro LA. Factors affecting wound healing. J Dent Res. 2010;89(3):219-29.
19. Chilkoti A, Dreher MR, Meyer DE. Design of thermally responsive, recombinant polypeptide carriers for targeted drug delivery. Advanced Drug Delivery Reviews. 2002;54:1093-111.
20. Despanie J, Dhandhukia JP, Hamm-Alvarez SF, MacKay JA. Elastin-like polypeptides: Therapeutic applications for an emerging class of nanomedicines. J Control Release. 2016;240:93-108.
21. Devalliere J, Dooley K, Hu Y, Kelangi SS, Uygun BE, Yarmush ML. Co-delivery of a growth factor and a tissue-protective molecule using elastin biopolymers accelerates wound healing in diabetic mice. Biomaterials. 2017;141:149-60.
22. Koria P, Yagi H, Kitagawa Y, Megeed Z, Nahmias Y, Sheridan R, et al. Self-assembling elastin-like peptides growth factor chimeric nanoparticles for the treatment of chronic wounds. Proc Natl Acad Sci U S A. 2011;108(3):1034-9.
23. Yeboah A, Cohen RI, Faulknor R, Schloss R, Yarmush ML, Berthiaume F. The development and characterization of SDF1alpha-elastin-like-peptide nanoparticles for wound healing. J Control Release. 2016;232:238-47.
24. McDaniel JR, Callahan DJ, Chilkoti A. Drug delivery to solid tumors by elastin-like polypeptides. Adv Drug Deliv Rev. 2010;62(15):1456-67.
25. Meyer DEC, A. Purification of recombinant proteins byfusion with thermally-responsive polypeptides. Nature Biotechnology. 1999;17:1112-5.
26. Hassouneh W, MacEwan SR, Chilkoti A. Fusions of elastin-like polypeptides to pharmaceutical proteins. Methods Enzymol. 2012;502:215-37.
27. Yeboah A, Maguire T, Schloss R, Berthiaume F, Yarmush ML. Stromal Cell-Derived Growth Factor-1 Alpha-Elastin Like Peptide Fusion Protein Promotes Cell Migration and Revascularization of Experimental Wounds in Diabetic Mice. Adv Wound Care (New Rochelle). 2017;6(1):10-22.
28. Guo ZJ, Niu HX, Hou FF, Zhang L, Fu N, Nagai R, et al. Advanced oxidation protein products activate vascular endothelial cells via a RAGE-mediated signaling pathway. Antioxid Redox Signal. 2008;10(10):1699-712.
29. Chen X, Zaro JL, Shen WC. Fusion protein linkers: property, design and functionality. Adv Drug Deliv Rev. 2013;65(10):1357-69.
30. Brito LA, Singh M. Acceptable levels of endotoxin in vaccine formulations during preclinical research. J Pharm Sci. 2011;100(1):34-7.
31. Schwarz H, Schmittner M, Duschl A, Horejs-Hoeck J. Residual endotoxin contaminations in recombinant proteins are sufficient to activate human CD1c+ dendritic cells. PLoS One. 2014;9(12):e113840.
32. Christensen T, Hassouneh W, Trabbic-Carlson K, Chilkoti A. Predicting transition temperatures of elastin-like polypeptide fusion proteins. Biomacromolecules. 2013;14(5):1514-9.

33. Li Y, Chang Y, Ye N, Dai D, Chen Y, Zhang N, et al. Advanced Glycation End Products Inhibit the Proliferation of Human Umbilical Vein Endothelial Cells by Inhibiting Cathepsin D. Int J Mol Sci. 2017;18(2).
34. Xiong F, Leonov S, Howard AC, Xiong S, Zhang B, Mei L, et al. Receptor for advanced glycation end products (RAGE) prevents endothelial cell membrane resealing and regulates F-actin remodeling in a beta-catenin-dependent manner. J Biol Chem. 2011;286(40):35061-70.
35. Wiesolek HL, Bui TM, Lee JJ, Dalal P, Finkielsztein A, Batra A, et al. Intercellular Adhesion Molecule 1 Functions as an Efferocytosis Receptor in Inflammatory Macrophages. Am J Pathol. 2020;190(4):874-85.
36. Shah M, Hsueh PY, Sun G, Chang HY, Janib SM, MacKay JA. Biodegradation of elastin-like polypeptide nanoparticles. Protein Sci. 2012;21(6):743-50.
37. Ayuk SM, Abrahamse H, Houreld NN. The Role of Matrix Metalloproteinases in Diabetic Wound Healing in relation to Photobiomodulation. J Diabetes Res. 2016;2016:2897656.
38. Park JH, Kang SS, Kim JY, Tchah H. The Antioxidant N-Acetylcysteine Inhibits Inflammatory and Apoptotic Processes in Human Conjunctival Epithelial Cells in a High-Glucose Environment. Invest Ophthalmol Vis Sci. 2015;56(9):5614-21.
39. Dunnill C, Patton T, Brennan J, Barrett J, Dryden M, Cooke J, et al. Reactive oxygen species (ROS) and wound healing: the functional role of ROS and emerging ROS-modulating technologies for augmentation of the healing process. Int Wound J. 2017;14(1):89-96.
40. Wang Q, Zhu G, Cao X, Dong J, Song F, Niu Y. Blocking AGE-RAGE Signaling Improved Functional Disorders of Macrophages in Diabetic Wound. J Diabetes Res. 2017;2017:1428537.
41. Hansen LM, Gupta D, Joseph G, Weiss D, Taylor WR. The receptor for advanced glycation end products impairs collateral formation in both diabetic and non-diabetic mice. Lab Invest. 2017;97(1):34-42.
42. Parnell LKS, Volk SW. The Evolution of Animal Models in Wound Healing Research: 1993-2017. Adv Wound Care (New Rochelle). 2019;8(12):692-702.

CHAPTER 3: MULTIFUNCTIONAL ELASTIN-LIKE POLYPEPTIDE FUSION PROTEIN COACERVATES INHIBIT RECEPTOR-MEDIATED PRO-INFLAMMATORY SIGNALS AND PROMOTE ANGIOGENESIS IN DIABETIC CHRONIC WOUNDS

Note: This chapter is reproduced from the following publication written by **Hwan June Kang**:

Hwan June Kang, Suneel Kumar, Biraja Dash, Henry C. Hsia, Martin L. Yarmush, François Berthiaume. "Multifunctional Elastin-like Polypeptide Fusion Protein Coacervates Inhibit Receptor-mediated Pro-inflammatory Signals and Promote Angiogenesis in Diabetic Chronic Wounds". *Nanomedicine: Nanotechnology, Biology and Medicine* (To be submitted, 2021).

3.1 Introduction

Several studies have reported impaired biological mechanisms in diabetic chronic wounds including decreased levels of growth factors [1], excessive and prolonged inflammation [2], impaired keratinocyte and fibroblast migration and proliferation [3], and poor angiogenesis [4]. Advanced glycation end-products (AGEs), which form when proteins or lipids are glycated in the presence of high levels of reactive sugars, are believed to be a major factor leading to the pathology of non-healing diabetic wounds [5]. AGEs, upon binding their receptors (RAGEs), trigger pro-inflammatory signals including increased generation of reactive oxygen species (ROS), persistent activation of the nuclear

transcription factor, NF-κB, and excessive pro-inflammatory gene expression [6, 7]. AGEs also have been shown to impair cellular functions of fibroblasts [8], keratinocytes [9, 10], endothelial progenitors [11], and endothelial cells [12], which play critical roles in wound healing. Furthermore, previous studies have found detrimental effects of AGEs in growth factor activities that are critical to the normal wound healing process, including epidermal growth factor (EGF) [13], keratinocyte growth factor (KGF) [14], and stromal cell-derived factor-1 (SDF-1) [11, 15].

Among growth factors whose activities are impaired in diabetic chronic wounds, SDF-1 is known to play a critical role in vascularization [16, 17], cell migration [18] and proliferation [19]. Sarkar et al. reported that exogenous application of SDF-1 in combination with a dermal skin substitute enhanced reepithelialization of dermal wounds in wild-type mice [16], suggesting exogenous SDF-1 as a potential treatment for diabetic chronic wounds since the expression of SDF-1 is decreased in the latter [15]. In fact, Restivo et al. showed that application of an SDF-1 expression plasmid restored wound healing to near normal in diabetic mouse wounds [20]. Our previous study also found that SDF-1 prepared in nanosized liposomes promoted sustained cell proliferation in mouse diabetic wounds [21]. In another study, Quan et al. reported that SDF-1 expressed in dermal fibroblasts promoted epidermal keratinocyte proliferation in normal and diseased skin [22].

Although these studies put forward SDF-1 as a potential candidate for treating diabetic chronic wounds, we previously reported that cellular responses to SDF-1 are significantly impaired in hyperglycemia, possibly due to the increased basal level of ROS, which abrogates the SDF-1-mediated ROS spike [23]. However, when a soluble form of RAGE (sRAGE), used as a competitive inhibitor of AGEs, was applied in combination

with SDF-1, the activity of SDF-1 was restored in in vitro cell culture experiments. Furthermore, full-thickness skin wounds of diabetic mice closed faster than a vehicle control or SDF-1 alone [23]. The study concluded that the application of sRAGE restored the baseline ROS level, SDF-1-induced superoxide spike and thus cell migration. Therefore, we hypothesized that a combinational delivery of sRAGE and SDF-1 could not only suppress AGE-RAGE-mediated generation of ROS, but may also promote cell migration and proliferation, angiogenesis and diabetic wound healing.

We recently developed an elastin-like polypeptide (ELP)-based delivery system for SDF-1 (SDF1-ELP) and the binding domain (V) of RAGE (vRAGE)-ELP [24, 25]. ELPs are derivative of tropoelastin with pentapeptide repeats of Valine-Proline-Glycine-Xaa-Glycine, where Xaa can be any amino acid except Proline [26, 27]. Fusion proteins with ELPs self-assemble into coacervates above a transition temperature and thus protect the bioactive parts of fusion proteins, for example, SDF-1 and vRAGE, from wound proteases [24, 25, 28]. SDF1-ELP coacervates were stable in elastase, promoted cell migration and vascularization in vitro, and showed superior in vivo efficacy compared to free SDF-1 [25, 28]. Furthermore, we have found that vRAGE-ELP could suppress ROS generation and pro-inflammatory gene expression in AGE-stimulated cultured endothelial cells and showed faster wound closure in diabetic mice compared to free sRAGE [24]. Combining these findings together, herein we aimed to investigate the co-delivery of SDF1-ELP and vRAGE-ELP on wound healing in an in vitro diabetes-mimicking cell culture system, and in vivo in full-thickness wounds on diabetic mice. Our results show that the co-delivery of vRAGE-ELP and SDF1-ELP promotes cell migration and proliferation, angiogenesis, and wound healing in diabetic mice.

3.2 Materials and Methods

3.2.1 Expression and Purification of SDF1-ELP and vRAGE-ELP

The design and cloning strategy of ELP fusion proteins have previously been described [24, 25]. Briefly, DNA encoding either SDF-1 or vRAGE was synthesized and fused to 50 pentapeptide repeats of ELP in a pET25B+ vector via a short linker sequence $(GGGGS)_4$. The ELP fusion proteins were expressed in *E. coli* (One Shot™ BL21 Star™ (DE3) Chemically Competent, Invitrogen™, Thermo Fisher Scientific, USA). The expressed SDF1-ELP and vRAGE-ELP proteins were purified by three cycles of "hot" and "cold" centrifugations to separate ELP proteins that aggregate into coacervates above a transition temperature and resolubilize below the transition temperature.

3.2.2 SDS-PAGE and Western Blot

The purified SDF1-ELP and vRAGE-ELP proteins were run on 4-20% precast gels and Tris/Glycine/SDS buffer (Bio-Rad Laboratories, USA). The SDS-PAGE gels were transferred onto nitrocellulose membranes (Bio-Rad Laboratories) for Western blotting. The membranes were then blocked with 1% BSA in TBS for one hour after which the membranes were incubated with anti-RAGE antibody (ab37647, Abcam, USA) or anti-human SDF-1 antibody (Peprotech, USA) overnight at 4°C. On the next day, the membranes were washed three times with PBST (PBS + 0.05% Tween 20). The membranes were then incubated with horseradish peroxidase (HRP) conjugated secondary antibody (goat anti-rabbit IgG, (H+L), HRP conjugated, Thermo Fisher Scientific) for 1

hour at room temperature. After washing with PBST three times, TMB substrate solution (1-Step™ Ultra TMB-Blotting Solution, Thermo Fisher Scientific) was added to membranes to detect the protein bands.

3.2.3 Determination of transition temperature

5 μM of vRAGE-ELP, 2 μM of SDF1-ELP or a combination of vRAGE-ELP (5 μM) and SDF1-ELP (2 μM) in PBS (100 μL total) were prepared in a 96-well plate in triplicate. The plate was placed in a plate reader to measure the turbidity of the protein solution. The temperature in the plate reader was increased from 25°C to 45°C in 1°C increments. Solution turbidity of each group was determined by monitoring the absorbance of the samples at 350 nm and averaging the measured values.

3.2.4 Size of ELP fusion protein coacervates

5 μM of vRAGE-ELP, 2 μM of SDF1-ELP or a combination of vRAGE-ELP (5 μM) and SDF1-ELP (2 μM) in 25 μL PBS were prepared in a 384 well plate (Corning, USA) to measure the sizes of fusion protein coacervates. The sizes of coacervates at 37°C were measured by dynamic light scattering (DynaPro Plate Reader, Wyatt Technology, USA).

3.2.5 Cell culture

Primary human umbilical vein endothelial cells (HUVECs) were purchased from Thermo Fisher Scientific. HUVECs were maintained in M200 media supplemented with low serum growth supplement (LSGS) kit (Thermo Fisher Scientific) and 100 U/mL

Penicillin-Streptomycin (Thermo Fisher Scientific). The HaCaT keratinocyte cell line was obtained from Dr. Bozena Michniak-Kohn. The keratinocytes were maintained in Dulbecco's Modified Eagle Medium (DMEM, Thermo Fisher Scientific) supplemented with 10% Fetal Bovine Serum (FBS, Thermo Fisher Scientific) and 100 U/mL Penicillin-Streptomycin (Thermo Fisher Scientific).

3.2.6 Cell viable number assay

Viable cell number was measured as described previously [24]. Briefly, HUVECs were seeded in a 96-well plate at a density of 2,000 cells per well and grown in M200 media supplemented with LSGS overnight. A control group of cells was exposed to 100 μg/mL of non-glycated bovine serum albumin (BSA, MilliporeSigma). All other groups described below were stimulated with 100 μg/mL of commercially available AGEs consisting of glycated BSA (Advanced Glycation End Product-BSA, MilliporeSigma) to mimic a diabetic condition. For the vRAGE-ELP treatment group, 100 μg/mL of AGEs were pre-incubated with 1 mg/mL of vRAGE-ELPs for 30 minutes 37°C to allow for the vRAGE-ELP coacervates to react with AGEs after which the mixture was added to cells in growth media. For SDF1-ELP treatment groups, AGE-stimulated cells were co-treated with various concentrations of SDF1-ELP (500 nM (~15 μg/mL), 1 μM (~30 μg/mL) or 2 μM (~60 μg/mL)) in growth media. For combination (vRAGE-ELP + SDF1-ELP) groups, 100 μg/mL of AGEs were pre-incubated with 1 mg/mL of vRAGE-ELPs for 30 minutes and added to cells in growth media. Cells were then co-treated with SDF1-ELP (500 nM, 1 μM or 2 μM). All groups were incubated for 24 hours at 37°C. The viable cell number

per well was measured using a 3-(4,5-dimethylthiazol-2-yl)-2,5-diphenyl-2H-tetrazolium bromide (MTT) assay (Vybrant MTT cell proliferation assay kit, Thermo Fisher Scientific).

3.2.7 In vitro angiogenesis assay

An in vitro tube formation assay was performed as previously described with a slight modification [28]. Briefly, 275 μL of Matrigel® Matrix (no phenol red, Corning) was spread evenly in two separate 24-well plates. The plates were left at room temperature for 10 minutes and incubated at 37°C for additional 30 minutes to allow the Matrigel to form gels. HUVECs were seeded onto the Matrigel at a density of 1.2×10^5 cells in 300 μL of medium M200 PRF (phenol red free) supplemented with LSGS. A control group of cells were treated with 100 μg/mL of BSA. Other groups of cells were treated with (1) 100 μg/mL of AGEs only, (2) 100 μg/mL of AGEs + 1 mg/mL of vRAGE-ELP, (3) 100 μg/mL of AGEs + 2 μM of SDF1-ELP, (4) 100 μg/mL of AGEs + combo (1 mg/mL of vRAGE-ELP + 2 μM of SDF1-ELP), and (5) 100 μg/mL of AGEs + 1 mg/mL of empty ELP. One plate was incubated for 6 hours and the other plate for 18 hours at 37°C. After incubation, cells were washed with Hank's balanced salt solution (HBSS) twice and stained with calcein AM (Thermo Fisher Scientific) at 8 μg/mL in HBSS for 30 minutes at 37°C. Cells were washed again with HBSS twice and the tube formation was imaged with fluorescence microscopy (Olympus IX81). The number of tubes per image field (four fields per group) was counted.

3.2.8 In vitro scratch wound healing assay

A 24-well cell culture plate was used for this assay. A line was drawn on the bottom of the 24-well plate horizontally using a permanent marker. Keratinocytes were plated at a density of 250,000 cells/well in 500 μL of growth media. Cells were incubated for at least 48 hours to achieve confluency. Once the cells were confluent, a scratch wound vertical to the pre-drawn line was created using a p200 pipette tip. Detached cells were removed by washing wells with PBS. Cells were then treated with (1) 100 μg/mL of AGEs only, (2) 100 μg/mL of AGEs + 1 mg/mL of vRAGE-ELP, (3) 100 μg/mL of AGEs + 2 μM of SDF1-ELP, (4) 100 μg/mL of AGEs + combo (1 mg/mL of vRAGE-ELP + 2 μM of SDF1-ELP), and (5) 100 μg/mL of AGEs + 1 mg/mL of empty ELP. A control group was treated with 100 μg/mL of non-glycated BSA and incubated at 37°C. The wounded area was imaged using a microscope camera (Olympus CKX41 and Infinity 2, Lumenera) at 0 hour, 24 hours, 48 hours and 72 hours after injury. The remaining wound area was measured using Image J software (NIH) and calculated as $(1 - \frac{remaining\ wound\ area}{initial\ wound\ area}) \times 100$.

3.2.9 In vivo wound closure study

An in vivo mouse study was conducted in accordance with a protocol approved by the Institutional Animal Care and Use Committee (IACUC) at Rutgers University. Genetically modified diabetic mice (BKS. Cg-Dock7^{m}+/+ Lepr^{db}/J) were purchased from the Jackson Laboratory (Bar Harbor, ME, USA) and used at the age of 10 weeks. A day before surgery, mice were anesthetized by isoflurane (Henry Schein, USA) inhalation and the hair on the back of mice was removed using a clipper, followed by Nair^{TM} cream application to remove residual hair. On the day of surgery, a 1 cm x 1 cm excisional full-thickness skin wound was created on the back of mice as described previously [24]. In

order to apply treatments (vehicle control, empty ELP, native sRAGE, and vRAGE-ELP), fibrin gels were prepared. 5 µM of empty ELP, 5 µM of vRAGE-ELP, 2 µM of SDF1-ELP or combo (5 µM of vRAGE-ELP + 2 µM of SDF1-ELP) were mixed in 80 µL of fibrinogen solution prepared by dissolving human fibrinogen (MilliporeSigma) in deionized water at a final concentration of 6.25 mg/mL. The treatments in fibrinogen were then placed in a 37ºC water bath for at least 10 minutes to initiate coacervate formation. The fibrinogen solution with treatments were then mixed with 20 µL of thrombin at 12.5 U/mL (MilliporeSigma). The mixture was then applied onto the wound and allowed to form a gel for 2 minutes. Tegarderm™ (3M, USA) was used to cover the wounds. The wound areas were photographed on days 1, 3, and 7, and weekly thereafter over a period of 42 days. The percent wound closure compared to the initial wound area was measured using Image J and calculated as $(1 - \frac{remaining\ wound\ area}{initial\ wound\ area}) \times 100$.

3.2.10 Wound tissue histology

On post-wounding day 42, skin samples from wounded areas were collected and fixed in 10% formalin for 24 hours before processing for histology. Tissue samples were paraffin-embedded and thin-sectioned (5 µm). The sectioned tissues were stained with Masson's trichrome stain to visualize tissue morphology. Pictures of stained tissue samples on glass slides were taken using a light microscope fitted with a camera (Olympus CKX41 and Infinity 2, Lumenera). Epidermal thickness and dermal thicknesses were measured using Image J.

3.2.11 Immunohistochemistry for CD31 positive cells

The sectioned tissues were stained by immunohistochemistry to detect CD31 positive cells. Antigen retrieval procedures were performed by incubating the sectioned tissues in Tris/EDTA pH 9.0 buffer overnight at 70°C. On the next day, the slides with sections were washed twice with TBS + 0.025% Triton X-100 for 5 minutes each. Non-specific binding sites were blocked by incubating the slides in TBS containing 1% BSA and 10% goat serum for 2 hours at room temperature. The slides were then incubated with anti-CD31 antibody (Abcam, ab182981, USA) diluted in TBS with 1% BSA at 1:2000 overnight at 4°C. On the next day, the slides were washed twice with TBS + 0.025% Triton X-100 for 5 minutes each. The slides were then incubated with 0.3% H_2O_2 for 15 minutes at room temperature. Next, the slides were incubated with goat anti-rabbit HRP-conjugated secondary antibody (Abcam, ab6721) diluted in TBS + 1% BSA (1:1000) for 1 hour at room temperature and rinsed for 5 minutes with TBS 3 times. The color was developed by adding DAB substrate kit (Abcam, ab64238) for 10 minutes at room temperature. The slides were rinsed in running tap water for 5 minutes and counterstained with hemoxylin. The stained sections were then mounted by adding 2-3 drops of mounting medium (Limonene mounting medium, Abcam) and covered with glass cover slips. The stained tissues were imaged using a microscope camera (Olympus CKX41 and Infinity 2, Lumenera). The number of CD31 positive cells per 10X magnification field were counted manually. A total of three animals per treatment group were used and two different tissue sections were analyzed per group.

3.2.12 Statistical analysis

GraphPad Prism 9 software (GraphPad Software Inc., San Diego, CA, USA) was used for statistical analysis. The p value was calculated by using ANOVA followed by post-hoc analysis with Tukey's test to identify differences among groups at specific time points. A value of $p < 0.05$ was considered statistically significant. Results are expressed as mean ± SEM.

3.3 Results

3.3.1 Identification of vRAGE-ELP and SDF1-ELP fusion proteins

Both vRAGE-ELP and SDF1-ELP fusion proteins in the purified final products were detected on Western blot using anti-RAGE or anti-SDF-1 antibodies, respectively (Figure 3.1). The predicted molecular weights of vRAGE-ELP and SDF1-ELP were previously reported to be 35.8kD and 31kD, respectively [24, 25]. The results showed single clear bands in the final product confirming that the purified proteins are SDF1-ELP (Figure 3.1, left) and vRAGE-ELP (Figure 3.1, right).

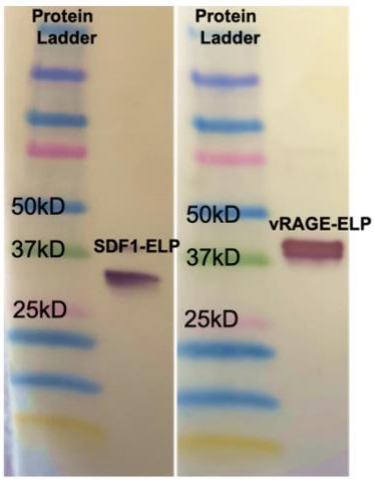

Figure 3.1 Western blot analysis of fusion proteins. Results from Western blotting experiments using anti-SDF1 antibody and anti-RAGE antibody confirmed the presence of fusion proteins, SDF1-ELP and vRAGE-ELP, respectively.

3.3.2 Transition temperature and size of vRAGE-ELP and SDF1-ELP coacervates

The transition temperature of vRAGE-ELP and SDF1-ELP at which they form coacervates were previously determined to be 30°C and 35°C, respectively [24, 25]. We once again examined the transition temperature of each fusion protein to ensure that they form coacervates at physiological temperature. The solution turbidity of either vRAGE-ELP or SDF1-ELP was monitored while increasing temperature. The solution turbidity sharply increased right above 30°C in vRAGE-ELP and 35°C in SDF1-ELP indicating the coacervate formation as expected (Figure 3.2A-B). We were then interested to monitor the solution turbidity of the combination of both fusion proteins. It is known that the same ELP portion, composed of the same guest residues and molecular weight, in different ELP fusion proteins can be used to induce better co-aggregation during the purification [29]. Therefore, we anticipated that vRAGE-ELP and SDF1-ELP would form a single coacervate when they are mixed since both fusion proteins have the exactly same ELP portion. As shown in Figure 3.2C, we observed a sharp increase in solution turbidity at 30°C, the transition temperature of vRAGE-ELP, which is lower than that of SDF1-ELP. Interestingly, the pattern of turbidity curve was similar to that of vRAGE-ELP. Next, we measured the size of each fusion protein or the combination of both fusion protein coacervates at 37°C, which is above the transition temperature of both fusion proteins, using dynamic light scattering. Figure 3.2D and 3.2E show a single peak indicating that vRAGE-ELP or SDF1-ELP formed uniform coacervates at 37°C. Furthermore, as suggested by the solution turbidity results, there was a single peak in the combination of vRAGE-ELP and SDF1-ELP (Figure 3.2F), implying a uniform formation of coacervates.

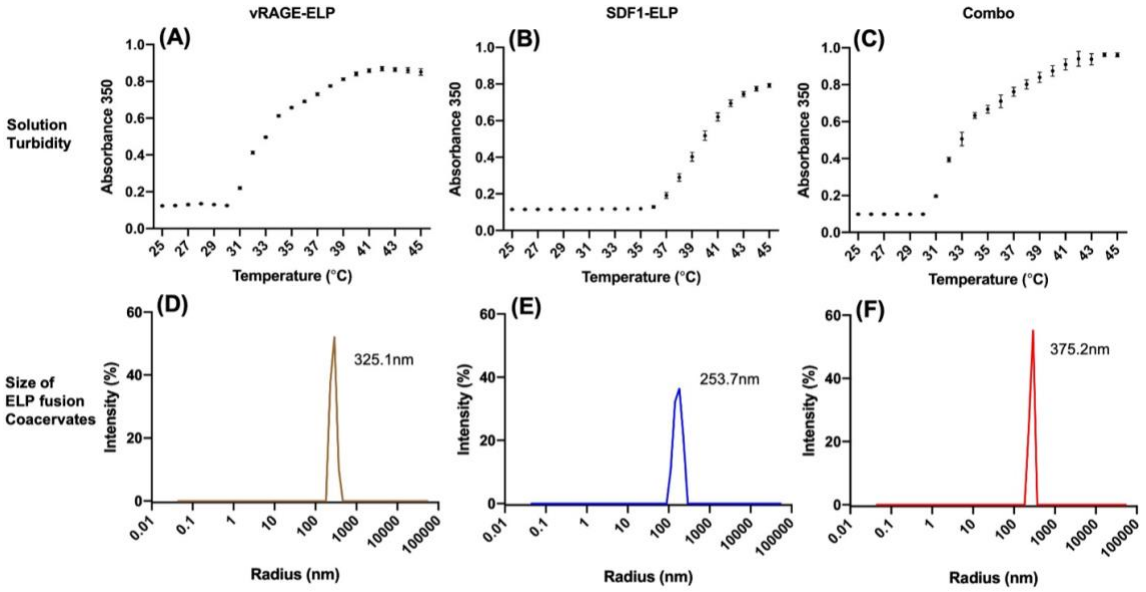

Figure 3.2 Transition temperature and size of ELP fusion coacervates. (A, B, C) Solution turbidity of vRAGE-ELP (5 μM), SDF1-ELP (2 μM) and combo (vRAGE-ELP 5 μM + SDF1-ELP 2 μM) increased after around 30℃, 35℃ and 30℃, respectively, indicating the formation of coacervates. N = 3. (D, E, F) Size of vRAGE-ELP (5 μM), SDF1-ELP (2 μM) and combo (vRAGE-ELP 5 μM + SDF1-ELP 2 μM) at 37℃. A single peak was observed in each group indicating uniformly formed coacervates.

3.3.3 Cell viable number

Our previous study showed that vRAGE-ELP restored the viability of HUVECs when the cells were exposed to AGEs, which mimics the diabetic environment, while empty ELPs without the vRAGE portion had no effect, suggesting that the vRAGE position of vRAGE-ELP is responsible for the bioactivity [24, 25]. Furthermore, other studies suggested that SDF1-ELP could promote tube formation [28] and increase viable cell number in HUVEC cultures (data not published). Therefore, we investigated whether the combination of vRAGE-ELP with SDF1-ELP could further increase cell viability. We used the previously optimized doses of AGEs (100 μg/mL) and vRAGE-ELPs (1 mg/mL) while we varied the concentration of SDF1-ELP to investigate the dose-dependent effect of

SDF1-ELP. AGE-stimulated cells showed decreased cell viability compared with the cells in the BSA control group ($p<0.0001$) (Figure 3.3). vRAGE-ELP treatment of AGE-stimulated cells recovered cell viability near to the BSA control group, confirming 1 mg/mL of vRAGE-ELP is enough to act as competitive inhibitor of AGEs, which is also consistent with our previous finding. AGE-stimulated cells treated with SDF1-ELP alone showed a trend of increasing cell viable number in a dose-dependent manner; however, there was no statistically significant difference between any of SDF1-ELP-treated groups and the AGE-stimulated group. When SDF1-ELP (500 nM (~15 μg/mL), 1 μM (~30 μg/mL) or 2 μM (~60 μg/mL)) was applied in combination with vRAGE-ELP, viable cell numbers increased in a dose-dependent manner. Furthermore, 2 μM of SDF1-ELP with vRAGE-ELP increased the cell viable number, which even exceeded that of the BSA control ($p<0.0001$) or vRAGE-ELP alone group ($p=0.0006$). These results suggest that the combination treatment has a synergistic effect in the presence of AGEs and thus a diabetic-like condition. Therefore, we used 2 μM of SDF1-ELP in following experiments.

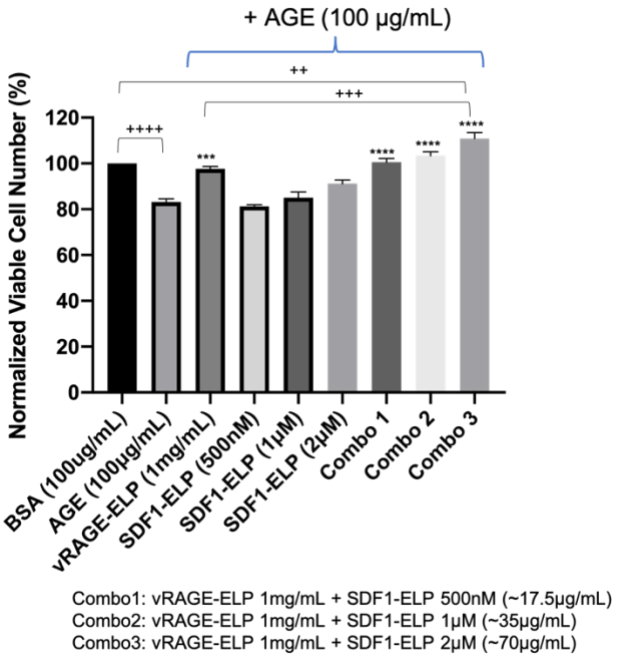

Combo1: vRAGE-ELP 1mg/mL + SDF1-ELP 500nM (~17.5μg/mL)
Combo2: vRAGE-ELP 1mg/mL + SDF1-ELP 1μM (~35μg/mL)
Combo3: vRAGE-ELP 1mg/mL + SDF1-ELP 2μM (~70μg/mL)

Figure 3.3 Effects of vRAGE-ELP and SDF1-ELP on endothelial cell viability under high AGE condition. Viable cell number was measured after 24 hours of incubation in each condition and normalized to the BSA control = 100%. Cell viability was significantly reduced when cells were treated with AGEs. Cells treated with vRAGE-ELP recovered viability closed to the BSA control while SDF1-ELP alone did not show significant increase compared to AGE group. When cells were co-treated with vRAGE-ELP and SDF1-ELP, cell viability values increased compared to AGE group. While lower doses of SDF1-ELP (500 nM and 1 μM) in combo 1 and combo 2 did not show significance compared with vRAGE-ELP alone, 2 μM dose in combo 3 exhibited a significant increase in cell viable number compared with vRAGE-ELP alone. Statistics: One-way ANOVA, Tukey's test. ++$p<0.01$, +++$p<0.001$, ++++$p<0.0001$, ***$p<0.001$, ****$p<0.0001$. Asterisks indicate comparisons with AGE group.

3.3.4 In vitro endothelial tube formation

We previously showed the ability of SDF1-ELP to promote angiogenesis in vitro in HUVEC cultures [28]. In the current study, we further investigated the effect of SDF1-ELP alone and in combination with vRAGE-ELP in AGE-stimulated HUVEC cultures to see whether SDF1-ELP still retains the ability to promote tube formation in the presence of AGEs with or without vRAGE-ELP inhibiting the AGE-RAGE binding. After 6 hours of incubation, endothelial cells in the BSA control began to form tubes while AGEs inhibited the tube formation (Figure 3.4A, top row). vRAGE-ELP-treated and SDF1-ELP-treated cells also started forming tubes, similar to the BSA control. Interestingly, the image of the combination group showed more mature formation of tubes compared to any other group. Note that the empty ELP used as a vehicle control did not show tube formation. After 18 hours of treatment, tube formation in AGE-stimulated group and empty ELP-treated group were still suppressed (Figure 3.4A, bottom row). In contrast, all the treatment groups (vRAGE-ELP, SDF1-ELP and combo) showed significantly increased numbers of tubes. To quantify the tube formation effects, the number of tubes per image field was counted and analyzed (Figure 3.4B). Our results indicate that all 3 treatment groups

(vRAGE-ELP alone, SDF1-ELP alone, and the combination of both) showed significant increases in tube formation at both time points compared to the AGE-stimulated group. Furthermore, the combination treatment showed a statistically significant difference compared to the BSA control at the earlier time point (6 hours after treatment) while vRAGE-ELP alone or SDF1-ELP alone did not show statistically significant differences compared to the BSA control, suggesting that synergistic effects of the combination began at an early time point.

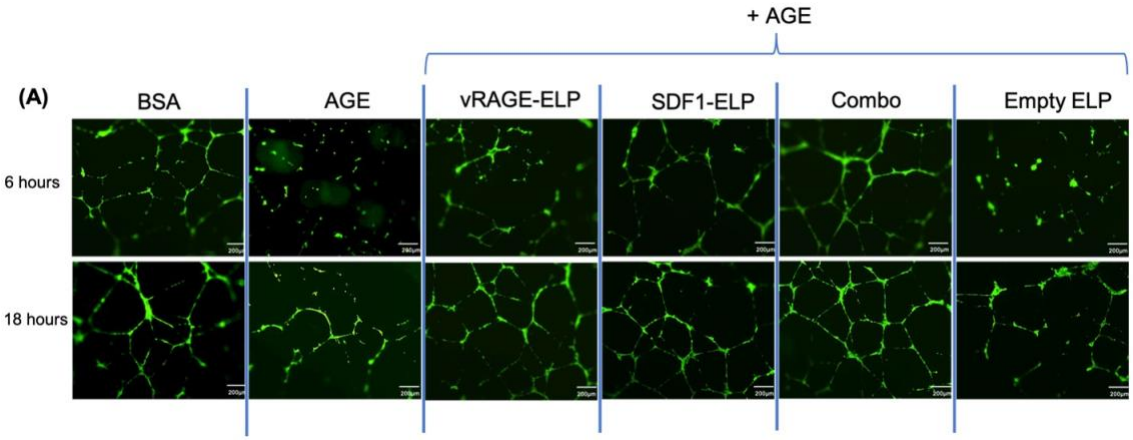

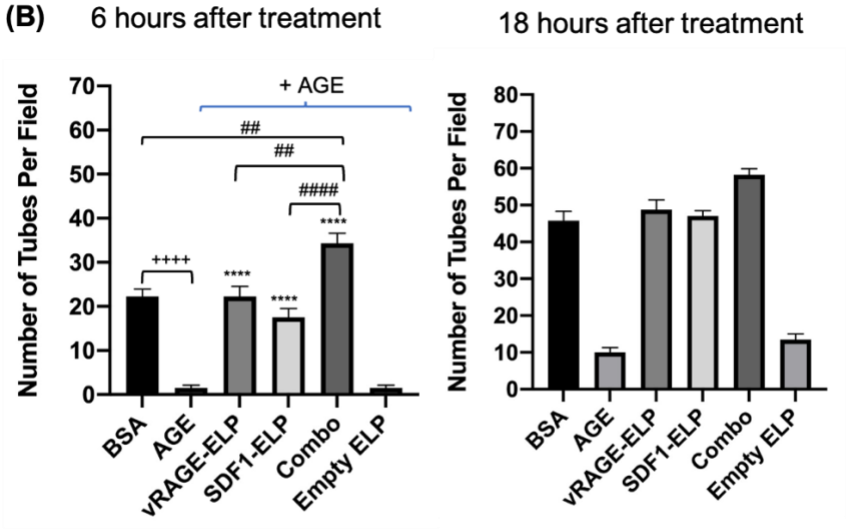

BSA: 100µg/mL
AGE: 100µg/mL
vRAGE-ELP: 1mg/mL
SDF1-ELP: 2µM (~70µg/mL)
Combo: vRAGE-ELP 1mg/mL + SDF1-ELP 2µM (~70 µg/mL)
Empty ELP: 1mg/mL

Figure 3.4 In vitro tube formation assay. (A) Representative images of tube formation in HUVEC culture on Matrigel. (B) Number of Tubes per Field. Tube formation in AGE group was suppressed compared to BSA control. In contrast, treatments with vRAGE-ELP, SDF1-ELP or Combo promoted tube formation. Interestingly, cells treated with combo showed significantly higher number of tubes at both time points compared with vRAGE-ELP or SDF-ELP alone. Note empty ELP treatment did not recover tube formation. Statistics: One-way ANOVA, Tukey's test. #$p<0.05$, ##$p<0.01$, #### $p<0.0001$, ++++$p<0.0001$, ***$p<0.001$, **** $p<0.0001$. Asterisks indicate comparisons with AGE group.

3.3.5 In vitro scratch wound healing assay

A previous study reported that SDF-1 promoted epidermal keratinocyte proliferation [22]. Other studies reported that AGEs impair cellular functions of keratinocytes [9, 10]. Therefore, we investigated the effects of vRAGE-ELP, SDF1-ELP, and the combination of both, on keratinocyte proliferation and migration using an in vitro scratch wound assay. Wound closure was delayed in AGE-stimulated keratinocytes compared to unstimulated controls, as expected (Figure 3.5). Treatments with vRAGE-ELP alone, SDF1-ELP alone and their combination promoted keratinocyte migration, while empty ELP did not have obvious effects (Figure 3.5A). Statistical analysis suggests that the wound closure rate in the combination treatment was higher compared to SDF1-ELP alone starting at 24 hours after treatment ($p=0.0376$) although there was no statistically significant difference between vRAGE-ELP alone and the combination (Figure 3.5B). By 72 hours after treatment, the scratch wound in the combination group closed almost 100% while wounds in other groups, including vRAGE-ELP alone and SDF1-ELP alone, still remained unclosed. Note that the wound closure in the AGE-stimulated group was markedly delayed compared to unstimulated controls at all time points. It should also be noted that wound closure in the combination group was significantly faster compared to the BSA control and exceeded the closure rates of the BSA control at all time points while

SDF1-ELP alone did not show statistically significant differences compared to the BSA control, suggesting a synergistic effect of the combination (Figure 3.5B).

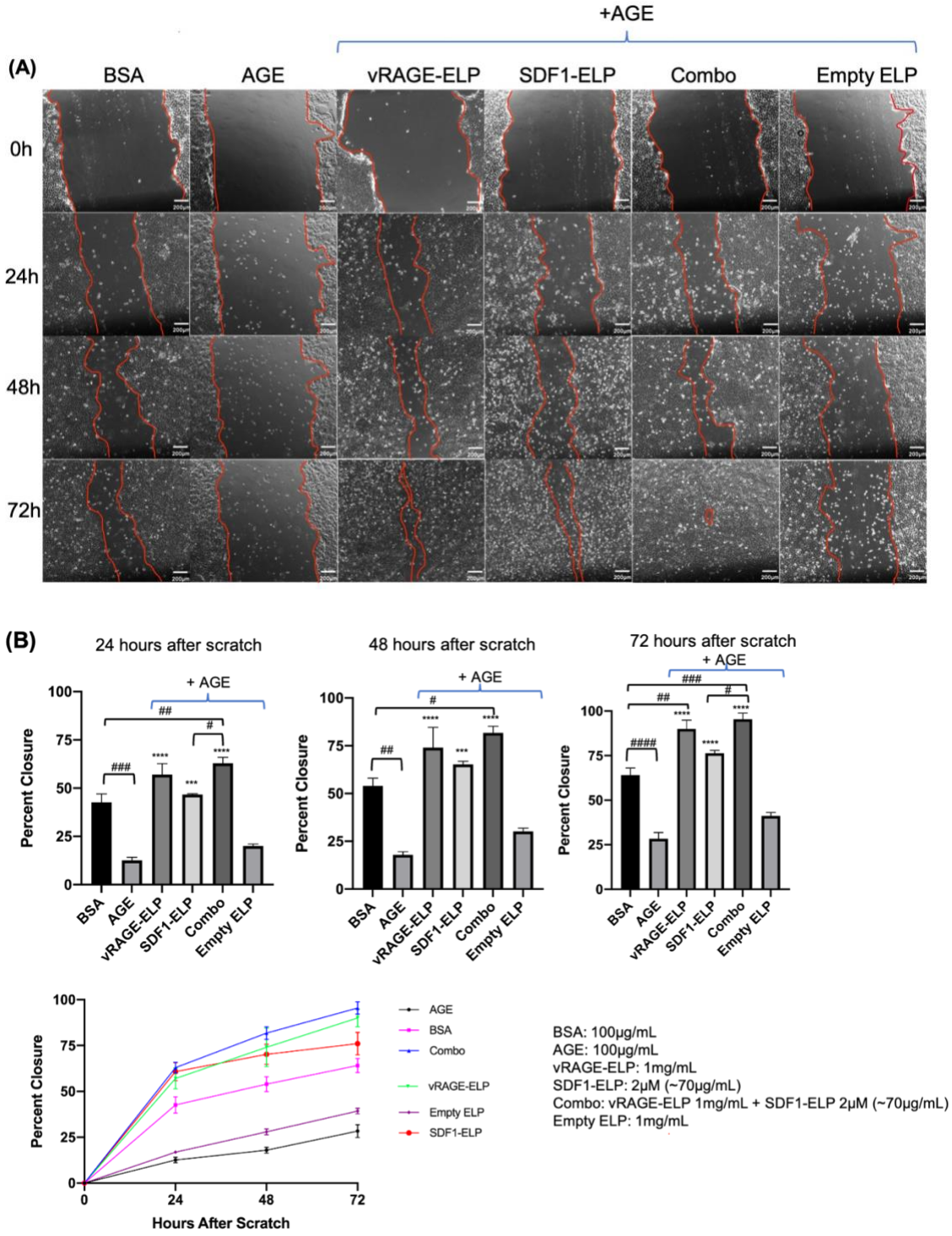

Figure 3.5 In vitro scratch wound closure. (A) Representative images of scratch wounds over time. On day 0, scratch wounds were created using a P200 pipette tip. Images were taken at 0, 24, 48 and 72 hours after scratch wounds were made in each treatment group. (B) Percent wound closure. Remaining wounded areas were measured using Image J software and percent wound closure rates were calculated by comparing with initial wound areas. All three treatments groups (vRAGE-ELP, SDF1-ELP and Combo) showed significantly increased closure rates at all time points compared with AGE-stimulated group. Furthermore, wound closure was accelerated in the combo treatment group compared to vRAGE-ELP or SDF1-ELP alone. N = 3. Statistics: One-way ANOVA, Tukey's test. #$p<0.05$, ##$p<0.01$, ###$p<0.001$, #### $p<0.0001$, ***$p<0.001$, **** $p<0.0001$. Asterisks: comparison with AGE group.

3.3.6 Effects of vRAGE-ELP, SDF1-ELP and combination of both on diabetic mouse wounds

To investigate the effects of vRAGE-ELP, SDF1-ELP and the combination of both in vivo, we created 1 cm by 1 cm excisional wounds in diabetic mice and treated the wounds once topically with fibrin gel, empty ELP, vRAGE-ELP, SDF1-ELP and the combination of vRAGE-ELP and SDF1-ELP. Representative images of wounded areas taken at regular time points are shown in Figure 3.6A. The percent wound closure rates were calculated, and the plot of percent wound closure comparing each group is shown in Figure 3.6B. Overall, wounds treated with either vRAGE-ELP alone, SDF1-ELP alone or the combination of both closed faster than the control groups, fibrin gel and empty ELPs. Wound closure in the vRAGE-ELP alone or the combination groups reached almost 100% on post-wounding day 35 while empty ELP-treated group and fibrin gel control group showed significantly delayed healing, with only of 75% and 50% closure, respectively (Figure 3.6B). It is noteworthy that wounds treated with the combination of vRAGE-ELP and SDF1-ELP showed significantly faster closure rates at earlier time points of days 14 and 21, suggesting a synergistic effect of both ELP fusion proteins.

Histology analysis of skin tissues shows that the epidermal and dermal layers in mice treated with fusion proteins were thicker than those in the other control groups (Figure 3.7A, top row). We also measured and averaged the epidermal and dermal thicknesses in each group by randomly selecting a few spots throughout sections. Both epidermis and dermis were thicker in mice treated with either vRAGE-ELP, SDF1-ELP or combo compared to the other control groups (Figure 3.7B-C) although there was no statistically significant difference between the treatment groups. To investigate whether the treatments promote angiogenesis as our in vitro results suggested, we performed immunohistochemistry to stain CD31 positive cells. The images shown in Figure 3.7A (bottom row) indicate that there was a remarkable increase in the number of CD31 positive cells in the combination groups. Note that only representative spots for the CD31 positive area are indicated with black triangles. Quantification of CD31 positive cells in each group shows that the number of CD31 positive cells in the combination treatment group was higher than fibrin gel or empty ELP control groups (Figure 3.7D). The number of CD31 positive cells in the combination group was also higher than SDF1-ELP or vRAGE-ELP alone groups; however, there were no statistically significant differences.

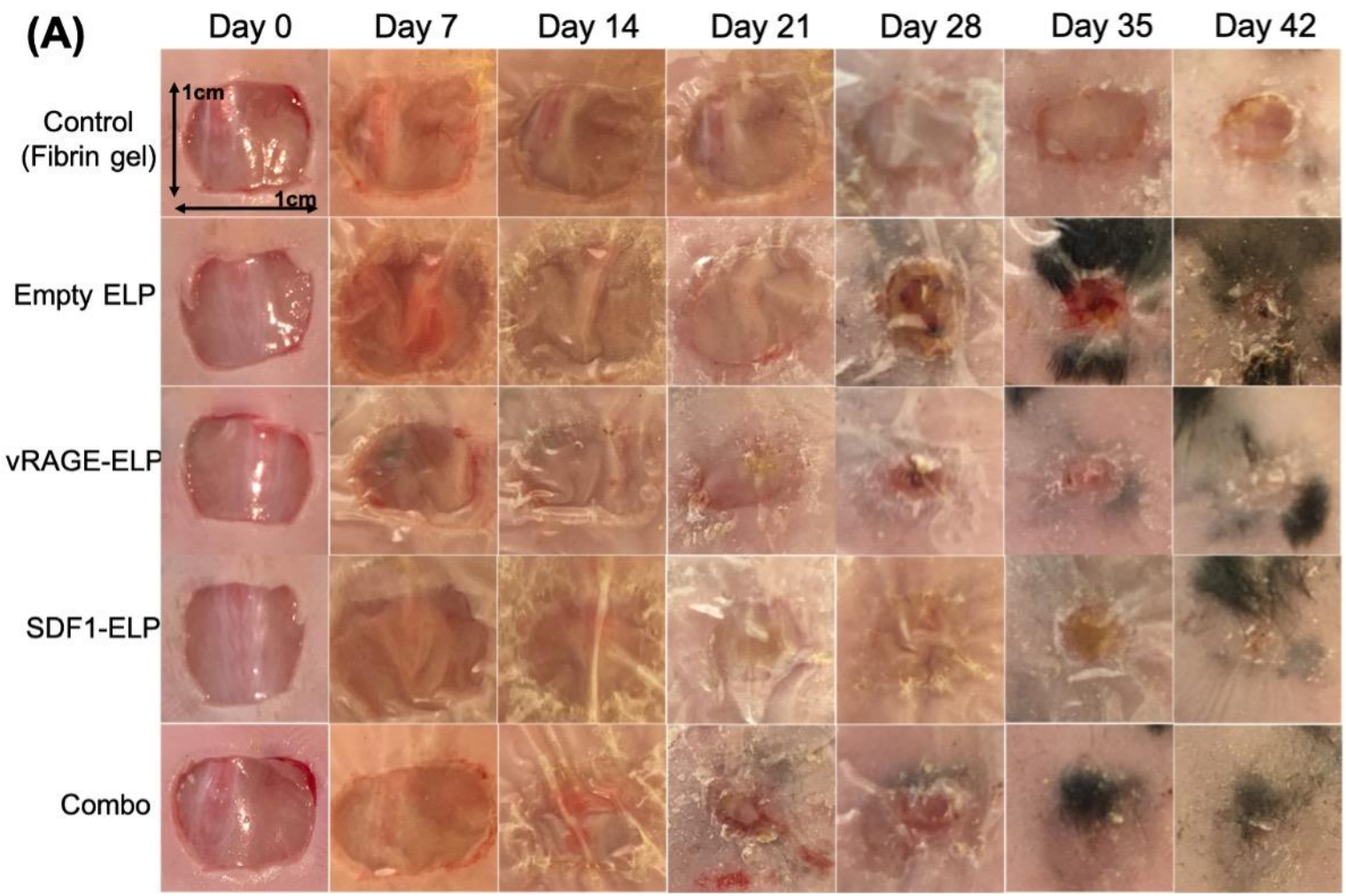
(A)
Day 0
Day 7
Day 14
Day 21
Day 28
Day 35
Day 42
1cm
1cm
Control
(Fibrin gel)
Empty ELP
vRAGE-ELP
SDF1-ELP
Combo

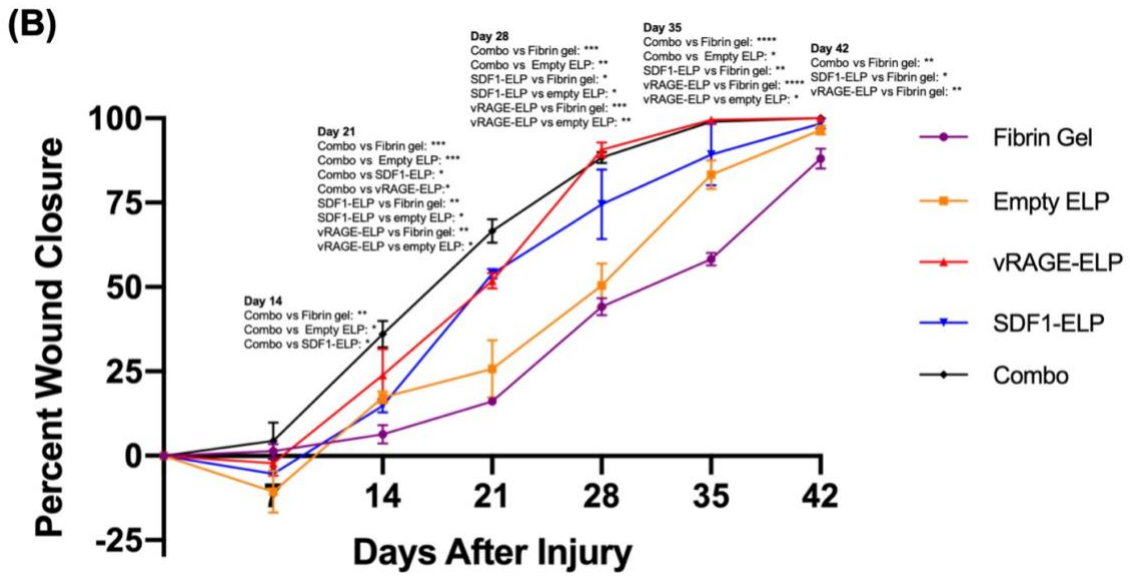

Figure 3.6 Wound healing in diabetic mice. (A) Representative images of excisional skin wounds in diabetic mice. Photos of wounded areas were taken every week. (B) Wound closure rate. Percent wound closure rates were measured using Image J and normalized to initial wound area. vRAGE-ELP and Combo group closed wound at day 35, faster than other treatment groups. Note the combo group shows faster wound closure rates at all time points. Statistics: One-way ANOVA, Tukey's test. *p<0.05, **p<0.01, ***p<0.001, **** p<0.0001. N=3.

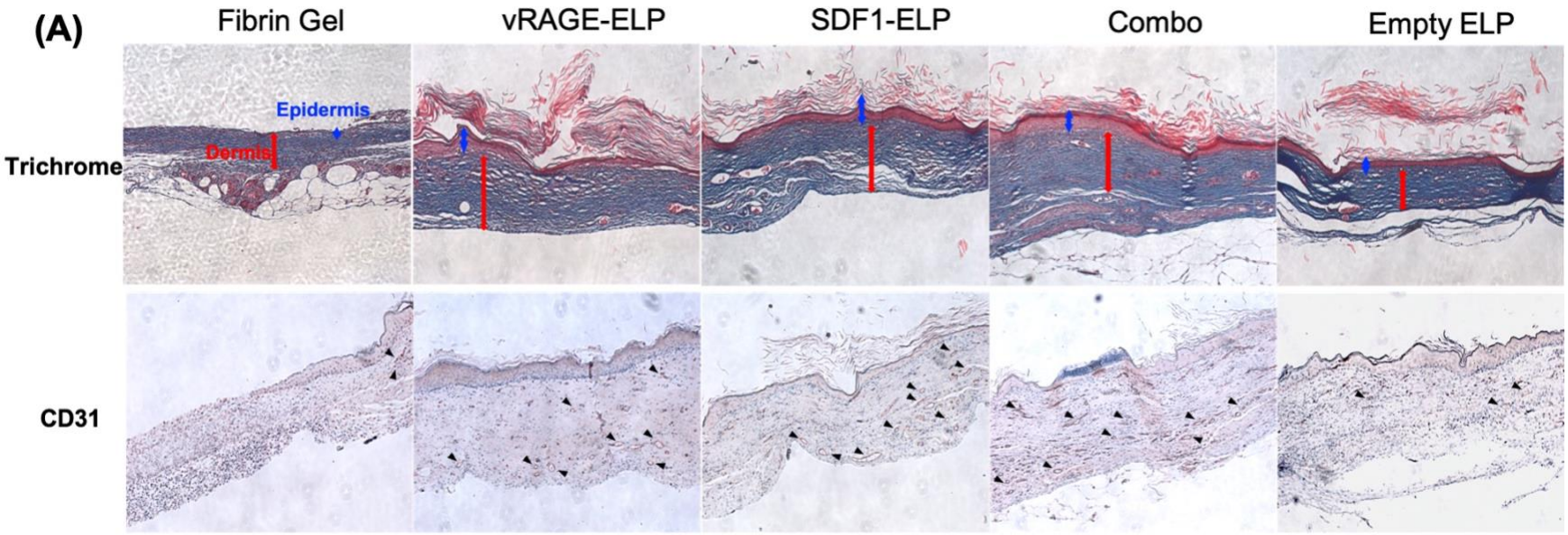
(A)
Fibrin Gel
vRAGE-ELP
SDF1-ELP
Combo
Empty ELP
Trichrome
Epidermis
Dermis
CD31

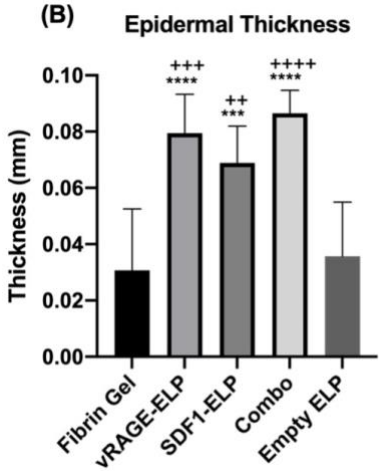
(B)
Epidermal Thickness
Thickness (mm)
0.10
0.08
0.06
0.04
0.02
0.00
+++
****
++
***
++++
****
Fibrin Gel
vRAGE-ELP
SDF1-ELP
Combo
Empty ELP

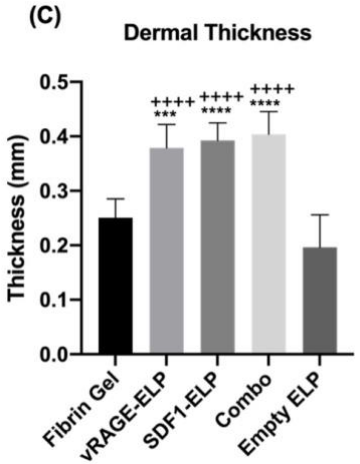
(C)
Dermal Thickness
Thickness (mm)
0.5
0.4
0.3
0.2
0.1
0.0
++++
***
++++
****
++++
****
Fibrin Gel
vRAGE-ELP
SDF1-ELP
Combo
Empty ELP

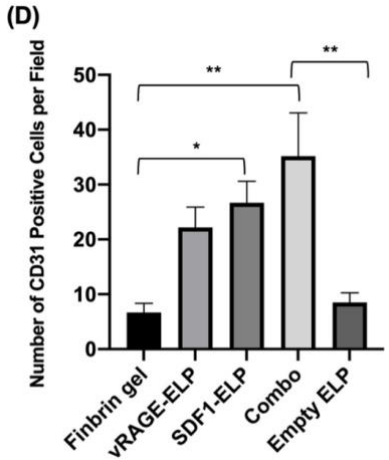
(D)
Number of CD31 Positive Cells per Field
50
40
30
20
10
0
**
**
*
Finbrin gel
vRAGE-ELP
SDF1-ELP
Combo
Empty ELP

Figure 3.7 Histology and Immunohistochemistry Analysis. (A) Representative images of Trichrome staining and CD31 staining on skin tissue collected at day 42. Epidermal and dermal layers are indicated in the figures. Black triangles indicate representative CD31 positive cells. (B) Thickness of epidermis. Values are averages of 6 randomly selected areas from two different sections per group. (C) Thickness of dermis. Values are averages of 6 randomly selected areas from two different sections per group. (D) Quantification of CD31 positive cells. The number of CD31 positive cells per 10X magnification field were counted manually. A total of three animals per treatment group were used and two different tissue sections were analyzed per group. One-way ANOVA followed by Tukey's test. *$p<0.05$, **$p<0.01$, ***$p<0.001$, ****$p<0.0001$, +++$p<0.001$, ++++$p<0.0001$

3.4 Discussion

Topical application of growth factors for diabetic chronic wounds have long been considered as the bioactivity and endogenous expression of growth factors are compromised in the diabetic wound environments [15]. To our knowledge, there are no available treatments that address the negative effects of AGE-RAGE-mediated signaling on the biological mechanisms, which includes the increased level of various proteases, which can quickly degrade bioactive peptides or growth factors, in diabetic chronic wounds [14, 23, 30]. Recently, we have developed an ELP-based delivery system for SDF-1 or vRAGE as potential therapeutics for chronic wounds. SDF1-ELP was shown to have similar biological activities in in vitro assays compared to free form of SDF-1 and significantly superior effects on in vivo diabetic mouse wound healing [25, 28]. Similarly, vRAGE-ELP showed abilities to recover the impaired biological mechanisms in AGE-stimulated in vitro cell cultures and to close diabetic mouse wounds faster than other vehicle controls [24]. Herein, we aimed to investigate whether the combination of both vRAGE-ELP and SDF1-ELP would have synergistic effects by inhibiting AGE-RAGE-mediated signaling and at the same time, promoting cell migration and proliferation, angiogenesis, and thus wound healing.

Both vRAGE-ELP and SDF1-ELP fusion proteins contain the same 50 ELP repeats (V40C2, where V = VPGVG and C = VPGVGVPGVGVPGCGVPGVGVPGVG). Theoretically, the same ELP repeats are expected to co-aggregate into coacervates [29, 31]. Our results suggest that vRAGE-ELP and SDF1-ELP can be intermixed into a few hundred nanometer-sized coacervates, which is evident from the solution turbidity measurements and size measurements by dynamic light scattering (Figure 3.2C and 3.2F). However, as our focus in the present study is on investigating the synergetic effects of two fusion proteins, which have different but critical roles in chronic wound healing, further studies may be required to better understand the physiochemical properties of two or more ELP fusion proteins when intermixed. For example, we have previously reported that about 8% of monomeric forms of SDF1-ELP released from coacervates coexist with SDF1-ELP coacervates and about 20% of monomeric forms of vRAGE-ELP coexist with vRAGE-ELP coacervates. It would be interesting to see whether these numbers stay the same or there is a different monomer release profile when two or more ELP fusion proteins are intermixed.

We used AGE-stimulated cell culture systems to investigate the bioactivities of vRAGE-ELP alone, SDF1-ELP alone, and the combination of both. This system has been optimized to mimic the diabetic condition with an elevated level of AGEs in vitro in our previous study [24]. vRAGE-ELPs were shown to act as competitive inhibitors, inhibit AGE-RAGE binding, and thus recover the impaired biological mechanisms. On the other hand, SDF1-ELP showed bioactivities in vitro and in vivo; however, the bioactivity of SDF1-ELPs had not been tested in diabetes-mimicking in vitro assays [25, 28]. Therefore, herein we first investigated the effect of SDF1-ELP on cell viable numbers in in vitro AGE-

stimulated cell culture. We found that although applications of SDF1-ELP alone showed a dimed effect on viable cell numbers compared to AGE-stimulated cells, there was no statistically significant difference even at higher dose of 2 μM (~60 μg/mL). This is probably due to the increased generation of intracellular ROS in the presence of AGEs, which can interfere with the activity of SDF-1. A previous study found that the ROS spike, which is normally triggered by active SDF-1, was suppressed in hyperglycemia and thus inhibiting the normal SDF-1 activity [23]. Therefore, we hypothesized that the activities of SDF1-ELP could be improved in AGE-stimulated conditions when vRAGE-ELPs are co-delivered and reduce the intracellular generation of ROS by inhibiting AGE-RAGE binding. Our results show that the combination of SDF1-ELP with vRAGE-ELP indeed had superior effects on increasing viable cell numbers in the presence of AGEs in a dose-dependent manner (Figure 3.3), indicating the synergetic effects of combination.

We further investigated the effects of SDF1-ELP in combination with vRAGE-ELP on in vitro angiogenesis and keratinocyte proliferation in the presence of AGEs as SDF-1 is known to promote endothelial vascularization and keratinocyte proliferation [16-19]. We also included an additional time point to see if the combination treatment begins to show better effects at earlier time points compared to other single-treatment groups. Our results show that not only did cells treated with the combination show superior effects on tube formation, but the effects also began to show up at an earlier time point compared to other treatment groups (Figure 3.4). Furthermore, the in vitro scratch wounds treated with the combination showed faster wound closure rates at all time points and closed almost 100% by 72 hours after injury while there were still open wounds in other treatment groups (Figure 3.5). Although vRAGE-ELP or SDF1-ELP alone still had positive effects on cell

viability (Figure 3.3), angiogenesis (Figure 3.4) and proliferation (Figure 3.5), it seems that a combination of vRAGE-ELP and SDF1-ELP has superior effects compared to the effect of each fusion protein alone.

A few studies have previously investigated the effects of free sRAGE, vRAGE-ELP, SDF-1 liposomes, SDF-1 with dermal scaffolds, SDF1-ELP [16, 21, 24, 25, 32] on diabetic mouse wounds, showing positive effects of each. Although the individual treatment option sounds promising, we questioned whether the combination of vRAGE-ELP and SDF1-ELP that can easily be intermixed and thus provide long-term stability could accelerate wound healing in vivo compared with vRAGE-ELP alone or SDF1-ELP alone. Our finding that the effects of the combination start at earlier time points in in vitro AGE-stimulated cell culture is consistent with the results from in vivo mouse wound healing studies. As shown in Figure 3.6, wounds treated with the combination began to show significantly faster healing starting on day 14 compared to any other treatment group. This is especially promising as healing of diabetic chronic wounds is significantly delayed and it is critical to accelerate wound closure to avoid potential infections and other complications [30, 33]. The epidermal and dermal layers were thicker in mice treated with the combination compared to vehicle controls, suggesting enhanced epithelization and formation of granulation tissue (Figure 3.7B-C). Furthermore, the number of CD31 positive cells was greater in the combination-treated group indicating enhanced angiogenesis (Figure 3.7D) compared to the control groups. Our results show no significant differences between the combination and SDF1-ELP only or between the combination and vRAGE-ELP in epidermal/dermal thickness or the number of CD31 positive cells. This

may be due to the fact that at the end of study, wounds have already almost closed in all those treatment groups and thus no detectable differences remain.

3.5 Conclusion

In conclusion, we report that co-delivery of novel vRAGE-ELP fusion protein and SDF1-ELP fusion protein recovers cellular functions and enhances wound healing in diabetic mice. The two fusion proteins can be intermixed into a few hundred nanometer-sized coacervates. To our knowledge, this is the first study that attempts to reverse the AGE-RAGE-mediated signaling as well as to promote cell proliferation and vascularization in one single treatment. Our results show that the application of SDF1-ELP in combination with vRAGE-ELP promotes cell proliferation and tube formation in vitro at earlier time points and significantly faster wound closure in diabetic mice. Although in this study, we have used only one of many growth factors fused to ELPs, vRAGE-ELP can potentially be used in combination with any other growth factor-ELP fusion protein, where vRAGE-ELP can enhance cellular responsiveness to growth factors by inhibiting AGE-RAGE binding and restoring impaired biological mechanisms by AGE-RAGE interaction.

3.6 References

1. Barrientos S, Brem H, Stojadinovic O, Tomic-Canic M. Clinical application of growth factors and cytokines in wound healing. Wound Repair Regen. 2014;22(5):569-78.
2. Tellechea A, Leal E, Veves A, Carvalho E. Inflammatory and Angiogenic Abnormalities in Diabetic Wound Healing: Role of Neuropeptides and Therapeutic Perspectives~!2009-09-05~!2009-09-20~!2010-03-04~! The Open Circulation & Vascular Journal. 2010;3(2):43-55.
3. Brem H, Tomic-Canic M. Cellular and molecular basis of wound healing in diabetes. J Clin Invest. 2007;117(5):1219-22.

4. Veith AP, Henderson K, Spencer A, Sligar AD, Baker AB. Therapeutic strategies for enhancing angiogenesis in wound healing. Adv Drug Deliv Rev. 2019;146:97-125.
5. Ahmed N. Advanced glycation endproducts--role in pathology of diabetic complications. Diabetes Res Clin Pract. 2005;67(1):3-21.
6. Barnes P, Karin M. Nuclear Factor-kB - a pivotal transcription factor in chronic inflammatory disease. The New England Journal of Medicine. 1997;336(15):1066-71.
7. Liu T, Zhang L, Joo D, Sun SC. NF-kappaB signaling in inflammation. Signal Transduct Target Ther. 2017;2.
8. Alikhani M, Maclellan CM, Raptis M, Vora S, Trackman PC, Graves DT. Advanced glycation end products induce apoptosis in fibroblasts through activation of ROS, MAP kinases, and the FOXO1 transcription factor. Am J Physiol Cell Physiol. 2007;292(2):C850-6.
9. Ming T. Effects of advanced glycation end-products (AGEs) on skin keratinocytes by nuclear factor-kappa B (NF-κB) activation. African Journal of Biotechnology. 2012;11(50).
10. Zhu P, Yang C, Chen LH, Ren M, Lao GJ, Yan L. Impairment of human keratinocyte mobility and proliferation by advanced glycation end products-modified BSA. Arch Dermatol Res. 2011;303(5):339-50.
11. Li H, Zhang X, Guan X, Cui X, Wang Y, Chu H, et al. Advanced glycation end products impair the migration, adhesion and secretion potentials of late endothelial progenitor cells. Cardiovascular Diabetology. 2012;11(46).
12. Schmidt AMH, O.; Chen J. X.; Li, J. F.; Crandall, J.; Zhang, J.; Cao, R.; Yan, S. D.; Brett, J.; Stern, D. Advanced Glycation Endproducts Interacting with Their Endothelial Receptor Induce Expression of Vascular Cell Adhesion Molecule-1 (VCAM-1) in Cultured Human Endothelial Cells and in Mice. J Clin Invest. 1995;96:1395-403.
13. Portero-Otín M, R P, Bellmunt MJ, Ruiz MC, Prat J, Salvayre R, et al. Advanced Glycation End Product Precursors Impair Epidermal Growth Factor Receptor Signaling. Diabetes. 2002;51(5):1535-42.
14. Koria P, Yagi H, Kitagawa Y, Megeed Z, Nahmias Y, Sheridan R, et al. Self-assembling elastin-like peptides growth factor chimeric nanoparticles for the treatment of chronic wounds. Proc Natl Acad Sci U S A. 2011;108(3):1034-9.
15. Satish L. Chemokines as Therapeutic Targets to Improve Healing Efficiency of Chronic Wounds. Adv Wound Care (New Rochelle). 2015;4(11):651-9.
16. Sarkar A, Tatlidede S, Scherer SS, Orgill DP, Berthiaume F. Combination of stromal cell-derived factor-1 and collagen-glycosaminoglycan scaffold delays contraction and accelerates reepithelialization of dermal wounds in wild-type mice. Wound Repair Regen. 2011;19(1):71-9.
17. Yamaguchi J, Kusano KF, Masuo O, Kawamoto A, Silver M, Murasawa S, et al. Stromal cell-derived factor-1 effects on ex vivo expanded endothelial progenitor cell recruitment for ischemic neovascularization. Circulation. 2003;107(9):1322-8.
18. Dar A, Goichberg P, Shinder V, Kalinkovich A, Kollet O, Netzer N, et al. Chemokine receptor CXCR4-dependent internalization and resecretion of functional chemokine SDF-1 by bone marrow endothelial and stromal cells. Nat Immunol. 2005;6(10):1038-46.

19. Florin L, Maas-Szabowski N, Werner S, Szabowski A, Angel P. Increased keratinocyte proliferation by JUN-dependent expression of PTN and SDF-1 in fibroblasts. J Cell Sci. 2005;118(Pt 9):1981-9.
20. Restivo TE, Mace KA, Harken AH, Young DM. Application of the chemokine CXCL12 expression plasmid restores wound healing to near normal in a diabetic mouse model. J Trauma. 2010;69(2):392-8.
21. Olekson MA, Faulknor R, Bandekar A, Sempkowski M, Hsia HC, Berthiaume F. SDF-1 liposomes promote sustained cell proliferation in mouse diabetic wounds. Wound Repair Regen. 2015;23(5):711-23.
22. Quan C, Cho MK, Shao Y, Mianecki LE, Liao E, Perry D, et al. Dermal fibroblast expression of stromal cell-derived factor-1 (SDF-1) promotes epidermal keratinocyte proliferation in normal and diseased skin. Protein Cell. 2015;6(12):890-903.
23. Olekson MP, Faulknor RA, Hsia HC, Schmidt AM, Berthiaume F. Soluble Receptor for Advanced Glycation End Products Improves Stromal Cell-Derived Factor-1 Activity in Model Diabetic Environments. Adv Wound Care (New Rochelle). 2016;5(12):527-38.
24. Kang H, Kumar S, Dash BC, Hsia HC, Yarmush ML, Berthiaume F. Self-assembled Elastin-like Polypeptide Fusion Protein Coacervates as Competitive Inhibitors of Advanced Glycation End-Products Enhance Diabetic Wound Healing. J Control Release. 2021;Submitted.
25. Yeboah A, Cohen RI, Faulknor R, Schloss R, Yarmush ML, Berthiaume F. The development and characterization of SDF1alpha-elastin-like-peptide nanoparticles for wound healing. J Control Release. 2016;232:238-47.
26. McDaniel JR, Callahan DJ, Chilkoti A. Drug delivery to solid tumors by elastin-like polypeptides. Adv Drug Deliv Rev. 2010;62(15):1456-67.
27. Meyer DEC, A. Purification of recombinant proteins byfusion with thermally-responsive polypeptides. Nature Biotechnology. 1999;17:1112-5.
28. Yeboah A, Maguire T, Schloss R, Berthiaume F, Yarmush ML. Stromal Cell-Derived Growth Factor-1 Alpha-Elastin Like Peptide Fusion Protein Promotes Cell Migration and Revascularization of Experimental Wounds in Diabetic Mice. Adv Wound Care (New Rochelle). 2017;6(1):10-22.
29. Hassouneh W, Christensen T, Chilkoti A. Elastin-like polypeptides as a purification tag for recombinant proteins. Curr Protoc Protein Sci. 2010;Chapter 6:Unit 6 11.
30. Guo S, Dipietro LA. Factors affecting wound healing. J Dent Res. 2010;89(3):219-29.
31. Christensen T, Trabbic-Carlson K, Liu W, Chilkoti A. Purification of recombinant proteins from Escherichia coli at low expression levels by inverse transition cycling. Anal Biochem. 2007;360(1):166-8.
32. Goova MT, Li J, Kislinger T, Qu W, Lu Y, Bucciarelli LG, et al. Blockade of Receptor for Advanced Glycation End-Products Restores Effective Wound Healing in Diabetic Mice. The American Journal of Pathology. 2001;159(2):513-25.
33. Sen CK. Human Wounds and Its Burden: An Updated Compendium of Estimates. Adv Wound Care (New Rochelle). 2019;8(2):39-48.

CHAPTER 4: CONCLUSIONS

4.1 Key Findings

The aim of this dissertation work was to (1) develop a fusion proteins (vRAGE-ELP) consisting of the binding domain of RAGE and ELP that can act as a competitive inhibitor of AGE in the diabetic chronic wound environment, (2) investigate the bioactivity of the fusion proteins in vitro and in vivo diabetic chronic wound models, and (3) investigate the synergistic effects of vRAGE-ELP when combined with another fusion protein (SDF1-ELP) that has been shown to accelerate wound healing and promote revascularization [1]. The recombinant vRAGE-ELP fusion proteins were successfully developed, and the physical characteristics of vRAGE-ELP, such as the transition temperature and the size of coacervates above the transition temperature, were determined. The effects of vRAGE-ELP on AGE-mediated signals were investigated in AGE-stimulated HUVEC culture. To investigate the effects of vRAGE-ELP on diabetic wound healing in vivo, genetically modified diabetic mice were treated with vRAGE-ELP and the wound closure was monitored and compared with other vehicle control groups. The synergistic effects of vRAGE-ELP in combination with SDF1-ELP were also investigated in AGE-stimulated in vitro HUVEC and keratinocyte culture systems as well as in vivo diabetic mouse model. This section summarizes key findings from these studies.

4.1.1 vRAGE-ELP self-assembles into coacervates and remains intact in the presence of elastase in vitro.

The transition temperature where vRAGE-ELPs self-assemble into coacervates was determined by monitoring protein solution turbidity at various temperatures. The solution turbidity sharply increased above 30°C, indicating the formation of coacervates. The size of vRAGE-ELP coacervates was measured using dynamic light scattering and the size range of vRAGE-ELP used in this dissertation study was estimated to be 400-1600nm in diameter. One of the most important properties of ELP fusion proteins is its relatively stable characteristic in highly proteolytic wound environment by forming coacervates [2-6]. To investigate the stability of vRAGE-ELP coacervates, vRAGE-ELP was incubated in elastase, whose level is elevated in chronic wounds. After a 7-day incubation in elastase or wound fluids, vRAGE-ELP remained intact while free sRAGE used as a control seemed to degrade over time. These results are consistent with previous findings where the same ELP portion was used to make SDF1-ELP fusion proteins [1]. Therefore, we conclude that vRAGE-ELP has the desired physical characteristics, such as the ability to form coacervates at physiological temperature and a good stability in the presence of protease.

4.1.2 vRAGE-ELP acts as a competitive inhibitor of AGE, inhibits AGE-RAGE binding and suppresses RAGE-mediated pro-inflammatory signals in vitro.

To investigate the ability of vRAGE-ELP as a competitive inhibitor of AGE, the binding of vRAGE-ELP to AGE was first examined using a commercial in vitro AGE-RAGE binding assay kit. The binding curve of vRAGE-ELP to AGE was similar to the binding curve of a positive control, sRAGE, to AGE, confirming that vRAGE-ELP binds to AGE and thus could act as a competitive inhibitor of AEGs. Consequently, to investigate whether vRAGE-ELP could inhibit RAGE-mediated pro-inflammatory signals in vitro,

HUVECs, which express RAGEs [7-9], were stimulated with commercially available AGEs to mimic diabetic wound conditions [10, 11]. When AGE-stimulated cells were treated with vRAGE-ELP, the level of intracellular ROS generation was decreased, cell viable numbers were recovered, and the expression of ICAM-1, one of the pro-inflammatory markers [12], was suppressed. As expected, empty ELP had little or no effects confirming it is vRAGE that is responsible for the bioactivity. These results indicate that vRAGE-ELP has potential to recover the impaired biological mechanisms resulted from AGE-RAGE interactions.

4.1.3 vRAGE-ELP significantly promotes wound closure in diabetic mice compared to other control groups including free sRAGE and empty ELP.

The effects of vRAGE-ELP on diabetic wound healing was investigated in vivo in diabetic mouse wounds. Full-thickness excisional skin wounds on the back of mice were treated with vRAGE-ELP, and the wound closure rate was compared with other control groups. The results show that wounds in mice treated with vRAGE-ELP closed faster than any other control group including free sRAGE. Statistically significant faster wound closure was observed throughout the wound healing process, where mice treated with vRAGE-ELP showed significantly faster wound closure starting on day 7, with over 90% wound closure on day 28, whereas wounds in other groups were only about 60-78% closed on day 28. Furthermore, the epidermal and dermal layers in mice treated vRAGE-ELP were thicker compared to other groups, indicating the superior bioactivity of vRAGE-ELP in diabetic wound healing.

4.1.4 vRAGE-ELP in combination with SDF1-ELP promotes cell proliferation, angiogenesis and wound closure in vitro.

In previous studies, SDF1-ELP was developed and showed its superior effects on cell migration and vascularization in vitro, and faster wound healing in vivo [1, 6]. Another study also suggested that in diabetic wounds with an elevated level of AGEs, the activity of SDF-1 is impaired possibly due to increased ROS levels [13]. Therefore, we investigated whether vRAGE-ELP, when used in combination with SDF1-ELP, has synergistic effects on in vitro AGE-stimulated cells. The combination of vRAGE-ELP and SDF1-ELP in AGE-stimulated HUVECs recovered the viable cell numbers beyond the baseline level while vRAGE-ELP alone recovered the viable cell numbers only close to the baseline, and SDF1-ELP alone had no statistically significant effect. In addition, the combination of vRAGE-ELP and SDF1-ELP promoted in vitro tube formation of AGE-stimulated HUVECs and scratch wound closure in AGE-stimulated keratinocytes. The effects of the combination were superior at earlier time points compared to vRAGE-ELP or SDF1-ELP alone treatments indicating the synergetic effects of the combination. These positive results suggest the combinational effects of vRAGE-ELP that can suppress the intracellular ROS level in AGE-stimulated environment and SDF1-ELP that can promote cell proliferation and angiogenesis.

4.1.5 vRAGE-ELP in combination with SDF1-ELP accelerates wound closure in diabetic mice and promotes revascularization in vivo.

vRAGE-ELP in combination with SDF1-ELP was topically applied to full-thickness excisional wounds of diabetic mice to investigate the synergetic effect of the

combination in vivo. Wounds in mice treated with the combination showed a faster trend of wound closure even at earlier time points (post-wounding days 14 and 21) compared to other treatment groups including vRAGE-ELP or SDF1-ELP alone. Furthermore, the results from immunohistochemistry for CD31 positive cells, which is used to demonstrate the presence of endothelial cells and thus angiogenesis, indicate more CD31 positive cells in the combination-treated group. These results together suggest that the combination of vRAGE-ELP and SDF1-ELP promotes healing of diabetic mouse wounds and angiogenesis.

4.2 Limitations

4.2.1 Clinical application of vRAGE-ELP

In this dissertation work, vRAGE-ELP was developed to be applied topically to the wound site. vRAGE-ELP also exhibited a sustained release profile. Therefore, the possibility of vRAGE-ELP to trigger any unwanted effects is expected to be minimal. However, the safety of vRAGE-ELP should be fully investigated before the use in clinic. While only one dose (5 μM), which is corresponding to 20 μg/100 μL of sRAGE that is previously used in literature [14], was tested in this project, more thorough animal studies should be carried out to examine the efficacy and safety of vRAGE-ELP at various doses.

4.2.2 In vitro diabetes-like cell culture model

Diabetic wound environment is extremely complex. While several previous studies used an in vitro cell culture system, where cells were cultured in media containing high

glucose to mimic the diabetic condition [15-17], there is no single in vitro model that perfectly mimics diabetic wound environment. The aim of this study was to evaluate the ability of vRAGE-ELP to act as a competitive inhibitor of AGE. Therefore, we adapted a cell culture model, where cells are stimulated with commercial AGEs, which are glycated BSA. While this specific in vitro model has been used in other studies as well [10, 11], diabetic wound environment may contain various other types of AGEs as AGEs are a group of complex and heterogenous compounds [18]. Furthermore, in this study, two types of mammalian cells, endothelial cells (HUVECs) and keratinocytes, were used to investigate the bioactivities of ELP fusion proteins in vitro. While endothelial cells and keratinocytes play critical roles in revascularization [19] and reepithelialization [20], respectively, wound healing process is much more complicated involving cross-communications of other cell types, such as fibroblasts [21] and endothelial progenitor cells [22], in addition to endothelial cells and keratinocytes. Therefore, there is still a critical need of developing a better in vitro diabetic model. Future studies may attempt to develop co-culture models involving several different types of cells that play important roles in wound healing.

4.2.3 In vivo mouse model

We used a genetically induced diabetic mouse model to investigate the bioactivity of vRAGE-ELP in vivo. Wounds in diabetic mice are widely used to study diabetic impaired wound healing [23, 24], as well as to carry out initial evaluations of potential therapeutics such as sRAGE and other ELP fusion proteins [1, 4-6, 14]. Furthermore, high levels of AGEs are found in diabetic mice [23], and RAGE expression is down-regulated in wounds of diabetic mice treated by sRAGE [14], thus making it an ideal system to study

the impact of AGE-mediated signaling, and its inhibition thereof, on wound healing. However, it should be noted that the time scale of onset of diabetes in these animals is on the order of weeks as compared to years and decades in humans. Furthermore, it should also be noted that the wound repair process in mice, where contraction and collagen formation typically occur [25], is not observed in human chronic wounds.

4.3 Future directions

4.3.1 vRAGE-ELP fusion protein monomers VS. coacervates

The aim of this dissertation work is to demonstrate bioactivity of vRAGE-ELP along with some biophysical data, and thus potential utility as a therapeutic for diabetic wound healing. We reported that about 20% of vRAGE-ELP monomers coexist with vRAGE-ELP coacervates. A previous study also reported that about 8% of SDF1-ELP monomers coexist with SDF1-ELP coacervates [1]. However, it is not well understood whether it is the monomer, coacervate, or both, that binds AGEs. vRAGE-ELP may impact multiple processes involved in the wound healing response that are impacted by the presence of AGEs. It is therefore likely that both monomers and coacervates contribute bioactivity in vivo. Furthermore, it is difficult to decouple the effect of total concentration, monomer concentration, and coacervate concentration due to the thermodynamic equilibrium that exists among them. Future studies may investigate the physical properties of vRAGE-ELP coacervates and vRAGE-ELP monomers to better understand its functional part.

4.3.2 Surface pharmacokinetics of vRAGE-ELP

The vRAGE-ELP fusion aggregates into coacervates at 30°C, which is well below the temperature of human wound beds or mouse skin [26, 27]. Therefore, vRAGE-ELP fusion coacervates are likely to remain in the temperature range above the transition temperature. In our study, to keep the ELP fusion coacervates from dispersing, we used fibrin gel as a delivery vehicle. However, surface pharmacokinetics of vRAGE-ELP over time and in different delivery vehicles have not been studied. In fact, pharmacokinetics also relates to the type of material used to apply the coacervates. This would be worthwhile to explore further in future studies. Furthermore, studies on the fate of ELP coacervates in in vitro cell culture systems and in vivo animal models may be conducted to understand cellular localization of vRAGE-ELP coacervates.

4.3.3 Stability of vRAGE-ELP in wound fluids

Our study showed that vRAGE-ELP remained intact in elastases for 7 days. However, the mechanism of protection from proteolysis is not well understood; our results showed that at 37°C, approximately 80% of the vRAGE-ELP protein was in coacervate form and 20% was in monomeric form. It is possible that the coacervate configuration decreases the contact surface area between vRAGE and surrounding proteases; however, we cannot exclude that even monomeric vRAGE-ELP itself may be more protease-resistant. Future studies may investigate whether monomeric vRAGE-ELP is also protease-resistant. This can be done by incubating vRAGE-ELP in the presence of protases at 37°C, filtering the monomeric forms out as described in the monomer release experiment, and performing protein analysis such as Western blot.

4.3.4 Combination of vRAGE-ELP with two or more ELP fusion growth factors

A previous study reported positive effects of KGF-ELP on chronic wounds, where the same ELP construct was used as in vRAGE-ELP [5]. In this dissertation work, we have already showed the synergistic effects of vRAGE-ELP in combination with SDF1-ELP. Therefore, it would be worthwhile to investigate the effects of vRAGE-ELP in combination with two or more other ELP fusion growth factors, such as vascular endothelial growth factor (VEGF) known to promote angiogenesis [28], and platelet derived growth factor (PDGF) known to stimulate chemotaxis and proliferation [29].

4.4 References

1. Yeboah A, Maguire T, Schloss R, Berthiaume F, Yarmush ML. Stromal Cell-Derived Growth Factor-1 Alpha-Elastin Like Peptide Fusion Protein Promotes Cell Migration and Revascularization of Experimental Wounds in Diabetic Mice. Adv Wound Care (New Rochelle). 2017;6(1):10-22.
2. Chilkoti A, Dreher MR, Meyer DE. Design of thermally responsive, recombinant polypeptide carriers for targeted drug delivery. Advanced Drug Delivery Reviews. 2002;54:1093-111.
3. Despanie J, Dhandhukia JP, Hamm-Alvarez SF, MacKay JA. Elastin-like polypeptides: Therapeutic applications for an emerging class of nanomedicines. J Control Release. 2016;240:93-108.
4. Devalliere J, Dooley K, Hu Y, Kelangi SS, Uygun BE, Yarmush ML. Co-delivery of a growth factor and a tissue-protective molecule using elastin biopolymers accelerates wound healing in diabetic mice. Biomaterials. 2017;141:149-60.
5. Koria P, Yagi H, Kitagawa Y, Megeed Z, Nahmias Y, Sheridan R, et al. Self-assembling elastin-like peptides growth factor chimeric nanoparticles for the treatment of chronic wounds. Proc Natl Acad Sci U S A. 2011;108(3):1034-9.
6. Yeboah A, Cohen RI, Faulknor R, Schloss R, Yarmush ML, Berthiaume F. The development and characterization of SDF1alpha-elastin-like-peptide nanoparticles for wound healing. J Control Release. 2016;232:238-47.
7. Kislinger TF, C.; Huber, B.; Qu, W.; Taguchi, A.; Yan, S.; Hofmann, M.; Yan, S.; Pischetsrieder, M.; Stern, D.; Schmidt A. Ne-(Carboxymethyl)Lysine Adducts of Proteins Are Ligands for Receptor for Advanced Glycation End Products That Activate Cell Signaling Pathways and Modulate Gene Expression. The Journal of Biological Chemistry. 1999;274(44):31740-9.
8. Wiesolek HL, Bui TM, Lee JJ, Dalal P, Finkielsztein A, Batra A, et al. Intercellular Adhesion Molecule 1 Functions as an Efferocytosis Receptor in Inflammatory Macrophages. Am J Pathol. 2020;190(4):874-85.
9. Xiong F, Leonov S, Howard AC, Xiong S, Zhang B, Mei L, et al. Receptor for advanced glycation end products (RAGE) prevents endothelial cell membrane resealing and regulates F-actin remodeling in a beta-catenin-dependent manner. J Biol Chem. 2011;286(40):35061-70.
10. Li Y, Chang Y, Ye N, Dai D, Chen Y, Zhang N, et al. Advanced Glycation End Products Inhibit the Proliferation of Human Umbilical Vein Endothelial Cells by Inhibiting Cathepsin D. Int J Mol Sci. 2017;18(2).
11. Schmidt AMH, O.; Chen J. X.; Li, J. F.; Crandall, J.; Zhang, J.; Cao, R.; Yan, S. D.; Brett, J.; Stern, D. Advanced Glycation Endproducts Interacting with Their Endothelial Receptor Induce Expression of Vascular Cell Adhesion Molecule-1 (VCAM-1) in Cultured Human Endothelial Cells and in Mice. J Clin Invest. 1995;96:1395-403.
12. Ahmed N. Advanced glycation endproducts--role in pathology of diabetic complications. Diabetes Res Clin Pract. 2005;67(1):3-21.
13. Olekson MP, Faulknor RA, Hsia HC, Schmidt AM, Berthiaume F. Soluble Receptor for Advanced Glycation End Products Improves Stromal Cell-Derived Factor-1 Activity in Model Diabetic Environments. Adv Wound Care (New Rochelle). 2016;5(12):527-38.

14. Goova MT, Li J, Kislinger T, Qu W, Lu Y, Bucciarelli LG, et al. Blockade of Receptor for Advanced Glycation End-Products Restores Effective Wound Healing in Diabetic Mice. The American Journal of Pathology. 2001;159(2):513-25.
15. Hu SC, Lan CE. High-glucose environment disturbs the physiologic functions of keratinocytes: Focusing on diabetic wound healing. J Dermatol Sci. 2016;84(2):121-7.
16. Khamaisi M, Katagiri S, Keenan H, Park K, Maeda Y, Li Q, et al. PKCdelta inhibition normalizes the wound-healing capacity of diabetic human fibroblasts. J Clin Invest. 2016;126(3):837-53.
17. Kruse CR, Singh M, Sorensen JA, Eriksson E, Nuutila K. The effect of local hyperglycemia on skin cells in vitro and on wound healing in euglycemic rats. J Surg Res. 2016;206(2):418-26.
18. Sharma C, Kaur A, Thind SS, Singh B, Raina S. Advanced glycation End-products (AGEs): an emerging concern for processed food industries. J Food Sci Technol. 2015;52(12):7561-76.
19. Yamaguchi J, Kusano KF, Masuo O, Kawamoto A, Silver M, Murasawa S, et al. Stromal cell-derived factor-1 effects on ex vivo expanded endothelial progenitor cell recruitment for ischemic neovascularization. Circulation. 2003;107(9):1322-8.
20. Florin L, Maas-Szabowski N, Werner S, Szabowski A, Angel P. Increased keratinocyte proliferation by JUN-dependent expression of PTN and SDF-1 in fibroblasts. J Cell Sci. 2005;118(Pt 9):1981-9.
21. Alikhani M, Maclellan CM, Raptis M, Vora S, Trackman PC, Graves DT. Advanced glycation end products induce apoptosis in fibroblasts through activation of ROS, MAP kinases, and the FOXO1 transcription factor. Am J Physiol Cell Physiol. 2007;292(2):C850-6.
22. Li H, Zhang X, Guan X, Cui X, Wang Y, Chu H, et al. Advanced glycation end products impair the migration, adhesion and secretion potentials of late endothelial progenitor cells. Cardiovascular Diabetology. 2012;11(46).
23. Hansen LM, Gupta D, Joseph G, Weiss D, Taylor WR. The receptor for advanced glycation end products impairs collateral formation in both diabetic and non-diabetic mice. Lab Invest. 2017;97(1):34-42.
24. Parnell LKS, Volk SW. The Evolution of Animal Models in Wound Healing Research: 1993-2017. Adv Wound Care (New Rochelle). 2019;8(12):692-702.
25. Gottrup F, Argen M, Karlsmark T. Models for use in wound healing research: A survey focusing on in vitro and in vivo adult soft tissue. Wound Repair Regen. 2000;8(2):83-96.
26. Dos Santos-Silva MA, Trajano ET, Schanuel FS, Monte-Alto-Costa A. Heat delays skin wound healing in mice. Exp Biol Med (Maywood). 2017;242(3):258-66.
27. Saadati F, Mahdikia H, Abbaszadeh HA, Abdollahifar MA, Khoramgah MS, Shokri B. Comparison of Direct and Indirect cold atmospheric-pressure plasma methods in the B16F10 melanoma cancer cells treatment. Sci Rep. 2018;8(1):7689.
28. Johnson KE, Wilgus TA. Vascular Endothelial Growth Factor and Angiogenesis in the Regulation of Cutaneous Wound Repair. Adv Wound Care (New Rochelle). 2014;3(10):647-61.
29. Goksen S, Balabanli B, Coskun-Cevher S. Application of platelet derived growth factor-BB and diabetic wound healing: the relationship with oxidative events. Free Radic Res. 2017;51(5):498-505.